Optimization of Radiation Therapy Treatment Planning Considering Setup Uncertainty and Radiobiological Effects

A Dissertation

Presented to

the Faculty of the Department of Industrial Engineering

University of Houston

In Partial Fulfillment

of the Requirements for the Degree

Doctor of Philosophy

in Industrial Engineering

by

Azin Khabazian

May 2019

Optimization of Radiation Therapy Treatment Planning Considering Setup Uncertainty and Radiobiological Effects

Azin Khabazian

Approved:

Chair of the Committee
Gino Lim, Professor,
Industrial Engineering

Committee Members:

Radhe Mohan, Professor,
Radiation Physics, The University of
Texas MD Anderson Cancer Center

Jiming Peng, Associate Professor,
Industrial Engineering

Taewoo Lee, Assistant Professor
Professor, Industrial Engineering

Wenhua Cao, Assistant Professor,
Radiation Physics, The University of
Texas MD Anderson Cancer Center

Suresh K. Khator, Associate Dean
Cullen College of Engineering

Gino Lim, Professor and
Chairman, Industrial Engineering

Dedicated to

My dear parents Ahmad and Fakhri

My devoted sister Arezoo and my brother Amir

with all my love

Acknowledgements

It is a pleasure to thank those who made this dissertation possible. First of all, my sincere gratitude goes to my advisor, Dr. Gino Lim for providing all the guidance, mentorship, warm encouragement, and patience throughout this program. It is incredibly lucky of me being his student. I am very grateful to Dr. Radhe Mohan and Dr. Wenhua Cao for giving me the opportunity to work with one of the greatest groups at one of the best cancer centers. It has been a pleasant experience working with them.

Many thanks to the dissertation committee members, Dr. Jiming Peng, Dr. Taewoo Lee, Dr. Wenhua Cao and Dr. Radhe Mohan for providing valuable comments that improved the contents of the work.

Big thank you to my wonderful friends, Aida, Aein, Amir, Aylar, Mahtab, Anahita, Navid, Zahed, and Shiva who made the past five years very enjoyable. I am so grateful to my dear friends Amir and Mahtab, for their support as well as their warm company, Navid and Anahita for their kindness and support during the past few years, and my lovely friend Aida, who I have shared difficult and joyful memories with. I am fortunate to have them all during my time in Houston.

The love, sacrifice and encouragement from my family has made it possible for me to complete the Ph.D study. My gratitude and love to my parents, my brother, Amir and my sister, Arezoo is more than that can be expressed in words. Finally, I would like to thank my twin sister and my best friend Aein, who was there to support me and cheer me up during difficult days. I am so lucky to have her in my life and by my side during this journey.

Many thanks to all of you!

Optimization of Radiation Therapy Treatment Planning Considering Setup Uncertainty and Radiobiological Effects

An Abstract

of a

Dissertation

Presented to

the Faculty of the Department of Industrial Engineering

University of Houston

In Partial Fulfillment

of the Requirements for the Degree

Doctor of Philosophy

in Industrial Engineering

by

Azin Khabazian

May 2019

Abstract

The clinical goal of radiation therapy is to maximize tumor cell killing while minimizing toxic effects on surrounding healthy tissues. A treatment protocol is used to decide on the treatment strategy and is a description of the desired radiation dose to the various regions of interest. Treatment planning then aims to find a plan as close to the treatment protocol as possible (Romeijn and Dempsey (2008)). Every step of radiation therapy is subject to some types of uncertainties (i.e., setup uncertainty, patient motion, and tumor shrinkage), which may compromise the quality of treatment. Basically, in treatment planning, a region of the patient where both tumor and organs at risk (OARs) are located with a certain probability is irradiated with a lower dose than the prescribed tumor dose. However, under uncertainty, the nearby healthy organs that should be irradiated by lower dose are always occupied by tumor voxels with a higher dose. Although the more ambitious goal is to damage the tumor cells so as to guarantee total tumor coverage for treatment, severe patient complications can occur when the surrounding healthy tissues receive an excessive amount of the radiation dose. Therefore, it is desired to develop an optimization approach to meet prescription requirements and tackle the uncertainties in radiation therapy treatments.

The proposed research attempts to overcome these limitations and find optimal beamlet intensity that will deliver a dose distribution close to the prescribed dose lead to a better sparing of healthy tissues.

First, to control the safety of the critical organs at risk during radiation as well as to provide sufficient tumor coverage, a Chance Constrained Programming (CCP) (Charnes and Cooper (1959)) approach is presented to handle setup uncertainty in radiation treatment planning that allows constraint violation up to a certain degree as it is the case in practice. We assume the uncertain dose distribution is governed by a known probability function and demonstrate that the proposed CCP model can solve the treatment planning problems efficiently.

Second, a CCP framework for radiation therapy treatment planning is considered, in

which the probability distribution of the random dose contribution is not completely specified, but is only known to belong to a given class of distributions. Sometimes, the information on hand for the random parameter might be limited to mean, covariance, and/or support of the uncertain data. In these situations, Distributionally Robust Chance Constrained Programming (DRCCP) (Calafiore and El Ghaoui (2006)) can be considered as a natural way to deal with uncertainties. An explicit convex condition is provided that guarantees the satisfaction of the probabilistic treatment planning constraints for any realization of the distribution within the given class.

Third, to systematically quantify the biological effects of radiation beams, a linear energy transfer (LET) is incorporated into the optimization of intensity modulated proton therapy (IMPT) plans. Because increased LET correlates with increased biological effectiveness of protons, high LETs in target volumes and low LETs in critical structures and normal tissues are preferred in an IMPT plan. Conventionally, the IMPT optimization criteria only includes dose-based objectives in which the relative biological effectiveness (RBE) is assumed to have a constant value of 1.1. In this study, we added LET-based objectives for maximizing LET in target volumes and minimizing LET in critical structures and normal tissues. We then explore the effect of this optimization to not only produce satisfactory dose distributions but also to achieve reduced LET distributions (thus lower biologically effective dose distributions) in critical structures and increased LET in target volumes compared to plans created using conventional objectives.

Moreover, to effectively treat a cancer patient with radiotherapy, an effective treatment strategy must be in place that considers dose delivery history and the patients' on-treatment biological changes. However, assessing the biological impacts of radiation on a tumor and the nearby healthy structures is not an easy task. But, the response of the cells to the radiation can be categorized by volume change, and these changes can be investigated by mathematical models that approximate reality. In this study, we seek to understand the importance of considering tumor shrinkage and proliferation during radiation treatment and how this affects the optimal prescribed dose in each fraction. We propose a stochastic sequential optimization structure under setup uncertainty of dose delivery, that optimizes

the dose in various fractions of an adaptive radiation therapy treatment plan by comparing the damage in tumor cells against the damage to the normal tissues volumetrically. Thus, while not prescribing specific strategies, this report provides the framework and guidance physicians to make apropriate decisions in implementing a safe and efficient treatment plan in their clinics on an individual patient.

Table of Contents

List of Figures

List of Tables

Chapter 1

Introduction

1.1 Background

Every year, approximately 1.7 million people in the United States alone that are newly diagnosed with cancer may benefit from radiation therapy (AmericanCancerSociety (2019)). With cancer affecting more individuals on a yearly basis, radiation therapy (RT) has become a key component in the successful treatment of this illness. In radiation therapy, radiation is delivered to the cancerous regions, to damage the DNA of the cells in the area being treated, interfering with their ability to divide and grow. As a result, radiation can kill cancerous tumor cells and stop them from regenerating. However, it will also damage healthy cells (Stone et al. (2003)). Thus, such treatment must be carefully planned so as to deliver sufficient dose to the tumor, while ensuring that the healthy tissue around the tumor is spared as much as possible. For some people, radiation may be the only treatment, but, most often it can be used in combination with other treatment methods (e.g. chemotherapy, immunotherapy, and surgery (Institute (2019)). According to American Cancer Society about half of the cancer patients receive a form of radiation therapy at some stage (AmericanCancerSociety (2019)).

1.1.1 Initial Treatment Planning Setup

To create a treatment plan, the starting point is to acquire the digital images of the internal anatomy. Medical teams use CT (Computed Tomography, see Figure 1.1), MRI (Magnetic Resonance Images) scans of the patient or position emission tomography (PET), to develop a radiation therapy plan. The images will go through a treatment planning

process called "simulation" so that a physician will precisely detect the target and critical structures. Cancerous areas are known as targets, while healthy organs located close to the targets are called critical structures or organs-at-risk (OARs). Healthy tissues are considered for the remaining portions.

Figure 1.1: CT simulator (21th Century Oncology (2019))

Typically, there are several clinical *targets* that we wish to treat, and several OARs that we would like to spare. The primary target, called *gross tumor volume* (GTV), includes areas where the disease is visible by any imaging modality. A secondary target, called *clinical target volume* (CTV), includes the GTV and an additional margin for possible microscopic disease (MD) extension that may not be visible in the images (see Figure 1.2). The third volume is the planning target volume (PTV) that allows for uncertainties in planning or treatment delivery. It is a geometric concept designed to ensure that the radiotherapy dose is actually delivered to the CTV. In some particular circumstances, a margin analogous to the PTV margin will be considered around an organ at risk to prevent the body from receiving a higher-than-safe dose, and this gives a planning-organ-at-risk volume. The concept of GTV, CTV, and PTV have been enormously helpful in optimizing the treatment modalities (which we will discuss further) and developing modern radiotherapy.

After the imaging and contouring phases, the details are used to set the treatment machine (linear accelerator (see Figure 1.3)). Along with the outlines of the structures, the physician will also prescribe a "treatment protocol". The treatment protocol is a description

Figure 1.2: Clinical *targets*

of the desired dose to the various regions of interest. A radiation oncologist specifies a set of requirements that have to be satisfied with any acceptable treatment plan. These requirements are in the form of a minimum prescription dose for target structure voxels and a maximum tolerance dose for nearby critical structure voxels. A prescription dose is the dose level necessary to destroy or damage target cells, while a tolerance dose is the level above which complications for healthy tissues may occur.

Figure 1.3: Treatment room and linear accelerator machine (Acceletronics (2019))

Treatment planning, then, refers to activities involved in finding the beam intensities that deliver a dose distribution as close to the prescribed dose as possible. Next, a human planner picks the parameters that are required as input to a treatment plan optimization software. These parameters are mostly the weights assigned to different objectives that

will guide the optimization algorithms to evaluate trade-offs which arise in balancing target radiation and healthy tissue sparing. The treatment planner usually works with commercial treatment planning software that uses an optimization procedure to find the treatment plan that best satisfies the treatment protocol requirements. Finally, after physician's approval, the treatment plan is delivered to the patient.

There are different types of beam modalities used for external beam radiation treatment such as photon beams and proton beams. In most cancer cases, the proton treatments are preferable to photon treatments due to the nature of the dose as a function of depth. For a given energy, the dose from proton beams increases as a function of depth of penetration in the patient until it reaches a peak (the "Bragg" peak) and then falls sharply to near zero (see Figure 1.4). This makes a more accurate dosage to the tumor cells but at the same time, is vulnerable to causing critical errors when uncertainty is present. For a photon beam, however, when the beam penetrates the skin, the dosage increases rapidly until it peaks. After peaking, there is an exponential reduction in dose as a function of the depth. Although photons are not able to focus the dose as well as protons, they are more robust to uncertainties such as patient setup errors and organ motion.

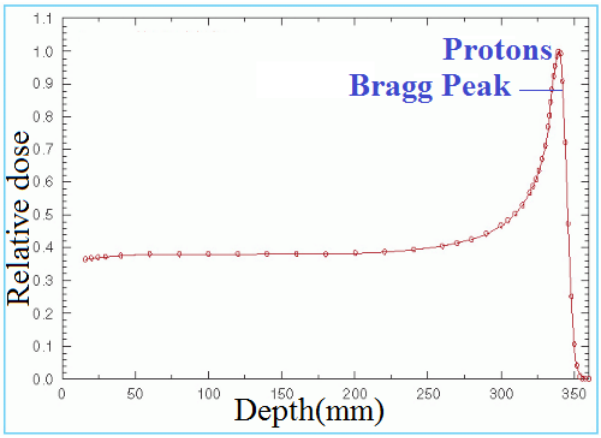

Figure 1.4: Characteristic depth-dose distribution of a proton beam (Key (2019))

External beams of radiation can be delivered in multiple ways. Fore example intensity modulated radiation therapy (IMRT) is designed to use beams of photon therapy to treat

tumor cells whereas Intensity modulated proton therapy (IMPT) is designed to use beams of proton particles. Their general aim is to increase local tumor control rates while keeping the radiation induced complications below desired thresholds. Intensity-modulated radiation therapy (IMRT) is a conventional cancer treatment method that aims to deliver a sufficient radiation dose to the target, based on tumor size, shape and location. Furthermore, IMRT allows a significant amount of control over the characteristics of the radiation delivered, by providing flexibility in the shapes of treatment beams, time of exposures, etc. (Webb (2004)). Each beam is divided into many thin beams ("beamlets") that can vary their intensity. This allows different doses of radiation to be given across the tumor. Similarly, in IMPT, the intensity of each beamlet or Bragg peak of each beam angle can be modulated independently. Due to characteristic of proton beams, intensity-Modulated Proton Therapy (IMPT) known as a highly precise type of radiation therapy, which can deliver highly conformal and homogeneous dose distributions to a target of complex shape while sparing adjacent healthy tissues as much as possible. Our work in this dissertation spans both of these treatment modalities.

1.1.2 Uncertainties in Radiation Therapy

Each step of the radiation treatment process involves uncertainties, both human and technology based, which significantly affects the quality of treatment. There are many sources of uncertainty that need to be taken into account in the course of a treatment planning. The segmentation of the target (tumor) and surrounding patient anatomy on the treatment beams is inherently uncertain and error prone. Patient positioning uncertainties are also relevant because the patient needs to be set up in the same position every day over the course of the treatment. Also, the clinical aspects of treatment simulation rely on the positioning and immobilization of the patient as well as on the data acquisition and beam geometry determination. Another class of uncertainty is motion effects which can be classified as inter-fraction and intra-fraction motion. The inter-fraction motion refers to motion between treatment sessions (also known as fractions), and intra-fraction motion refers to motion that occurs during a treatment session, such as breathing motion. Setup

uncertainty is caused by the setup procedure at the beginning of each fraction as well as the inter- and intra-fraction motion of the anatomy.

There are many reasons why errors occur, but they are usually divided into two categories: random and systematic errors. Systematic errors include setup error and organ motion on the CT scanner during treatment planning session, target delineation errors, and equipment calibration errors. Random errors include target movement during radiation delivery and day-to-day variation in the patient setup and equipment Van Herk (2004); Keller et al. (2003).

Among different ways of delivering radiation, proton therapy is more vulnerable than photon therapy to perturbations caused by various factors. The sharp fall-off of the dose at the end of the range of protons is their significant advantage, but it also makes them sensitive to various sources of uncertainty. To be effective, IMPT requires a high degree of precision and accuracy in delivery. In IMPT two important sources of uncertainty exist which are setup uncertainty (that is explained earlier) and range uncertainty. Range changes may originate from computed tomography (CT) artifacts, uncertainties in CT numbers, or conversion from CT numbers to stopping powers. Other possible sources of range uncertainties are tumor shrinkage and patient weight gain or loss (Unkelbach et al. (2009); Liu et al. (2012b)). These risks may result in deviation of the delivered IMPT dose distribution from the planned dose distribution, which may lead to unexpected treatment outcomes.

Immobilization devices are commonly used to reduce uncertainty by helping patients maintain consistent positioning, both during and between treatment (Bentel (1999)). Moreover, active breathing control (ABC) devices are used to reduce the effects of respiratory motion (Wong et al. (2005); Koshani et al. (2006)). The radiation treatment is then designed using the "ABC scan" as input. On the one hand, the ABC method better spares the OARs, while maintaining target coverage. On the contrary, this approach is time-consuming at imaging and treatment delivery. It is also expensive because of the device, and it is not useful for all of the patients. In addition, small discrepancies in the position of the target and surrounding patient anatomy are inevitable.

Other approaches used in practice to capture the geometrical uncertainties include convolution-based methods (Lujan et al. (1999); Chetty et al. (2003); Beckham et al. (2002)) and Multiple Instance of Geometry Approximation (MIGA) (McShan et al. (2006)). In convolution-based methods, uncertainties caused by daily setup procedures at the beginning of each treatment fraction, as well as the inter- and intra-fraction motion of the internal organs, are incorporated in dose calculations to calculate average dose values to tissues. MIGA, on the other hand, approximates the random setup variation by a discrete distribution of setup instances and performs a dose deposition matrix calculation for each setup instance.

In photon therapy, the safety margins (CTV, PTV) are designed to accommodate systematic and random uncertainties that might be introduced following the acquisition of the initial planning data. The underlying assumption in the determination of the CTV-to-PTV margin is that the CTV will be sufficiently covered with high (e.g., 95%) probability in the face of uncertainties. This approach may work for photon-based therapy because of the relatively small variations in photon dose distributions when patient anatomy changes (Liu et al. (2012b); Chen et al. (2012)). However, for IMPT, uncertainties can cause substantial perturbations in the dose distributions not only in the CTV-to-PTV margins, but also within the CTV, as well as in normal tissues lateral to the CTV. Thus, simply applying the concept of PTV cannot efficiently mitigate the impacts of uncertainties in radiation therapy (Fredriksson et al. (2011)) and alternative approaches are required.

1.1.3 Radiobiological Effects of Radiation Therapy

Absorbed radiation dose is an important quantity when predicting the biological effect. However, many factors affect the biological response to a given dose. The most important biological factors influencing the response of tumors and normal tissues to fractionated treatment (i.e. a treatment that is carried out as a series of small dosages over a period) are often called five R's (Khaled and Held (2012); Withers (1975)), such as repair, repopulation, redistribution, re-oxygenation, and radiosensitivity. These radiobiology effects were

initially described to provide a means of understanding the success or failure of localized radiotherapy. Repair is one of the primary reasons to fractionate radiotherapy. By splitting radiation dose into small parts, cells are allowed to repair sub-lethal damage (i.e., damage that can be repaired before the next fraction of radiation is delivered). Healthy cells are capable of repairing some of the radiation damage between fractions, whereas tumor cells have much less repair capability. In addition, the repair capacity of the cells depends on the time and the amount of dose. These two elements could significantly affect the capability of cells to treat themselves. Repopulation, i.e., the cell proliferation occurring during fractionated RT, occurs in both tumors and healthy tissue. Although repair of radiation damage between the fractions and proliferation of survival cells enhance the radiation tolerance of the normal tissue, the response of tumor is also influenced the treatment outcome. In fact, the damage and cell death that occur during the radiation may induce an increased rate of tumor proliferation. Hence, selecting the appropriate approach relies on an adequate balance between the tumor and normal tissue responses. In addition, redistribution and reoxygenation would also be expected to affect the total dose required for treatment. Redistribution refers to the fact that the cells exhibit differential radiation sensitivity while in the different phases of the cell cycle. Basically, normal cells interrupt typical cell cycling after exposure to ionizing radiation to allow for enough time for DNA repair, or in the case of extreme damage, prepare for cell death. This makes cells more sensitive and causes a therapeutic gain. Another major challenge for RT is the presence of hypoxic areas within solid tumors. A single fraction of irradiation preferentially kills the well-oxygenated cells. Reoxygenation of hypoxic areas occurs during fractionated treatment in part due to tumor shrinkage. This makes the cells more sensitive to subsequent radiation. The other factor is radiosensitivity which reminds us that for different cell types, the relative susceptibility of the cells to radiation is different.

Due to the radiobiological effects of radiation dose on the healthy and cancerous cells , the total amount of radiation that is to be delivered is split into fractional doses. Therefore, by splitting the dose over many days, healthy cells have a chance to recover between

fractions, while the cumulative dose of tumor cells destroy cancerous cells (Thames and Hendry (1987)). However, as the fractionated treatment is prolonged to longer times, the contribution of repopulation becomes greater.

The fact that the biological factors depend on the treatment schedule has significant implication for the planning of radiation therapy. Thus, understanding how radiation affects the underlying biological processes will give us an insight on investigating the optimal fractionation treatment plan. However, conventional radiation treatment plans mostly ignore the biological changes during the treatment and prescribe an equal amount dose for each stage.

One way to adapt doses and treatments is to make use of information acquired between fractions. This type of treatment modification, known as adaptive radiation therapy (ART), permits customized day-to-day dose delivery to mitigate treatment variations and incorporating them to re-optimize the treatment plan early on during therapy. There are multiple ways to optimize treatment dynamically. One way is to make use of feedback information obtained from the CT images throughout the course of therapy, which is known as online ART (Acharya et al. (2016)). However, one of the major challenges for on-line adaptive treatment is the length of time required to re-optimize the treatment plan. Planning time for a treatment varies depending on the complexity of the case and the experience of the planner. If treatment plans can be optimized and quality assured fast enough, we can adapt treatment using online ART ; otherwise, we can use offline ART, in which past CT images are used to adjust future treatment (Reilly et al. (2016); Yang et al. (2014); Qin et al. (2015)) . In a case that the existing technology cannot be used to observe such biological information, adaptive models can be developed to adjust a treatment dynamically. In this situation, the question arises as:

How should a treatment plan be adapted considering the dynamic nature of the natural biological processes in a patient body to improve the treatment outcome?

1.1.4 Quantification of the Biological Effectiveness of Radiation

Every radiation type has its special distribution of energy depositions. Two important physical quantities in radiation therapy that affect the biological outcome are the absorbed dose and the linear energy transfer (LET). In radiation therapy, not only the amount of energy deposited in a volume (the dose) is of importance but also how the energy depositions are distributed. This characteristic of radiation would also affect the biological responses of survival cells. As an example, high-LET radiation is believed to cause damage that is more difficult to repair compared to low-LET radiation (Goodhead (1994); Karlsson and Stenerlöw (2004)).

LET mainly indicates the quality of different types of radiation and is important because the biological effect of radiation (its relative biological effectiveness, RBE) depends on its average LET. Relative biological effectiveness (RBE) is defined as the ratio of the doses required by two radiations to cause the same level of effect. As defined, the RBE is a simple concept, but it is clinical compound because it is a function of particle type, dose, energy, dose per fraction, fraction number and the biological endpoints. When effects of equal doses of different types of radiation are compared, they produce different biological effects. The RBE can be expressed as a comparison of effects of different types of radiation.

To incorporate the biological aspects of radiation into modeling a treatment plan, alternative measures has been studied in the literature (e.g., the tumor control probability (TCP) and normal tissue complication probability (NTCP), the equivalent uniform dose (EUD) (Wu and Mohan (2002))) , among those RBE is a measure that uniquely describes the radiation quality.

Hence, we can classify the above issues with treatment planning optimization into following categories:

- Reliable and efficient intensity profile under uncertainty
- Fractionation scheduling considering the radio-biological effects
- Fluence map optimization under uncertainty considering the linear energy transfer (LET)

- Including relative biological effectiveness in a fluence map optimization under uncertainty

,which we will explain further in the Problem Description.

1.2 Problem Description

Optimization concept makes a significant contribution to the calculation of radiation therapy treatment plans. The objectives on target coverage and sparing different organs at risk are often conflicting, and there has been extensive research on how to prioritize the objectives (e.g., Wilkens et al. (2007)), and find the relative objective weights (e.g., Cotrutz and Xing (2003)). In such an optimization problem, designing treatment plans that meet prescription dose under uncertainty is one of the greatest challenges. Hence, the purpose of this section is to address and specify remaining challenges in this area, and then propose solution methods.

1.2.1 Reliable and Efficient Intensity Profile under Uncertainty

The typical decision variables for treatment planning are the intensities (or how long the beam is turned "on") of radiation beams and the angles from which to deliver the radiation. In this study, we focus on the optimization of beamlet intensities (called the fluence map optimization (FMO) problem) assuming the optimal beam directions are given. The resulting solution is called "intensity map", because it resembles a topological map where the height of a point on the map matches the intensity of the corresponding beamlet. This topic has received a lot of attention from the optimization community. Comprehensive reviews of the existing literature are provided in references (Shepard et al. (1999); Reemtsen and Alber (2009)). However, due to the challenges in this field of optimization, new approaches need to be developed for clinical problems. In this regard, one of the issues would be:

How can we identify the reliable intensity fluence map in a radiation therapy treatment planning under uncertainty?

Currently, the primary challenge in the optimization of radiation therapy problem is to address the treatment uncertainties. Therefore, investigation on the development of

stochastic optimization approaches is needed. In the last few years, stochastic models have been used to formulate uncertainties in IMRT treatment planning (e.g., Lof et al. (1995); Unkelbach and Oelfke (2004)). Robust optimization (RO) is also constructed to produce optimal and resilient plans that are more aggressive than traditional margin approaches, without sacrificing protection from uncertainty. For the recent studies who applied robust optimization in radiation therapy problems, we can refer to Chu et al. (2005); Olafsson and Wright (2006); Chan et al. (2006); Bortfeld et al. (2008); Pflugfelder et al. (2008); Fredriksson et al. (2011). Probabilistic and worst case robust optimization methods are the two main groups in the area of robust optimization in radiotherapy.

In RO, the uncertainty is often expressed using an uncertainty set that contains all possible scenarios of the uncertain data. Traditional RO models only consider the worst-case scenario of the unknown parameters and do not optimize for cases when non-worst-case scenarios inside the uncertainty set occur. Such an approach, while producing a treatment that is robust against uncertainty, is over-conservative and necessarily increases the radiation exposure of healthy tissue and organs-at-risk. In practice, an overestimation of uncertainties leads to a conservative decision resulting in an unnecessary deterioration of the objective function. In other cases, an aggressive decision may be preferred due to the physician expectations from treatment. Nevertheless, even under certain circumstances, it may not be possible to find beamlet intensities that satisfies two conflicting objectives, ensuring the tumor receives the required dose, while exposing healthy tissue to less dose.

Accordingly, a systematic way is required to evaluate the trade-off between treatment efficiency and reliability. That calls for using one of the major approaches in stochastic modeling programs, called chance-constrained programming (CCP). This approach that is recently applied to stochastic radiation therapy problems (Zaghian et al. (2018)), was first introduced by Charnes and Cooper (1959) and Miller and Wagner (1965), and has been widely studied as an alternative methodology for optimization under uncertainty (Geletu et al. (2013); van Ackooij et al. (2014); Kamjoo et al. (2016)). Its main feature is that the resulting decision ensures the probability of complying with constraints, i.e. the confidence

level of being feasible. When there is randomness in some or all data elements, and when the restrictions are required to be satisfied with at least some level of confidence less than one, CCP relaxes the constraints in deterministic mathematical programming and replaces them with probabilistic constraints. Thus, the relation between the treatment efficiency and reliability can be quantified using chance constrained programming.

However, there are some important issues concerning the CCP in an optimization problem. One of the issues using the CCP approach is that the feasible set of a chance constraint is usually nonconvex, which makes the optimization problem difficult to solve (Nemirovski and Shapiro (2006)). However, under some assumptions on an uncertain parameter, deterministic equivalent transformations have been developed in the literature (Charnes and Cooper (1959); Geletu et al. (2013)). Finding a feasible solution for the deterministic counterparts of the chance constraints is often computationally less burdensome than solving the original stochastic model.

Another difficulty is that the CCP tackles the problem in a way that uncertain parameters depend on the known probability distribution. In practice, distributional information of uncertainty may be partially available. This information might be limited to mean, covariance, and/or support of the uncertain data. Therefore, there is a need to develop a new approach to deal with uncertainties in a chance-constrained framework. This is addressed via distributionally robust chance-constrained programming (DRCCP) which is proposed by Calafiore and El Ghaoui (2006). In their study, they provided convex conditions that guarantee the satisfaction of the chance constraints when only partial information about the probability distribution is known. There are few other studies where they have explored DRCCP to ensure the probabilistic constraint irrespective of the probability distribution of the data (Zymler et al. (2013)). In general, within the CCP setting, one seeks to obtain the feasibility of the constraints with high probability. However, this is not the concern of robust optimization. In fact, in RO, the goal is to achieve feasibility under any realization of a predetermined uncertainty set. Hence, the primary motivation of CCP and DRCCP is to incorporate the concept of the confidence level to control the satisfactory of each chance

constraints. A confidence level, the probability that the constraints will hold under uncertainty, can help a physician in selecting an appropriate treatment plan based on the risk tolerance level for constraint violation.

1.2.2 Fractionation Scheduling Considering the Radio-biological Effects

The fact that the biological effect of radiation depends on the fractionation schedule has important implications for the planning of radiation therapy. Recently, with the improvement of models and imaging technologies, adaptive treatment planning problems, aiming at the optimal fractionation scheme and dose delivery over time, has tremendous potential. In a fractionated regime, radiation-induced responses of the tumor and normal tissues are used as feedback to modify and improve radiotherapy in to get the highest therapeutic gain. The complexities of how radiation affects the underlying biological processes make it difficult to determine how a treatment plan should be scheduled, however, it is crucial to understand the relationship between biological modeling assumptions and the resulting optimal treatment plan.

Thus, in addition to the radiation dose distribution of each beam as the general goals of optimization in an FMO, a physician needs to determine the best decomposition of a single treatment plan into several smaller fractions under uncertainty. Within these goals, we present the CCP fractionation model in an attempt to address the uncertainty issue in providing the safe treatment dose for each fraction considering repair and repopulation as the most important biological factors. The finding that healthy cells appear to have greater repair capability than tumors is one factor favoring the fractionated treatments. In fact, full repair may take about 6 to 8 hours and can be longer in such tissues under different circumstances. For simplicity, the recovery ratio can be measured as the proportion of surviving cells receiving a split dose divided by surviving cells receiving the total dose as a single dose. This ratio can be used to predict the normal cells' responses to the radiation during treatment. On the other hand, repopulation of tumor cells is much faster than the normal cells which could result in a treatment failure. These effects suggest that the

repopulation and repair need to be considered simultaneously in adapting a treatment.

The growth rate of the tumor is expected to be an exponential function of time and dose, and it could be varied due to the nutrition deprivation and other conditions (e.g. re-oxygenation). In this regard, various models have been developed in an attempt to describe and predict how tumor volume changes. However, the models for predicting the response of normal cell during the treatment has not been demonstrated. Thus, the main motivation for this study is the potential use of the appropriate model to link the biological changes for measuring the treatment outcome. We consider the effects of the tumor and healthy cells responses to the radiation which are characterized by volume changes. This is because tumor volume is well-known and extensively studied in the literature as a significant predictor of treatment outcome (Bral et al. (2009)). Various models have been developed in an attempt to describe and predict how tumor volume changes over time (Nieves and Ubriaco (2015); Huang et al. (2010)). One way of measuring these biological effects of irradiation is by the cell survival fraction. Nevertheless, a few studies worked on optimizing the fractionation dose considering the volumetric reaction of cells to the radiation.

1.2.3 Fluence Map Optimization under Uncertainty Considering Linear Energy Transfer

The first dosimetric quantity in radiotherapy optimization is the absorbed dose. This, however, does not guarantee a homogeneous distribution of Linear Energy Transfer (LET) values. Even though radiobiologists have been aware of the effect of energy variations in treatment, the differences in a treatment outcome were considered too small to be significant clinically. With improved treatment delivery techniques and powerful computational methods available, recent publications have sparked interest in LET measurements. Using LET, a biophysical model by Wilkens and Oelfke (2004) is a commonly studied method. There are few alternative studies in treatment planning problems considering LET (Grassberger et al. (2011)). In this work, our goal would be a simultaneous optimization of radiation energy and fluence under uncertainty.

1.2.4 Including Relative Biological Effectiveness in a Fluence Map Optimization under Uncertainty

Treatment planning is usually based on specific prescription doses to the target and constraints for the normal tissues, and not on clinical and biological endpoints of radiotherapy. While it would be preferable to base plans on the more clinically and biologically relevant parameters such as RBE. The biological effects of different beams can be optimized by the concept of relative biological effectiveness (RBE), that is the ratio of biological effectiveness of one type of radiation relative to another one, given the same amount of absorbed energy. RBE varies significantly as a function of dose, depth in the patient along the path of the protons, tissue and cell type, end-point and possibly other factors Wilkens and Oelfke (2004); Carabe-Fernandez et al. (2007) ; yet in radiation therapy (e.g. proton therapy), a physician currently utilizes a generic RBE of 1.1 for all situations. This value is based on averages of existing biologic data from past experiments performed under limited conditions. The fixed RBE value of 1.1 is recommended by the International Commission on Radiation Units and Measurements (ICRU) and is used in most clinical proton therapy centers Wilkens and Oelfke (2005). Nevertheless, the use of a constant RBE disregards the dependencies of the RBE on physical and biological properties. As a result, by incorporating RBE quantification and using other such biologic information into a treatment planning optimization, the plans could be generated preferentially in a way that the high RBE portions of the Bragg peaks are placed within the tumor volume. Hence, the biological optimization rather than the physical dose optimization would translate into both improved tumor control and reduced normal tissue exposure.

The potential clinical impact of a variable RBE for various situations is studied in the literature. Polster et al. (2015) utilized a tool for particle simulation for the implementation of eight biophysical models to predict RBE values based on LET and other elements. Few studies centered on model formulation and optimization of beamlet intensities considering RBE values. For an optimization model considering radiobiological effects, many studies were reported using the equivalent uniform dose (EUD) biological function problem. Alber

and Nüsslin (2001) presented an unconstrained optimization with interior penalty functions. Wilkens and Oelfke (2005) and Carabe-Fernandez et al. (2007) proposed RBE models based on variable radiobiological parameters for different tissues. Thus, some research on dose and RBE constrained based optimization in a probabilistic framework need to be addressed.

In summary, a treatment outcome depends on the physical and biological characteristic of radiation and anatomical information of a patient's body, and varies according to the dose, fractionation, LET, cell status before irradiation and other important factors. The respective roles of radiation treatment planning optimization are to study the feature of healthy and tumor cells in responding to radiation on one hand, and the complex mechanisms which may react to those factors as listed above, continue to be the subject of future radiobiological research. This is done hoping that better understanding of these factors may permit a scientific judgment on the existence treatment plans, and lead to the improvements which the risk of radiation-induced cancer reduced to zero.

1.3 Objectives and Contributions

The overall aim of this dissertation is to develop mathematical modeling methods to optimize and analysis the quality of a treatment plan in each fraction with the prediction of biological changes and considering the setup uncertainty under radiotherapy. In this Section, we briefly specify the first and second issues discussed in Section 1.2 and the way we approached the problems. Note that, we will address the remaining challenges in our future study. Through achieving the objectives, this research addresses the shortcomings of the existing approaches to handling uncertainties and satisfying prescription requirements in treatment planning optimization by presenting the following contributions.

- First, we present a chance constrained optimization approach to handling setup uncertainty in the problem of radiation therapy treatment planning. We describe testing the performance of the proposed CCP models regarding plan quality, robustness, and homogeneity for three patient datasets. Optimized CCP plans are also compared to the plans from a deterministic approach that does not take the uncertainties into

account. Dosimetric tests confirmed that the CCP can control setup uncertainty in target coverage and organs-at-risk sparing and this framework do not depend on tissue or patient specific.

- Then, we present the first distributionally robust chance-constrained approach to radiation treatments subject to setup uncertainty. This stochastic programming framework is an extension to CCP framework to mitigate other types of uncertainty. The DRCCP model is evaluated regarding affine and quadratic dependence of random dose contribution. The experimental studies are conducted in a small cancer case and prostate cancer case to illustrate the general feature of proposed DRCCP model.

- For the third work, we investigate the impact of incorporating LET criteria directly into IMPT optimization. Both dose and LET distributions could be optimized simultaneously in the proposed approach. Dose-averaged LET was used to indicate LET values in this study. The goal of this optimization was set to not only produce satisfactory dose distributions but also to achieve reduced LET distributions (thus lower biologically effective dose distributions) in critical structures and increased LET in target volumes compared to plans created using conventional objectives. In this study, five brain tumor patients who had been treated with proton therapy at our institution were selected. Two plans were created for each patient based on the proposed LET-incorporated optimization (LETOpt) and the conventional dose-based optimization (DoseOpt). The optimized plans were compared in terms of both dose (assuming a constant RBE of 1.1 as adopted in clinical practice) and LET. Both optimization approaches were able to generate comparable dose distributions. The LET-incorporated optimization achieved not only pronounced reduction of LET values in critical organs, such as brainstem and optic chiasm, but also increased LET in target volumes, compared to the conventional dose-based optimization. However, on occasion, there was a need to tradeoff the acceptability of dose and LET distributions. Our conclusion is that the inclusion of LET-dependent criteria in the IMPT optimization could lead to

similar dose distributions as the conventional optimization but superior LET distributions in target volumes and normal tissues. This may have substantial advantage in improving tumor control and reducing normal tissue toxicities.

- In the last part of this study, we investigate an alternative treatment mode where the radiation is allowed to be delivered in multiple fractions. We model the repair effect in addition to tumor repopulation and find the optimal fluence maps for each fraction of the radiotherapy simultaneously by considering the overall dose delivered to the patient. The optimization model decides how many doses to give in each fraction under the radio-biological changes and setup uncertainty. Under this problem setting, we show that safe fractionation dose has a particular threshold form. We investigate the benefit of this approach with computational studies on real prostate case patients. This sequential model reduces the treatment time and thus the comfort level of the patient. Furthermore, because the optimization exploits the opportunities provided in each fraction better treatment plans can be obtained.

1.4 List of Outcomes

1.4.1 Journal Publications

- Maryam Zaghian, Gino Lim, and Azin Khabazian (2018). "*A Chance-Constrained Programming Framework to Handle Uncertainties in Radiation Therapy Treatment Planning*," *European Journal of Operational Research*, 266(2), 736-745.

- Wenhua Cao, Azin Khabazian, Pablo Yepes, Gino Lim, Falk Poenisch, David Grosshans, Radhe Mohan (2017). "*Linear energy transfer incorporated intensity modulated proton therapy optimization*," *Physics in Medicine & Biology*, 63(1), **Featured Article**, 015013.

- Azin Khabazian, Maryam Zaghian, and Gino Lim (2019)."*A feasibility study of a risk-based stochastic optimization approach for radiation treatment planning under setup uncertainty*," (under revision) *Computers & Industrial Engineering Journal.*

- Gino Lim, Azin Khabazian, and Maryam Zaghian. "*Distributionally Robust Chance-Constrained Programming in radiation therapy treatment planning*," submitted to *Annals of Operations Research.*

- Azin Khabazian, and Gino Lim. "*Understanding Impacts of Radiobiological Parameters in Adaptive Radiation Treatment Planning under Setup Uncertainty*," to be submitted.

1.4.2 Conference Presentations

- Maryam Zaghian, Azin Khabazian, and Gino Lim, "*A Chance-Constrained Programming Framework to Handle Uncertainties in Radiation Therapy Treatment Planning*," INFORMS Annual Meeting, Philadelphia, Penn, Nov 2015.

- Maryam Zaghian, Azin Khabazian, and Gino Lim, "*Radiation Therapy Treatment Planning under Uncertainties: A Chance Constrained Programming Approach*," UH Graduate Re-search and Scholarship Projects (GRaSP), Houston, TX, Nov 2015.

- Maryam Zaghian, Azin Khabazian, and Gino Lim, "*Distributionally robust chance constrained programming in radiation therapy treatment planning*," IISE Annual Meeting, Anaheim, CA, May 2016.

- Azin Khabazian, Maryam Zaghian, and Gino Lim, "*Tractable Quadratic Approximations of Distributionally Robust Chance Constraints in Radiation Therapy Planning*," INFORMS Annual Meeting, Nashville, TN, Nov 2016.

- Azin Khabazian, Gino Lim, "*CCP Optimization with Time-Dependent Uncertainty in Radiation Therapy Planning*," INFORMS Computing Society Conference, Austin, TX, Jan 15, 2017.

- Azin Khabazian, Gino Lim, "*Optimization of Radiation Therapy Fractionation Dose Considering the Biological Effects*," INFORMS Annual Meeting, Houston, TX, Nov 2017.

- Azin Khabazian, Gino Lim, "*Understanding Impacts of Radiobiological Parameters in Adaptive Radiation Treatment Planning under Uncertainty*," INFORMS Annual Meeting, Phoenix, AZ, Nov 2018.

1.5 Organization

This dissertation is organized as follows. Chapter 2 is a comprehensive overview of the optimization models in FMO problem that deal with uncertainties. A review of the robust and chance-constrained optimization as well as the adaptive optimization of radiation treatment is also provided. In Chapter 3, we present our chance constrained approach to incorporate setup uncertainty in radiation therapy treatment planning optimization. We assumed that the uncertain dose distribution was governed by a known (or estimated) probability distribution function and demonstrated that the associated CCP models could help significantly in sparing organs-at-risk (OARs).

In Chapter 4, a distributionally robust chance-constrained treatment planning problem is derived. Our framework generalizes the presented CCP model for the case that uncertain parameter does not follow a particular distribution and is less conservative than robust approach. We demonstrate how this approach used to formulate the radiation therapy problems under the affine assumption of dose contribution. Then, we provide more precise deterministic equivalences of DRCCP model considering the quadratic format of random dose contribution. We evaluate the proposed DRCCP models in the context of a radiation therapy treatment planning problem.

In Chapter 5, we provide a feasibility study on incorporating linear energy transfer (LET) into the optimization of intensity modulated proton therapy (IMPT) plans. Two IMPT plans were created for each patient case, one using the conventional dose-based optimization and the other using the proposed LET-incorporated optimization. We compare the performance of our LET-incorporated IMPT optimization method with conventional dose optimization model in terms of both dose and LET distributions. Both optimization approaches were able to generate comparable dose distributions. The LET-incorporated optimization achieved not only pronounced reduction of LET values in critical organs, but

also increased LET in target volumes, compared to the conventional dose-based optimization. However, on occasion, there was a need to tradeoff the acceptability of dose and LET distributions. Our conclusion is that the inclusion of LET-dependent criteria in the IMPT optimization could lead to similar dose distributions as the conventional optimization but superior LET distributions in target volumes and normal tissues. This may have substantial advantage in improving tumor control and reducing normal tissue toxicities.

In Chapter 6, we provide an analysis of the biologically-based treatment planning model. This method not only allows for the correction of patient setup error but also allows dose recalculation and adaptive radiation therapy (ART), using the volumetric information to adjust the treatment plan of each fraction to the updated patient anatomy. We evaluate the effect of tumor repopulation and rapair capability of healthy tissues on optimal fractionation schemes based on the exponential survival rate of cancer cells as a function of dose delivery and resting time. The optimization problem consists of minimizing the number of surviving tumor cells under the constraints on maximum prescribed dose in OARs. We discuss the results from implementing the biologically-based CCP models at the end. Chapter 7 provides direction of the future research.

Chapter 2

Literature review

2.1 Fluence Map Optimization

The FMO problem is one of the most popular subproblems in treatment planning optimization, which has been extensively studied in the literature. The models that have been developed for the FMO are generally based on sets of conflicting treatment plan evaluation criteria. Thus, considering the treatment requirements, the typical approach in the FMO model has been to formulate the bound constraints and define an objective function that optimizes the value of a weighted sum of criteria (Shepard et al. (1999)). A wide range of optimization techniques have been used for FMO in IMRT, from linear programming (e.g., Hamacher and Küfer (1999); Holder (2003); Romeijn and Dempsey (2008); Lim et al. (2008)) to mixed-integer linear programming (e.g., Bednarz et al. (2002); Lee et al. (2003, 2006)) and penalty-based quadratic and nonlinear programming (e.g., Bortfeld (1997); Wu and Mohan (2002); Romeijn et al. (2003)). Several authors have proposed quadratic variational penalties (Spirou and Chui (1998); Chvetsov et al. (2005); Matuszak et al. (2007)), which promote smooth fluence profiles. In a recent paper, Aleman et al. (2014) employed the convex objective function that penalizes the deviation of delivered to desired dose. Dias et al. (2016) provided a voxel-based convex penalty nonlinear model to find the optimal fluence map. They consider each voxel to be penalized considering the square difference of the amount of dose received by the voxel and a given upper and/or lower bound.

Over the past few years, several researchers have studied the FMO problem (Romeijn et al. (2003); Lim et al. (2008); Zaghian et al. (2014)). However, due to the presence of uncertainties in radiation therapy, solving the FMO problem is computationally difficult in practice.

2.2 Treatment Plan Optimization under Uncertainty

Robust optimization is a methodology that govern the tumor coverage and OAR sparing under uncertainty simultaneously. Besides robust optimization, Chance-constrained programming (CCP) has been widely used in the literature to deal with optimization problems under uncertainty.. In the next section, we review the application of RO to a treatment planning in more detail. Then, we will explain the chance-constrained programming which is the focus of this study.

2.2.1 Robust Optimization

To date, robust optimization is one of the main approaches to deal with the uncertainties in a treatment planning problem. There are a handful of robust optimization approaches proposed to incorporate uncertainties into radiation therapy treatment plan optimization Baum et al. (2006); Unkelbach and Oelfke (2004); Bortfeld et al. (2008); Chan et al. (2006); Chan and Mišić (2013); Lomax (2008); Pflugfelder et al. (2008); Unkelbach et al. (2007, 2009); Liu et al. (2012b); Fredriksson et al. (2011). Research by Baum et al. (2006) and Unkelbach and Oelfke (2004) highlights the importance of robustness in radiation therapy Baum et al. (2006); Unkelbach and Oelfke (2004). Bortfeld et al. (2008) and Chan et al. (2006) use probability density functions that describe breathing motion, and provide a robust formulation of the problem of optimizing IMPT, generalizing existing mathematical programming formulations Bortfeld et al. (2008); Chan et al. (2006). They did not assume any fixed distribution for the patient breathing. Chan and Mišić (2013) generalized the existing single planning robust optimization approach to develop an adaptive robust optimization. Robust and stochastic optimizations are the two most widely used approaches for incorporating the uncertainties in treatment planning optimization problems. Chan et al. (2006) proposed a robust formulation of the treatment planning optimization problem using probability density functions of the uncertainty in breathing motion. They did not assume any fixed distribution for the patient breathing. Chu et al. (2005) and Olafsson and Wright (2006) showed that a robust linear optimization model can become a second-order cone

program when the ellipsoidal uncertainty set is taken into account. All of these robust optimization approaches involve solving a single planning problem before the start of treatment and using the resulting solution in all of the subsequent treatment sessions.

Worst-case robust optimization technique is another useful approach to handle uncertainties in treatment plan optimization. Two current approaches are the "worst-case dose" robust optimization Pflugfelder et al. (2008) and the "minmax" robust optimization approaches Fredriksson et al. (2011). (In reality, both are worst case approaches - the former is based on worst case dose in each voxel, whereas the latter considers the worst case value of the objective function for the dose distribution as a whole). Both of these approaches can work with either a linear programming (LP) model Cao et al. (2012) or a nonlinear programming (NLP) model Liu et al. (2012a). Some groups have proposed a worst case dose robust optimization approach using an LP model to consider range uncertainties Unkelbach et al. (2007, 2009); Chan (2007), whereas Pflugfelder et al. (2008) proposed a worst case dose distribution-based robust optimization approach using a nonlinear quadratic objective function. This approach can also be used with linear objective functions.Pflugfelder et al. (2008) and Liu et al. (2012a) developed a modification of the nonlinear worst case dose distribution-based robust optimization approach that additionally penalized hot spots within the target for better target dose homogeneity.

The minmax robust optimization approach was first proposed by Fredriksson et al. (2011). This nonlinear constrained model does not assume any probability distribution for the uncertainties. Chen et al. (2012) also reported a multicriteria minmax optimization approach utilizing a piecewise-linear convex constrained model, similar to the work by Fredriksson et al. (2011).

2.2.2 Chance Constrained Programming

Chance-constrained programming (Charnes and Cooper (1959)) is as one of the major approaches in modeling stochastic programs and has enjoyed widespread appeal and acceptance. If the uncertainty only affects the right-hand-side parameters of the single chance

constraints, deterministic equivalent transformations are linear and their corresponding feasible region is convex. On the other hand, when the uncertainty is in the left-hand-side parameters of the chance constraint, additional non-linearity will be introduced to the original problem by using deterministic equivalent transformations (Charnes and Cooper (1963)). Deterministic equivalents of the chance constraints are usually developed based on some distributional assumptions of the uncertain data (Kall et al. (1994); Prékopa (2013); Birge and Louveaux (2011)). Generalization of the chance constraints and relaxation of the distribution assumptions are recent developments in chance constrained programming. Without any major assumption on the distribution of random parameter, Pinter (1989) and Birge and Louveaux (2011) proposed upper bound and lower bound approximations on chance constraints. They used Chebyshev's, Bernstein's, and Hoeffding's inequalities to develop approximations.

Distributionally robust chance constraint has been found as a natural way to deal with uncertainties in a chance constrained framework. Calafiore and El Ghaoui (2006) converted the single chance constrained linear programs into convex second-order cone constraints for a wide class of probability distributions. They provide convex conditions that guarantee the satisfaction of the chance constraints for the given class of probability distribution. Assuming that the first and second order moments as well as the support of the random parameter are known, Zymler et al. (2013) developed models to approximate robust chance constraints. The chance constraints are approximated by worst-case CVaR constraints, which is motivated by the recent study described above (Chen et al. (2010)). However, the exact semidefinite programming (SDP) reformulations of the approximation are proposed. The reformulations are based on the theory of moment problems and conic duality arguments rather than the loose probabilistic inequalities. The approximation by Zymler et al. (2013) is proved to be exact for single chance constrained programming with either concave or (possibly non-concave) quadratic in random parameter. Robust individual chance constraints are shown to have manifestly tractable SDP representations in most cases in which CVaR approximation is exact.

As an immediate consequence, the treatment plans can be severely conservative for the tumor region, which leads to overdose on the surrounding healthy tissues. In an attempt to overcome these limitations and to potentially improve sparing of healthy tissues, we develop further a CCP framework of the FMO problem first introduced by Zaghian et al. (2018). We then develop a distributionally robust chance constrained structure for this problem to relax the assumption on uncertainty.

2.3 Biologically-based Treatment Planning Optimization

An important subproblem related to the FMO problem is the fractionation problem. In this type of optimization problem instead of having one single treatment, a treatment plan is divided into several sessions, called fractions. This is done to take advantage of the radio-biological effects of the normal and tumor cells during the treatment.

To this end, growing number of literatures has been devoted to adaptive radiation therapy. Lu et al. (2006) introduced the concept and strategy of adaptive fractionation therapy (AFT) which enables a quick and easy way to achieve a better therapeutic gain without planning. In this study, Lu et al. (2006) minimized the expected OAR dose for the remaining fractions in which they put constraints on the fraction size so that all fractions meet the lower and upper bounds, respectively. Chen et al. (2008) explored an adaptive fractionation scheme with biological optimization. There is another paper presented by Kim et al. (2012), in which a quantitative measure of the efficacy of dynamic treatment strategies is maximized. Dynamic biologically conformal radiation therapy (DBCRT) that is introduced in their paper, is used to exploit the mathematical modeling capabilities, and to achieve the best possible health outcome for each individual patient over several treatment sessions. Unkelbach et al. (2014) introduced a simple biological model that takes the trade off between tumor shrinkage and tumor cell repopulation into account. They reduce normal tissue dose by optimizing the time gaps and amount of dose which is delivered to the target in each treatment stage. ART can also be viewed as a problem of sequential decision making under uncertainty and as such, several studies have considered using dynamic

programming techniques. Ramakrishnan et al. (2012) establish a benchmark by using dynamic programming algorithm to solve the problem exactly. They have found out that the amount of decrease in dose to the OAR can vary significantly depending on the amount of motion in the anatomy, the number of fractions and the range of fraction sizes allowed. Saka et al. (2011) highlight the importance of adaptive intensity modulated radiation therapy. They present a promising iterative optimization approach that re-optimizes and updates the treatment plan periodically by incorporating the latest tumor geometry information. Kardar (2014) present a robust adaptive optimization approach, combined with conditional value-at-risk (CVaR) representation of dose volume constraint, considers tumor shrinkage as an uncertain parameter. They showed that robust adaptive planning improve sparing of healthy tissue without compromising the target coverage. Kim et al. (2009) mathematically explores the benefits of such fractionation schemes. This is achieved by building a stylistic Markov decision process (MDP) model, which incorporates some key features of the problem through intuitive choices of state and action spaces, as well as transition probability and reward functions.

Recently, researchers have shown a lot of interest in developing sophisticated optimization methods used in this step of radiation therapy (For review see Shepard et al. (1999); Reemtsen and Alber (2009)). Once the beamlet intensities are optimized, they are divided into fractional doses. Fractionation gives time to surrounding healthy tissue to recover and increases tumor control probability Thames and Hendry (1987).

Unlike the FMO problem, the fractionation problem has not been well studied in the literature, despite the evidence that the fractionation scheme bears significant impact on clinical outcomes (Bourhis et al. (2006); Ferreira et al. (2010); Ho et al. (2009); Hoffmann et al. (2008)). Although there have been numerous studies on the importance of the fractionation scheme, no consensus nor standardization exists with regards to how a fractionation scheme should be structured Ho et al. (2009) , and most previous studies focused on the number of fractions rather than mathematically optimizing the dose per fraction.

Chapter 3

A feasibility study of a risk-based stochastic optimization approach for radiation treatment planning under setup uncertainty

3.1 Introduction

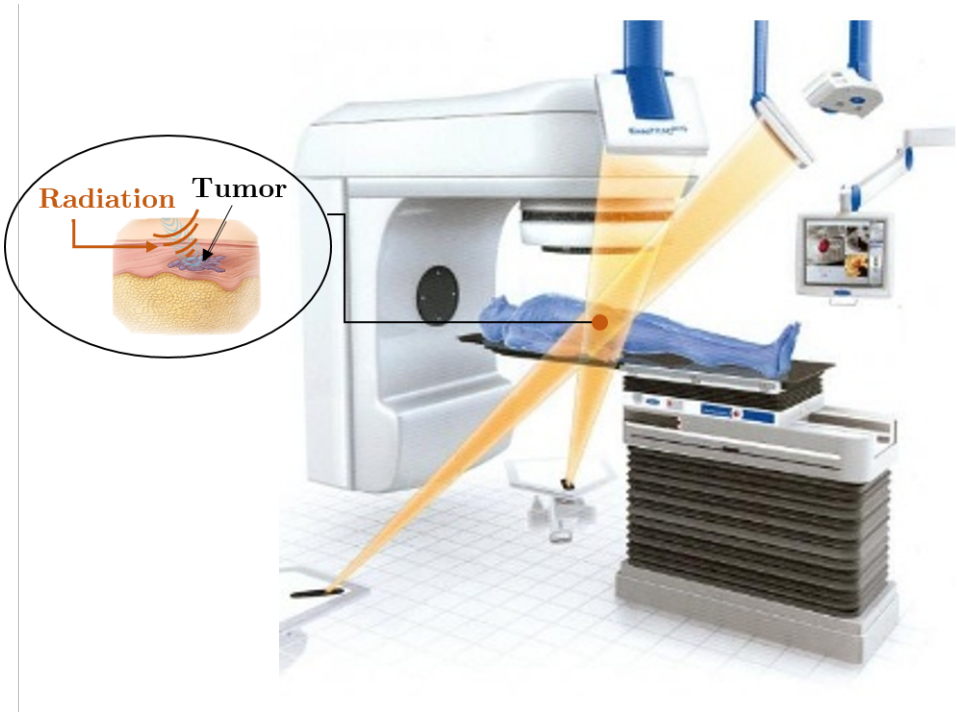

Figure 3.1: Illustration of a radiation therapy treatment planning.

According to the American Cancer Society, there were around 17.0 million new cancer cases diagnosed in 2019, and radiation therapy is used in more than half of the cases, some in conjunction with chemotherapy or surgery (AmericanCancerSociety (2019)). Radiation

therapy delivers radioactive particles to the tumor region to damage the DNA of the cells (see Figure 3.1). It is often unavoidable that the radiation can also harm healthy cells which may lead to radiation-induced side-effects (complications). The goal of radiation treatment planning is to shrink tumors (Erridge et al. (2003); Knap et al. (2010)) and kill cancer cells, while minimizing negative effects on healthy organs. This can be achieved by optimally choosing the amount of radiation to be delivered to the cancerous region. Two common radiation delivery modalities are photon-based intensity modulated radiation therapy (IMRT) (Lim and Cao (2012)), and proton-based intensity-modulated proton therapy (Cao et al. (2017); Bai et al. (2018)). Both methods decompose one open beam into many "beamlets" for each angle. The intensity of each beamlet can be modulated to achieve the optimal treatment effect; hence, clinical practitioners must determine how much radiation to deliver through each beamlet (i.e., beamlet intensity or weight) so that the target volume receives the prescription dose while healthy tissues receive a minimal or no dose. This is commonly known as a fluence map optimization (FMO) problem. Over the past few years, several mathematical models have been developed for the FMO problem (Romeijn et al. (2003); Zaghian et al. (2014); Cao et al. (2017)). However, in the presence of uncertainties in radiation therapy, solving the FMO problem is computationally challenging because it often involves millions of continuous and discrete variables.

Various uncertainties occur in treatment planning, such as in patient positioning, organ motion, breathing motion, dose calculation, beam energy, and others. Among these uncertainties, patient setup error is one of the most critical factors that can result in unpredictable treatment outcomes. Radiation therapy is often administered daily over a period of several weeks. For each treatment session, the patient needs to be set up on the treatment couch in the exact same position for each treatment. Due to the repeated positioning of patients, the actual and planned position of the patient with respect to the treatment can differ between each visit. As a consequence of patient setup error, the radiation dose received by each voxel can be different from the planned dose. Many existing studies highlight the importance of robustness in radiation treatment planning (Baum et al. (2006);

Unkelbach and Oelfke (2004); Bortfeld et al. (2008); Chan et al. (2006); Chu et al. (2005); Olafsson and Wright (2006); Pflugfelder et al. (2008); Liu et al. (2012b); Chan and Mišić (2013); Fredriksson et al. (2011)) and uncertainties are addressed using different models and assumptions (Shepard et al. (1999); Reemtsen and Alber (2009)).

As an extension of the deterministic (or nominal) optimization method, robust optimization (RO) is commonly used for incorporating the uncertainties in treatment planning optimization problems. An RO approach constructs a single solution that is feasible for all possible realizations of the parameter within an assumed uncertainty set. Chan et al. (2006) proposed a robust formulation of the treatment planning optimization problem using probability density functions of the uncertainty in breathing motion. Other studies have included scenario-based worst-case RO approaches (Pflugfelder et al. (2008); Liu et al. (2012b); Fredriksson et al. (2011)).

However, a drawback of RO is in the selection of the uncertainty set that contains all possible realizations of the unknown parameter in the optimization model. Because it is difficult to estimate the uncertainty set, the treatment plans are often developed under the worst-case scenario (Pflugfelder et al. (2008); Chan and Mišić (2013); Fredriksson et al. (2011)). As an immediate consequence, the treatment plans can be severely conservative for the tumor region, which leads to overdose on the surrounding healthy tissues (Chen et al. (2012); Casiraghi et al. (2013); Fredriksson and Bokrantz (2014)).

In an attempt to overcome the limitations of RO and to potentially improve sparing of healthy tissues, Zaghian et al. (2018) proposed a stochastic programming approach, specifically, chance-constrained programming (CCP). A key feature of CCP is to give treatment planners control of the probability that the constraints can hold under uncertainties. Hence, with the CCP approach a user can specify a level of confidence $(1-\alpha) \in [0,1]$ for violating the constraints, where higher confidence levels result in greater avoidance of constraint violations. As a result, treatment planners can bring their own experience in to the treatment planning and have better control of tumor coverage and radiation damage to healthy tissues. A similar approach has been reported by An et al. (2017) to develop an intensity-modulated

proton therapy plan using conditional-value-at-risk chance constraints. The minor drawback was that their comparison was based on the planning treatment volume-based method whereas RO is proposed to be a better approach in handling the uncertainties (Liu et al. (2012b)).

In CCP, an adjustable safety parameter is introduced for each of the constraints to certify the level of satisfaction on the probabilistic constraints with high confidence. These confidence levels represent prescribed safety tolerances or violation probabilities, which can provide additional information for decision makers in treatment planning. As a result, a treatment plan can be developed on the basis of the decision maker's risk preference for constraint violation while optimizing the treatment goal. In practice, the treatment goal is to spare the OARs (organs-at-risk) while delivering the prescribed dose to the tumor.

Most existing radiation treatment planning optimization models in RO do not allow constraint violation under uncertainty. But, the CCP approach allows the decision maker to adjust the level of conservatism of the robust solutions by specifying the level of constraint violations when the probability is derived with respect to sparing health organs. Therefore, the goal of the present study is to provide flexible treatment plans in terms of OAR sparing while satisfying the clinical target dose requirements. The presented model controls the frequency of constraint violations and provides optimized treatment plans along with user-defined confidence levels with the following objectives:

- Demonstrate the effectiveness of the CCP approach in creating treatment plans that are flexible to the dose requirements of the clinician-approved trade-offs among different organs (target and OARs).
- Provide a feasibility study of the clinical implementation of the CCP approach in radiation treatment planning under uncertainty.

We performed the experiments with five clinical cases from patients who received radiation treatment for cancer to verify the impact of using the confidence-based FMO model on the optimized plan quality in terms of healthy tissue sparing.

The rest of this paper is organized as follows. In Materials and Methods, we briefly describe our FMO model in terms of the set of fixed parameters and then explain how chance constraints for treatment planning can be constructed. Under distributional assumptions of uncertainty, the deterministic equivalence of the CCP framework is also elaborated. The results for two patients with prostate cancer, one with pancreatic cancer, one pediatric patient, and one patient with lung cancer are shown and discussed in the Results. We conclude the paper with the Discussion.

3.2 Materials and Methods

We begin by briefly reviewing the FMO problem in radiation therapy and discussing the deterministic constraints in our optimization problem. Next, we incorporate parameter uncertainty into optimization by formulating a probabilistic version of the optimization problem. The CCP approach is then described to solve the stochastic model.

3.2.1 Nominal formulation

The core task of FMO in radiation treatment planning is to find the optimal value of the beamlet intensity for all beamlets. Therefore, we define decision variables representing the intensity of beamlet $j \in \mathcal{J}$ as w_j, and the decision vector of all beamlet intensities as $\mathbf{w}$. The dose distribution is expressed as $\mathbf{D}_i(\mathbf{w})$ as a linear function of the variable w_j (Shepard et al. (1999); Lim (2008)) as

$$\mathbf{D}_i(\mathbf{w}) = \sum_{j \in \mathcal{J}} d_{ij} w_j = \mathbf{d}_i^T \mathbf{w}, \ \forall i \in \{\mathcal{T} \cup \mathcal{O}\},$$

where d_{ij} denotes the dose per intensity contribution to voxel i from beamlet j. The input parameters for radiation treatment planning models proposed in the present study are defined in Table 4.1. A cold spot is defined as a fraction of voxels in a structure receiving less than the desired prescribed radiation dose. A hot spot is defined as a fraction of voxels in a structure receiving more than the prescribed dose.

Table 3.1: Input parameters for radiation treatment planning models

Symbol	Definition
$\mathcal{T}$	A set of voxels in the clinical target volume
$\mathcal{O}$	A set of voxels in an organ-at-risk
$\mathcal{J}$	A set of all beamlets
λ_T^+	Penalty coefficient for hot spots on the target
λ_T^-	Penalty coefficient for cold spots on the target
λ_O	Penalty coefficient for hot spots on an organ-at-risk
α_T^+	Risk level for having cold spots on the target
α_T^-	Risk level for having hot spots on the target
α_O^+	Risk level for having hot spots on an organ-at-risk

The deterministic FMO model in radiation therapy (Lim et al. (2008)) can be represented as follows in constraints (2)-(6):

$$\min \quad -\lambda_T^- \theta_L + \lambda_T^+ \theta_U + \lambda_O^+ \varphi \tag{3.2.1}$$

s.t.

$$\mathbf{D}_i(\mathbf{w}) \geq \theta_L, \qquad \forall i \in \mathcal{T}, \tag{3.2.2}$$

$$\mathbf{D}_i(\mathbf{w}) \leq \theta_U, \qquad \forall i \in \mathcal{T}, \tag{3.2.3}$$

$$\mathbf{D}_i(\mathbf{w}) \leq \varphi, \qquad \forall i \in \mathcal{O}, \tag{3.2.4}$$

$$\underline{\theta}_L \leq \theta_L \leq \bar{\theta}_L, \ \underline{\theta}_U \leq \theta_U \leq \bar{\theta}_U, \ \textit{and} \tag{3.2.5}$$

$$\varphi, \mathbf{w} \geq \mathbf{0}, \tag{3.2.6}$$

in which various dose constraints are involved in the design of treatment plans. Here, θ_L (Gy) and θ_U (Gy) represent cold spot and hot spot control variables on the target, respectively, and φ (Gy) is the hot spot control variable on an organ-at-risk. Note that a cold spot is a portion of tissue that receives less than the desired radiation dose, and a hot spot is a portion of tissue that receives a dose higher than the desired dose (Lim et al. (2008)). Constraint (3.2.2) ensures a high likelihood of eradicating the tumor, whereas constraint (4.2.1) ensures a high likelihood that the functionality of critical structures is retained. Constraint (3.2.3) is to avoid overdose on the target. In this optimization model, our goal is

to find the beamlet intensities in such a way that deviations of the variables, θ_L, θ_U, and φ, can be minimized from their target values, i.e., $\min \theta_U - \theta_L$, $\min \varphi$. Parameters λ_T^+, λ_T^-, and λ_O^+ are for assigning different priority factors in the objective to penalize overdosing of the target, underdosing of the target, and overdosing of the OAR over the limit φ, respectively. In Constraint (3.2.5), $\underline{\theta}$ and $\bar{\theta}$ represent lower and upper bounds for variables θ_L and θ_U, respectively.

3.2.2 CCP formulation

Under setup uncertainty, the random dose delivered to voxel i is denoted by

$$\tilde{\mathbf{D}}_i(\mathbf{w}) = \tilde{\mathbf{d}}_i' \mathbf{w},$$

where $\tilde{\mathbf{d}}_i$ denotes the random dose contributed by all beamlets per unit weight and is received by voxel i. A classic approach to the solution of constraints (3.2.2)-(4.2.1) under random uncertainty is to enforce the constraints in probability by introducing a risk level α, which is called a chance-constrained linear program.

To construct chance constraints for radiation treatment planning optimization under patient setup uncertainty, we introduce α_i as a desired safety factor of each structure i, and we rewrite the constraints in probability as follows:

$$P\{\tilde{\mathbf{D}}_T(\mathbf{w}) \geq \theta_L\} \geq 1 - \alpha_T^-, \tag{3.2.7}$$

$$P\{\tilde{\mathbf{D}}_T(\mathbf{w}) \leq \theta_U\} \geq 1 - \alpha_T^+, \ \textit{and} \tag{3.2.8}$$

$$P\{\tilde{\mathbf{D}}_O(\mathbf{w}) \leq \varphi\} \geq 1 - \alpha_O^+. \tag{3.2.9}$$

The dose calculated using any feasible solution of constraints (4.2.2)-(4.2.5) will be between the lower and upper boundary control parameters prescribed for each structure, with a specified confidence level for each voxel. Typically, the same dose is prescribed to all voxels in the target, so we assume equal confidence levels for all voxels in the same structure for each set of constraints. In other words, the resulting dose of any feasible solution of

constraints (4.2.2)-(4.2.5) is greater than θ_L with confidence level $(1-\alpha_T^-)\%$ and less than θ_U with confidence level $(1-\alpha_T^+)\%$ for the target voxel, and it is also less than φ with confidence level $(1-\alpha_O^+)\%$ for each OAR voxel, in the face of uncertainty.

Unfortunately, there is often a conflict between the lower and upper bound constraints, which will lead to an infeasible solution in practice. To avoid infeasibility of the optimization problem, we may allow some or all of these constraints to be violated up to a certain level. We can easily penalize the violations of the lower and upper bounds on the amount of dose received by each voxel in the objective function. In this regard, assuming that confidence levels $(1-\alpha_i)$ are given, we developed model (4.2.3), in which θ_L, θ_U, and φ are considered as decision variables

$$
\begin{aligned}
&\min \quad -\lambda_T^-\,\theta_L + \lambda_T^+\,\theta_U + \lambda_O^+\,\varphi && && (3.2.10)\\
&s.t. && &&\\
&P\{\tilde{\mathbf{D}}_T(\mathbf{w}) \geq \theta_L\} \geq 1-\alpha_T^-, && \forall i \in \mathcal{T}, &\\
&P\{\tilde{\mathbf{D}}_T(\mathbf{w}) \leq \theta_U\} \geq 1-\alpha_T^+, && \forall i \in \mathcal{T}, &\\
&P\{\tilde{\mathbf{D}}_O(\mathbf{w}) \leq \varphi\} \geq 1-\alpha_O^+, && \forall i \in \mathcal{OAR}, &\\
&Constraints\ (3.2.5)-(4.2.4). &&&
\end{aligned}
$$

Next, we solve the CCP model (4.2.3) by treating uncertain parameters as continuous random variables with a known probability density function.

3.2.3 CCP models under distributional assumptions

One of the computational challenges in solving a CCP model comes from the fact that the chance constraints may not be convex (Nemirovski and Shapiro (2006)). However, a CCP model can be made convex in a few special cases. For example, if the uncertainty parameter $(\tilde{\mathbf{d}}_i)$ has a log-concave probability density, the corresponding chance constraints will be convex (Zaghian et al. (2018)).

In this section, we consider two special probability distribution functions of random parameter $\tilde{\mathbf{d}}_i$, normal and uniform distribution. We focus on the normal distribution because it is widely used and has attractive analytical properties that facilitate further analysis (Chan et al. (2009)). As follows from the central limit theorem (Bertsekas and Tsitsiklis (2002)), a large set of independent identically distributed random variables approach a normal distribution regardless of the underlying probability distribution. So, the normality assumption will also help extend the analysis to multiple sources of uncertainty. Thus, we constructed the deterministic equivalent of a CCP framework on the basis of the normality assumption of a random parameter (Zaghian et al. (2018)) (see Appendix A) as well as a uniform distribution (see Appendix B). Note that we used normal and uniform probability distributions that are widely used in practice as an example to describe the setup uncertainty (Chan et al. (2009); Engelsman et al. (2005)).

3.3 Clinical cases and planning details

We evaluated the relative performance of the CCP models on the basis of treatment plan information obtained from five cancer patients (two patients with prostate cancer, one with pancreatic cancer, one pediatric patient, and one patient with lung cancer) who received radiation therapy at The University of Texas MD Anderson Cancer Center.

By assuming that the setup uncertainty ranged between -5 mm and $+5$ mm (Manning et al. (2001); Wong et al. (2005)), we generated four representative scenarios in addition to the nominal scenario (Liu et al. (2012b); Casiraghi et al. (2013)) for the patient setup uncertainty. The first- and second-order moments of the uncertain dose contributions were calculated for each case under normal and uniform distributional assumptions. Under these assumptions, the respective minimum and maximum doses to the target were 95% ($\underline{\theta}_L = 0.95$) and 105% ($\bar{\theta}_U = 1.05$) of the prescribed dose in all plans. The values of weight factors λ_T^-, λ_T^+, and λ_O^+ are often selected on the basis of the planner's preference. Table 4.4 lists the planning parameters for the five clinical cases analyzed in the present study. For each case, the number of beams, number of voxels within each volume, and the corresponding

dose-volume requirements were provided.

Table 3.2: Anatomical structures and dose requirements for five clinical cases used in our analysis

Cancer Case [1]	Volume	NO. of Beams	Constraints
Prostate I (IMRT)	Target: 1000	6	Prescription: 76 Gy Receiving $\geq$ 96% of θ_L Receiving $\leq$ 105% of θ_U
	OAR (rectum): 5848 OAR (bladder): 10603		
Prostate II (IMRT)	Target: 6375	6	Prescription: 76 Gy Receiving $\geq$ 95% of θ_L Receiving $\leq$ 105% of θ_U
	OAR (rectum): 5719 OAR (bladder): 7850		
Pancreas (IMRT)	Target: 1244	12	Prescription: 54 Gy Receiving $\geq$ 99% of θ_L Receiving $\leq$ 101% of θ_U
	OAR (liver): 50391 OAR (spinal cord): 489 OAR (left kidney): 9116 OAR (right kidney): 5920		Max dose: 45 Gy
Lung (IMPT)	Target: 5716	3	Prescription: 70 Gy Receiving $\geq$ 95% of θ_L Receiving $\leq$ 107% of θ_U
	OAR (heart): 8287 OAR (spinal cord): 481 OAR (esophagus): 389		
Pediatric (IMPT)	Target: 9307	3	Prescription: 64 Gy Receiving $\geq$ 95% of θ_L Receiving $\leq$ 105% of θ_U
	OAR (brainstem): 1118 OAR (optic chiasm): 17		

Different treatment plans were generated for each of the clinical cases: one with the deterministic approach, one with the robust worst-case optimization and the others using the CCP treatment planning models. The models were solved using a commercial linear optimization solver, CPLEX (IBM Analytics (2019)). Note that the beam angles were optimized (Lim et al. (2014)) and confirmed by clinicians in advance.

A family of dose-volume histograms (DVHs) for the comparison of different models were applied. We used the DVH family band width method (Trofimov et al. (2012)) that displayed all DVHs of the five dose distributions corresponding to the four scenarios of

setup uncertainty in addition to the nominal scenario. DVH indices comparing tumor dose coverage, homogeneity, and OAR sparing are also discussed in detail in the next section.

3.4 Results

3.4.1 Plan quality and robustness

Plans optimized by the chance-constrained and nominal (or deterministic) optimization models for one of the patients with prostate cancer are compared in Figures 3.2a-3.2f. The DVHs corresponding to the nominal dose distribution (i.e., no uncertainty) are displayed along with the DVH bands for deterministic and chance-constrained models. The solid line indicates DVHs for the nominal dose distribution and the shaded area shows the DVH family band plotted on the basis of various shifted setup scenarios. For all plans, the nominal DVHs (solid lines) were almost equally good, which shows that the clinical constraints were satisfied. However, Figure 3.2a shows that the band of the DVH along the target is wider for the deterministic model than for the CCP models (DVHs in Figures 3.2c and 3.2e), which shows that the target coverage of the deterministic model was worse than that of the CCP models.

Moreover, as would be expected, the DVH bands on OARs that are illustrated on the right side of Figure 3.2 are reduced by the CCP approach under two different distributional assumptions. In fact, these figures explain how controlling the violation of the clinical constraints using CCP models resulted in improved OAR sparing compared with the deterministic model. Overall, this comparison demonstrates that by incorporating setup uncertainty information in the optimization, the sensitivity of the plans against errors can be reduced.

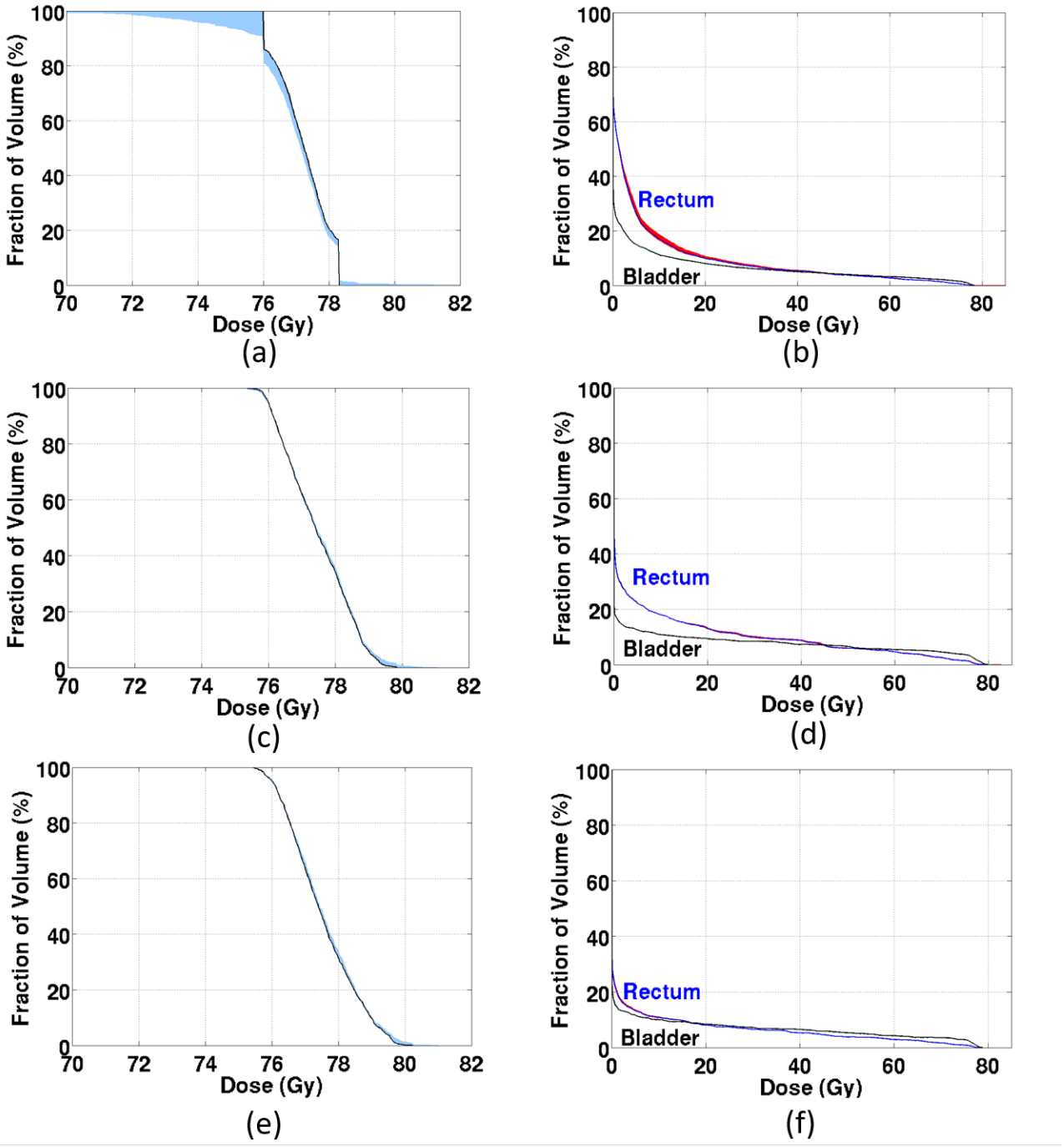

Figure 3.2: Dose-volume histogram bands for target and organs-at-risk dose distributions covering all setup uncertainties, resulting from (a, b) the deterministic approach, (c, d) chance-constrained programming under the normality assumption, and (e, f) chance-constrained programming under the uniformity assumption. (Zaghian et al. (2017)).

3.4.2 Robust optimization:

The plans were optimized to evaluate the robustness of treatment plans using CCP and RO under random setup errors, and corresponding DVHs for the target and OARs were analyzed for each of the setup scenarios.

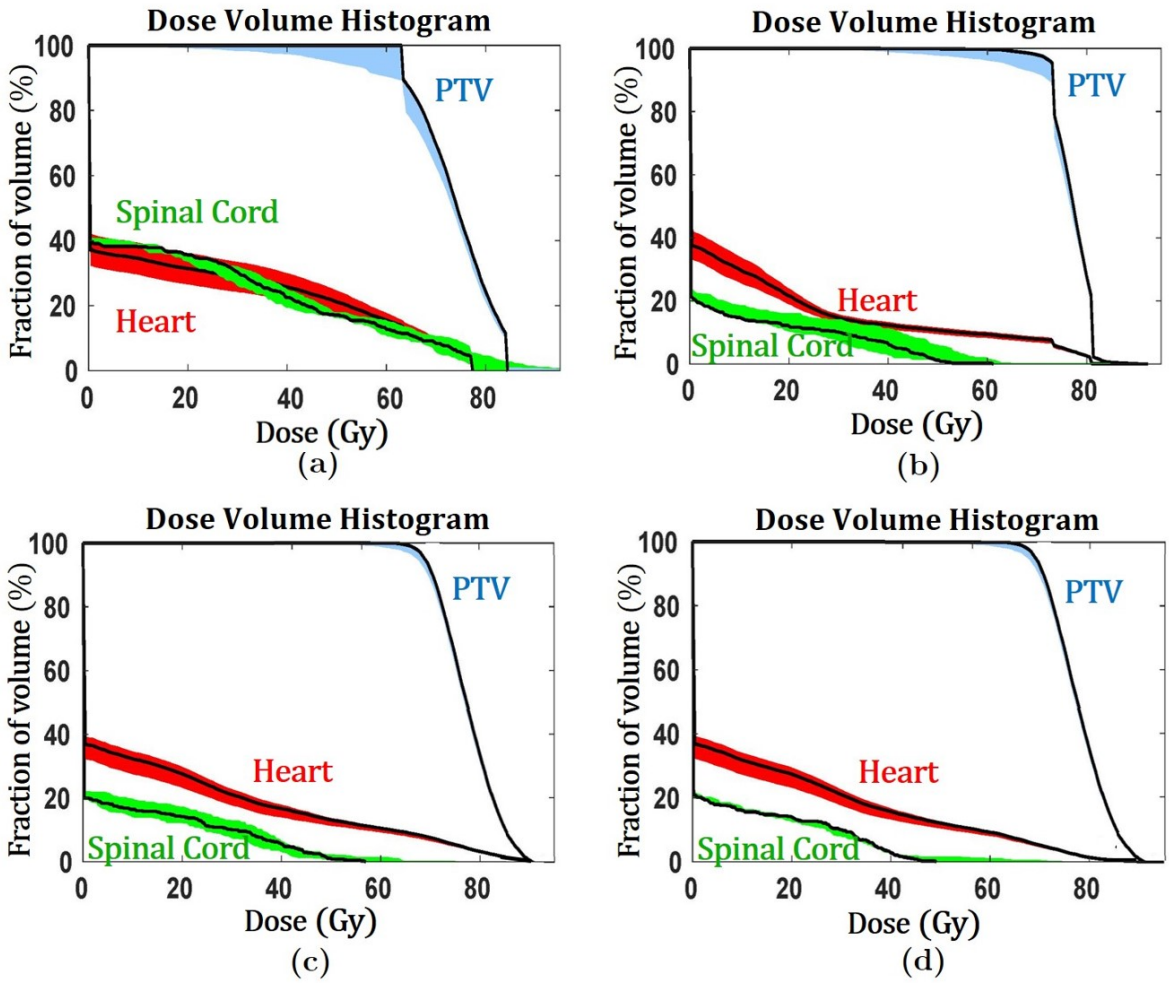

Figure 3.3: Lung cancer dose-volume histogram bands for planned target volume (PTV) and organs-at-risk dose distributions covering all setup uncertainties, resulting from (a) the deterministic approach, (b) robust optimization, (c) chance-constrained programming under the normality assumption, and (d) chance-constrained programming under the uniformity assumption.

Figure 3.3 shows the DVH family band for the lung cancer case, based on treatment plans developed using the deterministic approach, RO, and CCP under normal (CCP-N) and CCP under uniform probability distributions (CCP-U). Figures in Appendix C show

the results for the two prostate cancer cases, the pancreatic, and the pediatric cancer cases, respectively. The DVHs in Figure 3.3 show that all nominal plans (black line) met the clinical prescription criteria in both covering the tumor and sparing OARs, and the target was robustly covered for all plans, as indicated by the narrow DVH family band (shaded area) compared with the deterministic approach. Based on the experiments presented in the paper, the confidence-based CCP models outperformed the robustly optimized plan by improving the protection of critical organs under the nominal and setup scenarios. The shaded area around the nominal DVHs of the spinal cord in the robust plan (Figure 3.3b) is wider than that in the CCP plans (Figure 3.3c and 3.3d). As shown in Figures 3.3c and 3.3d, the maximum doses to the normal cells around the target from the CCP plans met the tolerances without sacrificing the robustness of the plan to setup uncertainty, which demonstrates the flexibility of the CCP approach compared to the RO method in creating clinically reasonable plans.

To further illustrate the performance of the biologically-based CCP models, we explored the effect of CCP models on sparing of normal tissues around the tumor for the five clinical cases. Table 3.3 reports radiation dose statistics associated with OAR DVHs for each case based on the plans optimized by the CCP models and worst-case RO approach. The values in the nominal scenario as well as the average and worst-case values considering all setup scenarios are presented. The table shows that the proposed CCP models delivered smaller radiation doses to the normal organs than the RO approach for all cases for each of the three measures: nominal, worst-case, and average dose.

Table 3.3 shows the radiation dose statistics on healthy organs for all cancer cases as explained by An et al. (2017): D_1 (Gy), the amount of dose received by more than 1% of the organ. The CCP approach reduced the nominal dose of D_1 for the rectum in Prostate case I as compared to RO: 75.64 Gy for CCP-N and 72.39 Gy (vs. 76.46) in case of CCP-U. The average dose of D_1 (Gy) on the bladder was also reduced when the CCP approach was used on each of the nominal, worst-case, and average scenario. We observed similar results for Prostate case II shown in Table 3.3. For the Pancreas case, the maximum nominal

doses of D_1 on healthy organs were 35.42 Gy and 28.46 Gy for liver and spinal cord using the RO model, respectively. Those values were reduced to 22.48 Gy and 28.05 Gy using CCP-N, and to 23.51 Gy and 28.10 Gy using the CCP-U model for the liver and spinal cord, respectively. Similar results were observed by comparing the results of maximum dose (D_1 (Gy)) on the liver and spinal cord for worst-case and average case scenarios. For this case, the maximum radiation dose on the spinal cord was slightly lower for CCP plans, whereas there were significant improvements in protecting the liver by reducing the amount by at least 12.94 Gy when compared to the RO plan. For a better illustration of the dose volume histogram plotted for the liver in the Pancreas case, the percentage of the liver volume receiving more than 30 Gy, $V_{30}\%$, was compared for all the plans. Both CCP-N and CCP-U reduced $V_{30}\%$ by 2.18% and 2.03%, respectively, over the robust plan. It can be seen that the CCP plans delivered the least amount of dose to the healthy tissue, especially, in the liver. For the case of the lung cancer, the CCP result in a slightly higher dose of D_1 (Gy) (maximum dose) for the heart. However, this was a necessary compromise to provide a plan with better sparing of the spinal cord, which can be severely damaged if it is over-dosed.

Both CCP under the normality assumption and CCP under the uniformity assumption appeared to provide better control than the RO approach in terms of sparing of normal tissues, which can be achieved by controlling the tolerance levels assigned to each structure's dose requirements and studying the relationship between dose requirements and plan conservatism. In a CCP setting, the confidence level of satisfying the target dose requirement can be adjusted on the basis of the physician's preference to avoid overly conservative treatment plans. As a result, with the CCP method the OAR protection can be improved, and this will prevent side effects due to radiation and lead to better quality of life for patients.

Table 3.3: Comparison of chance-constrained models (CCP-N and CCP-U with $\alpha = 95\%$) and the worst-case robust optimization (RO) method on healthy organ sparing. The values are derived from the dose-volume histograms. [2]

	Prostate I		Prostate II		Pancreas		
	Rectum	Bladder	Rectum	Bladder	Liver		Spinal Cord
CCP-N	D_1 (Gy)	D_1 (Gy)	D_1 (Gy)	D_1 (Gy)	V_{30}%	D_1 (Gy)	D_1 (Gy)
nominal	75.64	77.27	77.35	77.19	0.23	22.48	28.05
worst-case	75.93	77.27	77.36	77.31	0.35	23.20	28.24
average	75.74	77.22	77.33	77.22	0.26	22.76	28.12
CCP-U							
nominal	72.39	77.25	76.97	77.69	0.38	23.51	28.10
worst-case	72.88	77.29	77.06	77.72	0.46	24.34	29.33
average	72.51	77.24	76.98	77.69	0.39	23.71	28.36
RO							
nominal	76.46	77.27	77.39	78.24	2.41	35.42	28.46
worst-case	77.45	77.38	77.76	78.24	2.73	36.60	32.00
average	76.71	77.28	77.46	78.24	2.50	35.88	29.84

	Lung			Pediatric	
	Heart	Spinal Cord		Brainstem	Optic Chiasm
CCP-N	D_1 (Gy)	D_1 (Gy)	V_{40}%	D_1 (Gy)	D_1 (Gy)
nominal	85.03	49.88	5.40	60.92	14.38
worst-case	85.03	61.88	6.44	61.24	14.68
average	84.50	51.18	5.02	61.07	14.44
CCP-U					
nominal	81.23	44.52	2.70	60.92	14.38
worst-case	82.22	59.52	2.91	61.24	14.64
average	81.23	47.63	2.74	60.91	14.44
RO					
nominal	81.05	50.21	6.02	61.24	14.38
worst-case	81.15	61.79	11.23	61.24	14.70
average	81.10	53.26	6.44	61.23	14.50

Next, we evaluated the robustness of the CCP plans in terms of tumor dose coverage. Table 3.4 shows the tumor DVH indices achieved by our confidence-based CCP models and worst-case RO approach. For each clinical case, the first row shows the dose homogeneity index (HI) that is often used as an objective measure of treatment plan quality (Yoon et al. (2007)). HI is calculated by

$$HI = \frac{D_{95}}{D_5},\ 0 \leq HI \leq 1,$$

where D_5 and D_{95} are the dose coverage at 5% and 95% volume of the target: the larger

[2] D_1 denotes the amount of dose received by more than 1% percent of the organ, and V_{30}% denotes the percentage of the organ volume receiving dose of more than 30 Gy.

(closer to 1) the value of HI, the better the dose homogeneity.

To quantify the plan robustness under uncertainty, we listed the width of the DVH band at D_5 and D_{95} in the second and third rows. The nominal HI values for all clinical cases except the patient with lung cancer were equally high, and the DVH band-widths from the CCP models were better than those from the RO model (as shown in Figure 3.3 and figures in Appendix C). For the patient with lung cancer, the nominal HI values were slightly lower for the CCP plans, whereas the indices of DVH band width from the CCP models outperformed those from the RO plan. This means that the target coverage of the plans generated by the CCP models under two different distributional assumptions was more robust when compared with the RO plan for shifted setup uncertainty.

Table 3.4: Homogeneity index for clinical cases examined in our analysis.

Case[3]		CCP-N	CCP-U	RO
Prostate cancer I	HI (nominal)	0.96	0.95	0.96
	D_5 DVH band	0.05	0.05	0.05
	D_{95} DVH band	0.01	0.05	0.01
Prostate cancer II	HI (nominal)	0.96	0.96	0.96
	D_5 DVH band	0.03	0.05	0.05
	D_{95} DVH band	0.01	0.02	0.02
Pancreatic cancer	HI (nominal)	0.97	0.97	0.97
	D_5 DVH band	0.10	0.15	0.26
	D_{95} DVH band	0.15	0.20	0.35
Lung cancer	HI (nominal)	0.88	0.88	0.90
	D_5 DVH band	0.15	0.13	0.15
	D_{95} DVH band	3.00	3.54	9.19
Pediatric cancer	HI (nominal)	0.86	0.86	0.86
	D_5 DVH band	0.12	0.15	0.16
	D_{95} DVH band	0.05	0.03	0.04

3.4.3 Sensitivity Analysis

This section discusses the sensitivity of CCP models to the choice of a distribution. We designed an experiment to test the performance of the proposed model when the assumed dose distribution for treatment planning was different from the true distribution, which is

[3]HI:homogeneity index, DVH: dose-volume histogram

not known in advance. For example, treatment plans may have been developed based on the assumption that the set up error follows a normal distribution (CCP-N) when, in fact, the true probability distribution was Uniform. The parameter values resulting from those experiments on Prostate case I are shown in Table 3.5.

Table 3.5: Cold- and hot-spot control parameters on target (θ_L and θ_U) and hot-spot control parameter on OARs (φ) optimized for Prostate I.

Assumption	Approach	θ_L (Gy)	θ_U (Gy)	φ (Gy)
Normally distributed	CCP-N	76.00	77.52	76.00
	CCP-U	72.20	81.32	79.04
Uniformly distributed	CCP-N	76.00	82.08	78.28
	CCP-U	74.48	76.00	74.48

First, we compare the treatment plans under the two distributional assumptions in terms of the *uniformity* of the planned dose distribution on the target (Lim et al. (2007)). In radiation therapy, the uniformity is the difference between the maximum dose and the minimum dose received on the target, which is measured by $\theta_U - \theta_L$. Ideally, we wish to achieve a treatment plan whose gap is close to zero. In Table 3.5, when the random data was assumed to follow a normal probability distribution, the uniformity value of the CCP-N based treatment plan (i.e., $1.52\ Gy = 77.52 - 76.00$) is smaller than the CCP-U based plan ($9.12\ Gy = 81.32 - 72.20$). However, when the random data was assumed to follow a uniform probability distribution, we observed the opposite result as the uniformity value of CCP-N (6.08) is larger than that of CCP-U (1.52).

Next, we compared the performance of the proposed model (CCP-N/CCP-U) with the maximum threshold on OARs obtained based on the respective distributional assumption. As it is shown from the last column of Table 3.5, the plan by CCP-N resulted in a consistently lower upper threshold limit on OARs ($\varphi = 76.00$ Gy) than did CCP-U ($\varphi = 79.04$ Gy) under the normal probability distribution assumption. A similar observation was made when the random parameter was assumed to follow a uniform distribution (from the last two rows in Table 3.5).

3.5 Discussion

In the present work, we explored the CCP optimization framework using five clinical cases. Treatment plans were optimized for robustness, quality, and homogeneity under patient setup errors. In practice, the treatment goal is to spare the OARs while delivering the prescribed dose to the tumor. However, these conflicting objectives are often difficult to achieve. In a worst-case scenario, critical organs will necessarily receive more doses when a plan robustly covers the target. Conversely, the target will not receive a sufficient radiation dose when a plan robustly spares a nearby critical structure. Thus, the level of the plan conservatism needs to be determined under uncertainty, and this can be decided by adjusting the tolerance levels introduced in the CCP approach. Our results showed that the confidence-based CCP model was a user-centric optimization tool that can help obtain a good balance between the plan quality and robustness. Our analysis covered five clinical cases under two probability assumptions of random setup uncertainty using the same clinical limitations and directions. Our numerical results for the clinical cases showed that the CCP approach was capable of controlling the robustness of the model while attaining high-quality solutions. We believe that the CCP plans demonstrated here will be applicable to many different types of clinical cases under different probability assumptions of uncertainty.

Chapter 4

Distributionally Robust Chance-Constrained Programming in Radiation Therapy Treatment Planning

4.1 Introduction

Radiation treatment (RT) planning is the process of designing an appropriate treatment in such a way that the tumor region receives the prescribed radiation dose, while the critical structures receive as small dose as possible to minimize the risk of side effects to healthy tissues. RT delivery machines are capable of controlling the intensities of the beamlets (i.e., many small rays of radiation beams) to achieve the RT goal, and radiation is delivered to patients from multiple angles to achieve a conformal and uniform dose distribution to the target volume.

RT affects both the tumor volumes and the healthy tissues around the tumor. Exposure to an excessive amount of radiation can cause permanent damage in healthy cells. Therefore, a fractionation scheme is often used in which about 2 Gy of radiation is delivered to the patient each day to allow the healthy tissues to recover between treatments. Hence, treatment can take several weeks to complete, with the patient having to visit the clinic five times a week.

There are several known uncertainties in RT planning that should be carefully considered to avoid serious degradation in treatment quality: patient setup uncertainty (Chu et al. (2005)), uncertain dose deposition by the beam because of the type of tissue (Unkelbach et al. (2007)), and patient breathing motion (Bortfeld et al. (2008)). The effect of these

uncertainties on the delivery of the planned dose distribution should be mitigated appropriately to ensure that the correct dose is deposited in the tumor and the patients are treated safely.

To address parameter uncertainty, various robust planning models have been developed in RT planning. Worst-case robust optimization is commonly used in the medical community to provide tumor coverage under uncertainty while minimizing exposure to healthy organs (Pflugfelder et al. (2008); Fredriksson et al. (2011); Liu et al. (2012b)). Treatment plans developed using such approaches primarily focus on the worst-case scenario for the tumor volume, which may result in unnecessarily conservative plans that cover the tumor region well at the risk of exposing nearby healthy organs to high doses of radiation. Hence, physicians may prefer a treatment planning model that strikes a balance between a high probability of tumor control and a low risk of side effects.

Over-conservatism in the model can be avoided using a stochastic optimization technique such as chance-constrained programming (CCP) (Calafiore and El Ghaoui (2006)). In CCP, chance constraints are used to relax the constraints in a deterministic optimization model and replace them with probabilistic ones. Each chance constraint can be associated with the level of confidence for satisfying the underlying deterministic constraint. The confidence level can be helpful to treatment planners who are trying to balance a set of conflicting objectives, i.e., delivering a therapeutic dose to the tumor while limiting the dose to the organs-at-risk (OARs) (Zaghian et al. (2018); An et al. (2017)).

The means by which CCP deals with a parameter uncertainty depends on the probability distribution of the uncertain parameter, which is typically not known in advance. However, there may be limited information about a possible family of distributions, on the basis of prior observations. In these situations, distributionally robust CCP (DRCCP) is an appropriate method of addressing uncertainties in a chance-constrained framework (Calafiore and El Ghaoui (2006); Zymler et al. (2013); Chen et al. (2010)).

A few studies have used DRCCP to account for uncertainties in the parameters of optimization models, irrespective of the probability distribution of the data. When only partial

information about the probability distribution is known, convex conditions can be used that guarantee the satisfaction of the chance constraints for any possible distribution, with respect to the given information (Calafiore and El Ghaoui (2006)). Chen et al. (2010) considered a variety of uncertainty sets and showed that there was a relationship between the bounds on the conditional-value-at-risk measure and different approximations of individual chance-constrained problems in robust optimization. Accordingly, Zymler et al. (2013) developed models to approximate robust chance constraints, assuming that the first-order (FO) and second-order (SO) moments or the support of the random parameter is known. They approximated the distributionally robust chance constraints using worst-case conditional-value-at-risk constraints in a study that was motivated by another study by Chen et al. (2010).

The goal of our study was to account for the uncertainties in the treatment planning optimization process using a DRCCP approach in which the robustness of each clinical objective can be considered and optimized separately. For this, we developed a confidence-based robust optimization model to determine acceptable treatment plan quality, subject to the treatment dose constraints. We considered setup uncertainty within a family of distribution probabilities and incorporated it in the proposed model to find the highest possible tolerance level at which the clinical goals were satisfied for all possible setup errors. As many types of uncertainties can be considered in this way, the proposed framework may be further used to account for various uncertainty sources and treatment modalities.

We evaluated the proposed DRCCP approach under two assumptions of the uncertainty set: in the first class, we consider the common situation in which the coefficients of the linear program are known to have a finite mean and lie in independent intervals. A computationally tractable approximation is provided to enforce of the probability constraint, robustly with respect to the parameter distribution. In the second class, we assumed that the FO and SO moments (or the mean and the covariance) were known. Again, the probabilistic constraints were enforced over all possible distributions, compatible with given moments. For this class, the SO cone counterparts of the robust chance constraints were developed

while considering the linear function of the random dose variable. To improve the performance of the approximation models, we developed two novel quadratic approximations of the random dose distribution with a higher order of uncertainties.

All proposed optimization models include the probability of the meeting planning goals as a variable in the objective function to minimize the degree of clinical constraint violation. It can thereby reach the highest probability for which the goals can be fulfilled. The model simultaneously provides an optimized treatment plan and a corresponding confidence level and controls the level of plan conservatism against which the treatment plan is robust to the uncertainty.

To illustrate the general features of the proposed DRCCP approaches, we performed experimental studies in a small test case, followed by a prostate cancer case. We illustrated how well the DRCCP approaches fit the data under distributional uncertainty and compare in terms of their efficiency. In addition, the quality, robustness, and confidence of the plans generated using different models and under different assumptions are evaluated and analyzed for a real prostate cancer patient. The improved plan quality, as determined by Quadratic Majorant (QM) and SO dependence approximations, is also highlighted.

Our specific contributions in this paper are as follows:

- Assuming that our information about the uncertain dose is limited to the FO and SO moments or the interval and mean of the random parameter, we relax the distributional assumptions on the chance constraints and DRCCP approaches. Depending on the type of information we have on the random parameter, the robust chance constraints are transformed into the corresponding SO cone counterparts, and the confidence levels of the constraints are maximized.

- To make the treatment plans more homogeneous, we developed two quadratic approximations of the distributionally robust chance constraints under the assumption that the FO and SO moments of the random parameter are known. These quadratic models provide more precise deterministic approximations of the robust chance constraints.

- We propose a hybrid solution in which a solution of the DRCCP-SOCP is used as a starting point for other DRCCP approaches with quadratically approximated chance constraints.

In Section 4.2, we list the probabilistic constraints based on the parameters interpreted in Table 4.1. We then explain how chance constraints for treatment planning are constructed. In Section 4.3, we define DRCCP and then, propose four approaches. Experimental studies using a small test case and a clinical prostate case are presented in Section 4.4. Section 4.5 contains our conclusions.

4.2 Treatment planning chance constraints

Table 4.1: Notation

$\mathcal{T}$	Set of voxels in clinical target volume
$\mathcal{OAR}$	Set of voxels in organ-at-risk
$\mathcal{J}$	Set of all beamlets
θ_L	Cold spot control parameter on target
θ_U	Hot spot control parameter on target
φ	Hot spot control parameter on OAR
λ_T^+	Penalty coefficient for hot spots on target
λ_T^-	Penalty coefficient for cold spots on target
λ_{OAR}	Penalty coefficient for hot spots on OAR
α_T^+	Risk of hot spots on target
α_T^-	Risk of cold spots on target
α_{OAR}^+	Risk of hot spots on OARs
w_j	Intensity of beamlet j
d_{ij}	The dose contributed by the j^{th} beamlet per unit weight to voxel i

We considered decision variable $\mathbf{w}$ as the intensity of beamlets, and $\mathbf{D}_i(\mathbf{w})$ as the total dose in voxel $i \in \{\mathcal{T} \cup \mathcal{OAR}\}$, which is given by

$$\mathbf{D}_i(\mathbf{w}) = \mathbf{d}_i^{'}\mathbf{w} = \sum_{j \in \mathcal{J}} d_{ij} w_j,$$

where $\mathbf{d}_i$ represents the dose contribution from all beamlets to voxel i. Under uncertainties,

the random dose delivered to voxel i is denoted by

$$\tilde{\mathbf{D}}_i(\mathbf{w}) = \tilde{\mathbf{d}}_i^{'}\mathbf{w},$$

where $\tilde{\mathbf{d}}_i$ denotes the vector of random doses contributed by all beamlets per unit weight; it is received by voxel i.

Because of the effect of radiation on the tumor and the surrounding normal tissue, we place a lower and upper dose limits (θ_L and θ_U) on the target to control the cold spots and hot spots on target voxels, respectively. In addition, to spare healthy tissues from the toxic effects of radiation, we limit the dose to a specific level, φ, which is a structure-specific parameter.

Using these definitions, we have three types of constraints:

$$\mathbf{D}_i(\mathbf{w}) \geq \theta_L, \qquad \forall i \in \mathcal{T}, \tag{4.2.1}$$

$$\mathbf{D}_i(\mathbf{w}) \leq \theta_U, \qquad \forall i \in \mathcal{T}, \ and \tag{4.2.2}$$

$$\mathbf{D}_i(\mathbf{w}) \leq \varphi, \quad \forall i \in \mathcal{OAR}, \tag{4.2.3}$$

where $\mathbf{D}_T(\mathbf{w})$ is the nominal equivalent of the $\tilde{\mathbf{D}}_T(\mathbf{w})$. Under uncertainty, the constraint (4.2.1)-(4.2.3) can be expressed in a chance-constrained framework by introducing a confidence level and enforcing the constraint in probability as represented here under:

$$P\{\tilde{\mathbf{D}}_i(\mathbf{w}) \geq \theta_L\} \geq 1 - \alpha_T^-, \qquad \forall i \in \mathcal{T}, \tag{4.2.4}$$

$$P\{\tilde{\mathbf{D}}_i(\mathbf{w}) \leq \theta_U\} \geq 1 - \alpha_T^+, \qquad \forall i \in \mathcal{T}, \ and \tag{4.2.5}$$

$$P\{\tilde{\mathbf{D}}_i(\mathbf{w}) \leq \varphi\} \geq 1 - \alpha_{OAR}^+, \qquad \forall i \in \mathcal{OAR}, \tag{4.2.6}$$

where $1 - \alpha_T^-$, $1 - \alpha_T^+$, and $1 - \alpha_{OAR}^+$ are the confidence levels for avoiding cold spots and hot spots on target voxels and sparing voxels in OARs.

4.3 Distributionally robust chance constraints

How to best solve a stochastic problem depends on what is known about the probability distribution of the uncertain dose contribution parameters. However, in many cases, it is impossible to accurately estimate this distribution. In this section, we introduce distributionally robust chance constraints and illustrate deterministic counterparts to address the problem of RT planning.

A distributionally robust chance constraint should be enforced robustly with respect to an entire family of probability distributions on the random data. We considered the following robust chance-constrained problem:

$$\max_{w_j,\alpha_T^+,\alpha_T^-,\alpha_{OAR}^+} \quad \lambda_T^-(1-\alpha_T^-) + \lambda_T^+(1-\alpha_T^+) + \lambda_{OAR}(1-\alpha_{OAR}^+) \tag{4.3.1}$$

s.t.

$$\inf_{\tilde{\mathbf{d}}_i \sim D} \; P\{\tilde{\mathbf{d}}_i^{'}\mathbf{w} \geq \theta_L\} \geq 1-\alpha_T^-, \qquad \forall i \in \mathcal{T}, \tag{4.3.2}$$

$$\inf_{\tilde{\mathbf{d}}_i \sim D} \; P\{\tilde{\mathbf{d}}_i^{'}\mathbf{w} \leq \theta_U\} \geq 1-\alpha_T^+, \qquad \forall i \in \mathcal{T}, \tag{4.3.3}$$

$$\inf_{\tilde{\mathbf{d}}_i \sim D} \; P\{\tilde{\mathbf{d}}_i^{'}\mathbf{w} \leq \varphi\} \geq 1-\alpha_{OAR}^+, \qquad \forall i \in \mathcal{OAR}, \; \textit{and} \tag{4.3.4}$$

$$\mathbf{w} \geq 0. \tag{4.3.5}$$

To tractably solve this model, we first defined a family of probability distributions, D, that was under consideration. In Section 3.1, we assumed that the mean and bounded interval of the uncertain parameter were known, and in Section 3.2, we made assumptions about the FO and SO moments of the uncertain parameter distribution.

4.3.1 Known FO moment and bounded intervals

The uncertain dose contribution vector $\tilde{\mathbf{d}}_i$ is assumed to have a known mean $\hat{d}_i$ and known bounds on its support, i.e., we know $\ell_{ij}^- < \ell_{ij}^+$, such that $P(\tilde{d}_{ij} \in [\ell_{ij}^- + \hat{\mathbf{d}}_i, \ell_{ij}^+ + \hat{\mathbf{d}}_i]) = 1$. The family of distributions on random vector $\tilde{\mathbf{d}}_i$ that satisfies the above condition is denoted with $(\hat{\mathbf{d}}_i, \mathbf{L}_i)_I$, where $\mathbf{L}_i$ is a diagonal matrix of interval widths $(\ell_{ij}^+ - \ell_{ij}^-)$.

Proposition 4.3.1 is related to that described in a study by Calafiore and El Ghaoui (2006) and provides a computationally tractable approximation that ensures feasibility at the chance constraints (4.3.9) - (4.3.11).

Proposition 4.3.1. Consider the following constraints:

$$\hat{\mathbf{d}}_i^{'}\mathbf{w} - \sqrt{(1/2)\ln(1/\alpha_T^-)}\,\|\mathbf{L}_i\mathbf{w}\| \geq \theta_L, \qquad \forall i \in \mathcal{T}, \tag{4.3.6}$$

$$\hat{\mathbf{d}}_i^{'}\mathbf{w} + \sqrt{(1/2)\ln(1/\alpha_T^+)}\,\|\mathbf{L}_i\mathbf{w}\| \leq \theta_U, \qquad \forall i \in \mathcal{T},\ and \tag{4.3.7}$$

$$\hat{\mathbf{d}}_i^{'}\mathbf{w} + \sqrt{(1/2)\ln(1/\alpha_{OAR}^+)}\,\|\mathbf{L}_i\mathbf{w}\| \leq \varphi, \qquad \forall i \in \mathcal{OAR}. \tag{4.3.8}$$

For any $\{\alpha_T^-, \alpha_T^+, \alpha_{OAR}^+\} \in (0,1)$, every feasible solution of the constraints (4.3.6) - (4.3.8) is feasible for the chance constraints (4.3.9) - (4.3.11), respectively.

$$\inf_{\tilde{\mathbf{d}}_i \sim (\hat{\mathbf{d}}_i, \mathbf{L}_i)} P\{\tilde{\mathbf{D}}_i(\mathbf{w}) \geq \theta_L\} \geq 1 - \alpha_T^-, \qquad \forall i \in \mathcal{T}, \tag{4.3.9}$$

$$\inf_{\tilde{\mathbf{d}}_i \sim (\hat{\mathbf{d}}_i, \mathbf{L}_i)} P\{\tilde{\mathbf{D}}_i(\mathbf{w}) \leq \theta_U\} \geq 1 - \alpha_T^+, \qquad \forall i \in \mathcal{T},\ and \tag{4.3.10}$$

$$\inf_{\tilde{\mathbf{d}}_i \sim (\hat{\mathbf{d}}_i, \mathbf{L}_i)} P\{\tilde{\mathbf{D}}_i(\mathbf{w}) \leq \varphi\} \geq 1 - \alpha_{OAR}^+, \qquad \forall i \in \mathcal{OAR}. \tag{4.3.11}$$

Proof. Let $\mathbf{w}$ be a feasible solution of the constraints (4.3.9) - (4.3.11). For each $\tilde{\mathbf{d}}_i \sim (\hat{\mathbf{d}}_i, \mathbf{L}_i)_I$,

$$P\{\tilde{\mathbf{D}}_i(\mathbf{w}) < \theta_L\} \leq \alpha_T^-, \qquad \forall i \in \mathcal{T}, \tag{4.3.12}$$

$$P\{\tilde{\mathbf{D}}_i(\mathbf{w}) > \theta_U\} \leq \alpha_T^+, \qquad \forall i \in \mathcal{T},\ and \tag{4.3.13}$$

$$P\{\tilde{\mathbf{D}}_i(\mathbf{w}) > \varphi\} \leq \alpha_{lOAR}^+, \qquad \forall i \in \mathcal{OAR}. \tag{4.3.14}$$

First, consider the constraint (4.3.9). By definition, for the random dose contribution in independent intervals:

$$P\{\tilde{\mathbf{d}}_i^{'}\mathbf{w} \geq \theta_L\} = P\{\hat{\mathbf{d}}_i^{'}\mathbf{w} + \sum_j \xi_j \geq \theta_L\}, \qquad \forall i \in \mathcal{T}$$

$$= P\{-\sum_j \xi_j \leq \hat{\mathbf{d}}_i^{'}\mathbf{w} - \theta_L\}, \qquad \forall i \in \mathcal{T}, \tag{4.3.15}$$

where $\mathbf{E}(\xi_j) = 0$, and ξ_j is independent and bounded in intervals of width $|w_j|(\ell_{i1}^{+} - \ell_{i1}^{-})$. From Hoeffding's inequality (Hoeffding (1963)),

$$P\{\tilde{\mathbf{d}}_i^{'}\mathbf{w} \leq \theta_L\} \leq exp[\frac{-2(\hat{\mathbf{d}}_i^{'}\mathbf{w} - \theta_L)^2}{\|\mathbf{L}_i\mathbf{w}\|^2}], \qquad \forall i \in \mathcal{T}. \tag{4.3.16}$$

Thus, inequality (4.3.17) is required

$$exp[\frac{-2(\hat{\mathbf{d}}_i^{'}\mathbf{w} - \theta_L)^2}{\|\mathbf{L}_i\mathbf{w}\|^2}] \leq \alpha_T^{-}, \qquad \forall i \in \mathcal{T}, \tag{4.3.17}$$

from which the constraint (4.3.6) follows.

Constraints (4.3.7) and (4.3.8) were also proven in a similar fashion to that of (4.3.6).

The resulting model (DRCCP-I) is:

$$\max_{w_j, \alpha_T^{+}, \alpha_T^{-}, \alpha_{OAR}^{+}} \quad \lambda_T^{-}(1-\alpha_T^{-}) + \lambda_T^{+}(1-\alpha_T^{+}) + \lambda_{OAR}(1-\alpha_{OAR}^{+}) \tag{4.3.18}$$

s.t.

$$\hat{\mathbf{d}}_i^{'}\mathbf{w} - \sqrt{(1/2)\ln(1/\alpha_T^{-})}\,\|\mathbf{L}_i\mathbf{w}\| \geq \theta_L, \qquad \forall i \in \mathcal{T},$$

$$\hat{\mathbf{d}}_i^{'}\mathbf{w} + \sqrt{(1/2)\ln(1/\alpha_T^{+})}\,\|\mathbf{L}_i\mathbf{w}\| \leq \theta_U, \qquad \forall i \in \mathcal{T},$$

$$\hat{\mathbf{d}}_i^{'}\mathbf{w} + \sqrt{(1/2)\ln(1/\alpha_{OAR}^{+})}\,\|\mathbf{L}_i\mathbf{w}\| \leq \varphi, \qquad \forall i \in \mathcal{T}, \; and$$

$$\mathbf{w} \geq 0. \tag{4.3.19}$$

4.3.2 Finite FO and SO moments

We assumed that the uncertain coefficient $\tilde{\mathbf{d}}_i$ depends affinely on a random variable $\tilde{\epsilon}_{ij}$ whose distribution is unknown, but the FO and SO moments are known to be finite.

$$\mathbf{d}_i(\tilde{\epsilon}) = \mathbf{d}_i^0 + \sum_{j \in J} \mathbf{e}_j \tilde{\epsilon}_{ij},$$

where $\mathbf{d}_i^0$ vector is equal to $E(\tilde{\mathbf{d}}_i)$, and elements of $\mathbf{e}_j$ vectors are 0, except for the j^{th} element, which is 1. For ease of notation, the auxiliary functions $\mathbf{y}_i^j(\mathbf{w})$ are introduced; these are defined by

$$\mathbf{y}_i{}^0(\mathbf{w}) = \mathbf{d}_i{}^{0'}\mathbf{w},$$

$$\mathbf{y}_i{}^j(\mathbf{w}) = \mathbf{e}_j^{'}\mathbf{w}.$$

The random dose per voxel i is defined as

$$\tilde{\mathbf{D}}_i(\mathbf{w}) = \mathbf{y}_i^0(\mathbf{w}) + \mathbf{y}_i^{'}(\mathbf{w})\tilde{\epsilon}_i,$$

where $\mathbf{y}_i{}^{'}(\mathbf{w})$ is affine in $\mathbf{w}$ for every voxel i. Thus, the chance constraints in (4.3.2)-(4.3.4) are rewritten in constraints (4.3.20)-(4.3.22).

$$\inf_{\tilde{\mathbf{d}}_i \sim D} P\{\mathbf{y}_i^0(\mathbf{w}) + \mathbf{y}_i^{'}(\mathbf{w})\tilde{\epsilon}_i \geq \theta_L\} \geq 1 - \alpha_T^-, \qquad \forall i \in \mathcal{T}, \tag{4.3.20}$$

$$\inf_{\tilde{\mathbf{d}}_i \sim D} P\{\mathbf{y}_i^0(\mathbf{w}) + \mathbf{y}_i^{'}(\mathbf{w})\tilde{\epsilon}_i \leq \theta_U\} \geq 1 - \alpha_T^+, \qquad \forall i \in \mathcal{T},\ and \tag{4.3.21}$$

$$\inf_{\tilde{\mathbf{d}}_i \sim D} P\{\mathbf{y}_i^0(\mathbf{w}) + \mathbf{y}_i^{'}(\mathbf{w})\tilde{\epsilon}_i \leq \varphi\} \geq 1 - \alpha_{OAR}^+. \qquad \forall i \in \mathcal{OAR}. \tag{4.3.22}$$

The next three Propositions in this section provide convex SO cone approximations for the distributionally robust chance constraints when the mean and variance are known.

Proposition 4.3.2. Let random vector $\tilde{\epsilon}_i$ have a known mean of 0 and covariance matrix $\sigma^2(\tilde{\epsilon}_i)$ and consider the following model (DRCCP-SOCP):

$$\max_{w_j, \alpha_T^+, \alpha_T^-, \alpha_{OAR}^+} \quad \lambda_T^-(1-\alpha_T^-) + \lambda_T^+(1-\alpha_T^+) + \lambda_{OAR}(1-\alpha_{OAR}^+) \tag{4.3.23}$$

s.t.

$$\mathbf{y}_i^0(\mathbf{w}) - \sqrt{(1-\alpha_T^-)/\alpha_T^-}\,\|\sigma(\tilde{\epsilon}_i)\mathbf{y}_i(\mathbf{w})\| \geq \theta_L, \qquad \forall i \in \mathcal{T}, \tag{4.3.24}$$

$$\mathbf{y}_i^0(\mathbf{w}) + \sqrt{(1-\alpha_T^+)/\alpha_T^+}\,\|\sigma(\tilde{\epsilon}_i)\mathbf{y}_i(\mathbf{w})\| \leq \theta_U, \qquad \forall i \in \mathcal{T}, \tag{4.3.25}$$

$$\mathbf{y}_i^0(\mathbf{w}) + \sqrt{(1-\alpha_{OAR}^+)/\alpha_{OAR}^+}\,\|\sigma(\tilde{\epsilon}_i)\mathbf{y}_i(\mathbf{w})\| \leq \varphi, \qquad \forall i \in \mathcal{OAR},\ and \tag{4.3.26}$$

$$\mathbf{w} \geq 0.$$

Every feasible solution of the constraints (4.3.24) - (4.3.26) is feasible for the chance constraints (4.3.20) - (4.3.22), respectively.

Proof. Let $\mathbf{w}$ be a feasible solution of the constraints (4.3.24) - (4.3.26). For each $\tilde{\mathbf{d}}_i \sim (\hat{\mathbf{d}}_i, \sigma^2(\tilde{\mathbf{d}}_i))$

$$P\{\mathbf{y}_i^0(\mathbf{w}) + \mathbf{y}_i^{'}(\mathbf{w})\tilde{\epsilon}_i < \theta_L\} \leq \alpha_T^-, \qquad \forall i \in \mathcal{T}, \tag{4.3.27}$$

$$P\{\mathbf{y}_i^0(\mathbf{w}) + \mathbf{y}_i^{'}(\mathbf{w})\tilde{\epsilon}_i > \theta_U\} \leq \alpha_T^+, \qquad \forall i \in \mathcal{T}, \ and \tag{4.3.28}$$

$$P\{\mathbf{y}_i^0(\mathbf{w}) + \mathbf{y}_i^{'}(\mathbf{w})\tilde{\epsilon}_i > \varphi\} \leq \alpha_{OAR}^+, \qquad \forall i \in \mathcal{OAR}. \tag{4.3.29}$$

First, consider the constraint (4.3.20). From the upper-sided Chebyshev inequality (Bertsimas and Popescu (2005)), we have

$$\sup_{(\hat{\mathbf{d}}_i, \sigma^2(\tilde{\mathbf{d}}_i))} P\{-\mathbf{y}_i^{'}(\mathbf{w})\tilde{\epsilon}_i \geq \mathbf{y}_i^0(\mathbf{w}) - \theta_L\} = \frac{1}{1 + (r_i^-)^2}, \qquad \forall i \in \mathcal{T}, \tag{4.3.30}$$

where

$$\begin{aligned} &(r_i^-)^2 = inf \quad \tilde{\epsilon}_i^{'}\, \sigma^{-1}(\tilde{\epsilon}_i)\, \tilde{\epsilon}_i, \qquad \forall i \in \mathcal{T}, \\ &s.t. \\ &\qquad \mathbf{y}_i^{'}(\mathbf{w})\tilde{\epsilon}_i \leq \theta_L - \mathbf{y}_i^0(\mathbf{w}), \qquad \forall i \in \mathcal{T}. \end{aligned} \tag{4.3.31}$$

Considering constraint (4.3.31), we notice that, if $\theta_L - \mathbf{y}_i^0(\mathbf{w}) \geq 0, \forall i \in \mathcal{T}$, then $\tilde{\epsilon}_i = \mathbf{0}, \forall i \in \mathcal{T}$ and $(r_i^-)^2 = 0, \forall i \in \mathcal{T}$. Assuming $\theta_L - \mathbf{y}_i^0(\mathbf{w}) < 0, \forall i \in \mathcal{T}$, then $(r_i^-)^2, \forall i \in \mathcal{T}$ is minimized if constraint (4.3.31) holds true for equality. Hence, for any voxel inside the target:

$$\begin{aligned} &\tilde{\epsilon}_i = \frac{\theta_L - \mathbf{y}_i^0(\mathbf{w})}{\mathbf{y}_i^{'}(\mathbf{w})}, \qquad \forall i \in \mathcal{T}, \\ &(r_i^-)^2 = [\frac{\theta_L - \mathbf{y}_i^0(\mathbf{w})}{\mathbf{y}_i^{'}(\mathbf{w})}]^{'}\, \sigma^{-1}(\tilde{\epsilon}_i)\, [\frac{\theta_L - \mathbf{y}_i^0(\mathbf{w})}{\mathbf{y}_i^{'}(\mathbf{w})}], \qquad \forall i \in \mathcal{T}. \end{aligned} \tag{4.3.32}$$

According to equation (4.3.30), the chance constraint (4.3.27) is satisfied if and only if

$$\frac{1}{1+(r_i^-)^2} \leq \alpha_T^-, \qquad \forall i \in \mathcal{T},$$

that is equivalent to:

$$(r_i^-)^2 \geq \frac{1-\alpha_T^-}{\alpha_T^-}, \qquad \forall i \in \mathcal{T}, \tag{4.3.33}$$

from which the constraint (4.3.24) follows.

The constraints (4.3.25) and (4.3.26) can be derived in a similar fashion to (4.3.24). □

The two models presented in Sections 4.3.1 and 4.3.2 can be effective approaches to solving stochastic problems under two different conditions. Proposition 4.3.1 when information about random data is limited to an interval with a known upper bound, lower bound, and mean. Proposition 4.3.2 can be used to convert the stochastic problem into a deterministic approximation, in terms of the mean and covariance of the uncertain parameter. This deterministic approximation can also be improved. We next describe two refined approaches of the model in Proposition 4.3.2 that are useful if the FO and SO moments of the uncertain data are known.

4.3.2.1 QM approximation:

To be more precise when considering uncertainties, a sentence that includes the SO of a random vector can be added to the random dose. As a result, the random dose function will have both the linear and quadratic terms that follow the QM (Zymler et al. (2013)) of the constraint:

$$\tilde{\mathbf{D}}_i(\mathbf{w}) = \mathbf{y}_i^0(\mathbf{w}) + \mathbf{y}_i^{'}(\mathbf{w})\tilde{\epsilon}_i + L\,\tilde{\epsilon}_i^{'}\|\mathbf{y}_i(\mathbf{w})\|^2\tilde{\epsilon}_i,$$

where L is defined as a constant parameter.

Proposition 3 is similar to proposition 2; it illustrates the deterministic approximations

of the QM chance constraints.

Proposition 4.3.3. Let random vector $\tilde{\epsilon_i}$ belong to family D of probability distributions that have a mean of 0, and a known $\sigma^2(\tilde{\epsilon}_i)$; consider the following constraints:

$$\mathbf{y}_i^0(\mathbf{w}) + L\,\sigma^2(\tilde{\epsilon_i})\|\mathbf{y}_i(\mathbf{w})\|^2 - \sqrt{(1-\alpha_T^-)/\alpha_T^-}\times$$
$$((\mathbf{y}_i(\mathbf{w}))^2\sigma^2(\tilde{\epsilon_i}) + L^2\|\mathbf{y}_i(\mathbf{w})\|^4\sigma^2(\tilde{\epsilon_i}^2))^{1/2} \geq \theta_L, \qquad \forall i \in \mathcal{T}, \tag{4.3.34}$$

$$\mathbf{y}_i^0(\mathbf{w}) + L\,\sigma^2(\tilde{\epsilon_i})\|\mathbf{y}_i(\mathbf{w})\|^2 + \sqrt{(1-\alpha_T^+)/\alpha_T^+}\times$$
$$((\mathbf{y}_i(\mathbf{w}))^2\sigma^2(\tilde{\epsilon_i}) + L^2\|\mathbf{y}_i(\mathbf{w})\|^4\sigma^2(\tilde{\epsilon_i}^2))^{1/2} \leq \theta_U, \qquad \forall i \in \mathcal{T},\ \textit{and} \tag{4.3.35}$$

$$\mathbf{y}_i^0(\mathbf{w}) + L\,\sigma^2(\tilde{\epsilon_i})\|\mathbf{y}_i(\mathbf{w})\|^2 + \sqrt{(1-\alpha_{OAR}^+)/\alpha_{OAR}^+}\times$$
$$((\mathbf{y}_i(\mathbf{w}))^2\sigma^2(\tilde{\epsilon_i}) + L^2\|\mathbf{y}_i(\mathbf{w})\|^4\sigma^2(\tilde{\epsilon_i}^2))^{1/2} \leq \varphi, \qquad \forall i \in \mathcal{OAR}. \tag{4.3.36}$$

Every feasible solution of the constraints (4.3.34) - (4.3.36) is feasible for the chance constraints (4.3.37) - (4.3.39), respectively.

$$\inf_{\tilde{\mathbf{d}}_i \sim D} P\{\mathbf{y}_i^0(\mathbf{w}) + \mathbf{y}_i^{'}(\mathbf{w})\tilde{\epsilon}_i + L\,\tilde{\epsilon}_i^{'}\|\mathbf{y}_i(\mathbf{w})\|^2\tilde{\epsilon}_i \geq \theta_L\} \geq 1-\alpha_T^-,$$
$$\forall i \in \mathcal{T}, \tag{4.3.37}$$

$$\inf_{\tilde{\mathbf{d}}_i \sim D} P\{\mathbf{y}_i^0(\mathbf{w}) + \mathbf{y}_i^{'}(\mathbf{w})\tilde{\epsilon}_i + L\,\tilde{\epsilon}_i^{'}\|\mathbf{y}_i(\mathbf{w})\|^2\tilde{\epsilon}_i \leq \theta_U\} \geq 1-\alpha_T^+,$$
$$\forall i \in \mathcal{T},\ \textit{and} \tag{4.3.38}$$

$$\inf_{\tilde{\mathbf{d}}_i \sim D} P\{\mathbf{y}_i^0(\mathbf{w}) + \mathbf{y}_i^{'}(\mathbf{w})\tilde{\epsilon}_i + L\,\tilde{\epsilon}_i^{T}\|\mathbf{y}_i(\mathbf{w})\|^2\tilde{\epsilon}_i \leq \varphi\} \geq 1-\alpha_{OAR}^+,$$
$$\forall i \in \mathcal{OAR}. \tag{4.3.39}$$

Proof. The proof of this proposition is a minor modification of Proposition4.3.2.

4.3.2.2 SO dependence approximation:

Here, the dependence of random dose contributions $\mathbf{d}_i$ is not affine; instead, they depend quadratically on the random vector $\tilde{\epsilon_i}$:

$$\mathbf{d}_i(\tilde{\epsilon}) = \mathbf{d}_i^0 + \sum_{j \in J} \mathbf{e}_j \tilde{\epsilon}_{ij} + q \sum_{j \in J} \mathbf{e}_j \tilde{\epsilon}_j^2,$$

where q is the scalar parameter. The random dose per voxel i is defined by

$$\tilde{\mathbf{D}}_i(\mathbf{w}) = \mathbf{y}_i^0(\mathbf{w}) + \mathbf{y}_i^{'}(\mathbf{w})\tilde{\epsilon}_i + q\mathbf{z}_i^{'}(\mathbf{w})\tilde{\epsilon}_i^2,$$

where the auxiliary functions $\mathbf{y}_i{}^{'}(\mathbf{w})$ and $\mathbf{z}_i^{'}(\mathbf{w})$ are affine in $\mathbf{w}$ for every voxel i, and $\mathbf{z}_i^{'}(\mathbf{w})$ is introduced as

$$\mathbf{z}_i^{'}(\mathbf{w}) = \mathbf{e}_j^{'}\mathbf{w}.$$

Proposition 4.3.4 is similar to Propositions 2 and 3; it proposes deterministic approximations of the distributionally robust chance constraints (4.3.12) - (4.3.14)

Proposition 4.3.4. Let the random vector $\tilde{\epsilon_i}$ have a mean of 0, and a known $\sigma^2(\tilde{\epsilon}_i)$ and consider the following constraints:

$$\mathbf{y}_i^0(\mathbf{w}) + q\mathbf{z}_i^{'}(\mathbf{w})\, \sigma^2(\tilde{\epsilon}_i^2) - \sqrt{(1-\alpha_i^-)/\alpha_i^-}\, (\mathbf{y}_i(\mathbf{w}))^2\, \sigma^2(\tilde{\epsilon}_i) + (q^2\mathbf{z}_i(\mathbf{w}))^2\, \sigma^2(\tilde{\epsilon}_i^2))^{1/2} \geq \theta_L, \quad \forall i \in \mathcal{T}, \tag{4.3.40}$$

$$\mathbf{y}_i^0(\mathbf{w}) + q\mathbf{z}_i^{'}(\mathbf{w})\, \sigma^2(\tilde{\epsilon}_i^2) + \sqrt{(1-\alpha_i^+)/\alpha_i^+}\, (\mathbf{y}_i(\mathbf{w}))^2\, \sigma^2(\tilde{\epsilon}_i) + (q^2\mathbf{z}_i(\mathbf{w}))^2\, \sigma^2(\tilde{\epsilon}_i^2))^{1/2} \leq \theta_U, \quad \forall i \in \mathcal{T},\ \textit{and} \tag{4.3.41}$$

$$\mathbf{y}_i^0(\mathbf{w}) + q\mathbf{z}_i^{'}(\mathbf{w})\, \sigma^2(\tilde{\epsilon}_i^2) + \sqrt{(1-\alpha_i^+)/\alpha_i^+}\, (\mathbf{y}_i(\mathbf{w}))^2\, \sigma^2(\tilde{\epsilon}_i) + (q^2\mathbf{z}_i(\mathbf{w}))^2\, \sigma^2(\tilde{\epsilon}_i^2))^{1/2} \leq \varphi, \quad \forall i \in \mathcal{OAR}. \tag{4.3.42}$$

Every feasible solution of the constraints (4.3.40) - (4.3.42) is feasible for the chance constraints (4.3.43) - (4.3.45), respectively. In fact, the approximations of the distributionally robust chance constraints in (4.3.2)-(4.3.4) are rewritten in constraints (4.3.43) - (4.3.45).

$$\inf_{\tilde{\mathbf{d}}_i \sim D} P\{\mathbf{y}_i^0(\mathbf{w}) + \mathbf{y}_i^{'}(\mathbf{w})\tilde{\epsilon}_i + \mathbf{z}_i^{'}(\mathbf{w})\tilde{\epsilon}_i^2 \geq \theta_L\} \geq 1 - \alpha_T^+, \qquad \forall i \in \mathcal{T}, \tag{4.3.43}$$

$$\inf_{\tilde{\mathbf{d}}_i \sim D} P\{\mathbf{y}_i^0(\mathbf{w}) + \mathbf{y}_i^{'}(\mathbf{w})\tilde{\epsilon}_i + \mathbf{z}_i^{'}(\mathbf{w})\tilde{\epsilon}_i^2 \leq \theta_U\} \geq 1 - \alpha_T^-, \qquad \forall i \in \mathcal{T},\ and \tag{4.3.44}$$

$$\inf_{\tilde{\mathbf{d}}_i \sim D} P\{\mathbf{y}_i^0(\mathbf{w}) + \mathbf{y}_i^{'}(\mathbf{w})\tilde{\epsilon}_i + \mathbf{z}_i^{'}(\mathbf{w})\tilde{\epsilon}_i^2 \leq \varphi\} \geq 1 - \alpha_{OAR}^+, \quad \forall i \in \mathcal{OAR}. \tag{4.3.45}$$

Proof. The proof of this proposition is a minor modification of Proposition 4.3.2.

4.4 Experiments and results

In this section, we present numerical results that provide important insights about the four DRCCP approaches and the CCP approaches, under distributional assumptions. Our initial goal was to illustrate the key features of the DRCCP approaches using a small test case; a square target surrounded by an L-shaped OAR geometry. We then demonstrated the strength of the DRCCP approaches using a prostate cancer case.

4.4.1 A small test case

The geometry for our small example is shown in Figure 4.1 with one rectangular target shown in white and one L-shaped OAR shown in gray. The tumor and the OARs have six pixels of equal dimension. Each pixel can be identified by its horizontal (x) and vertical (y) coordinates. Two perpendicular beams contribute to the voxels. Because the position of the patient may be different from one session to the next, the actual dose contribution of the beamlets can be uncertain during treatment sessions. Depending on the available information about the data distribution, different DRCCP approaches can be used to optimize the weights of the beamlets under setup uncertainty.

If the mean and the bounded intervals of the setup error are known, the DRCCP-I

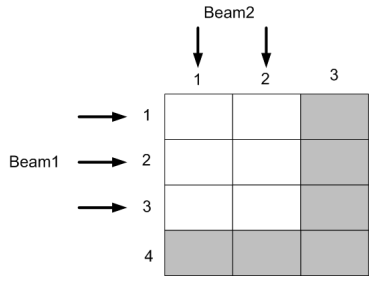

Figure 4.1: A gray L-shaped OAR; the white square shows the tumor region.

approach (4.3.18) can be used to generate distributionally robust treatment plans. If only the FO and SO moments of the unknown parameter are available, any of the DRCCP-SOCP, DRCCP-QM, and DRCCP-SO approaches can be used to optimize beamlet intensities.

Figure 4.2 illustrates the optimized dose to each voxel in a nominal setup generated by all four approaches. In general, all plans can effectively cover the target volume and control dose to the OAR. DRCCP-I outperformed DRCCP-SOCP in providing more homogeneous dose distribution within the target. The maximum dose in DRCCP-I was 1.09, the minimum dose to the target voxels was 0.93, and the gap was 0.16. Note that the gap difference from DRCCP-SOCP was 0.21. These gaps were a result of the random parameter following a uniform distribution. The DRCCP-I is also used when the interval of the uncertain dose contribution is known. Thus, the DRCCP-I approach can be a better fit to the uncertain parameter under the uniform distribution assumption.

Both the DRCCP-QM and DRCCP-SO approaches generally outperformed the DRCCP-SOCP by delivering a more homogeneous dose to the target while delivering a lower dose to the OARs. For example, in the SOCP approach, the given minimum and maximum doses to the target were between 0.91 and 1.12, while these values were 0.91 and 1.06 for the SO dependence and QM approaches, respectively. Hence, the plans generated by the SO and QM approaches were more homogeneous than was the SOCP approach. Moreover, the dose to the OAR structure was better controlled by DRCCP-QM and DRCCP-SO: the maximum dose to the OARs from DRCCP-QM and DRCCP-SO, was 0.22, while the maximum dose to the OAR using DRCCP-SOCP was 0.3. The target coverage homogeneity and OAR sparing provided by the DRCCP-QM and DRCCP-SO approaches were comparable. The

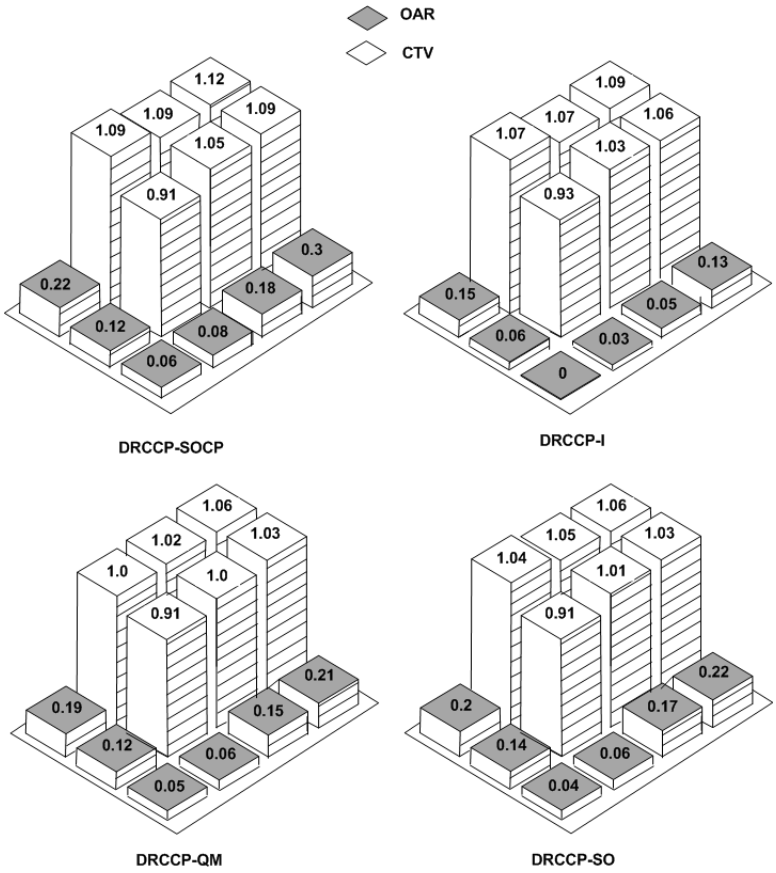

Figure 4.2: Depiction of the optimal nominal dose, generated by the DRCCP-SOCP, DRCCP-I, DRCCP-QM, and DRCCP-SO approaches, deposited in each voxel for the model described in Section 4.4.1.

results are intuitive because both SO and QM approximate the DRCCP approach more accurately than does the SOCP approach.

To evaluate the robustness of the DRCCP approaches, we generated two types of random data using uniform and normal distributions (CCP-U and CCP-N) that were consistent with the given information of uncertain parameters. The mean and standard deviation of the dose to the target and the OAR voxels generated from all models are presented in Table 4.2. We verified the effectiveness of the DRCCP approach and found similar results as those for the plan generated by the CCP approach under a distributional assumption.

As shown in Table 4.2, when the model was solved using the CCP-N approach for the dose and the realized distribution was uniform, the dispersion of a dose set received by the target ($\sigma_{CCP-N} = 0.102$) was higher than that using the SOCP approach ($\sigma_{SOCP} = 0.096$).

Table 4.2: Mean and standard deviation of the dose from the shifted setups for the voxels in the target and OARs generated by all DRCCP and CCP approaches under distributional assumptions

(a) Considering uniform distribution for $\tilde{d}_i$

Approach	Target		OAR	
	Mean	SD	Mean	SD
CCP-N	0.92	0.102	0.12	0.118
DRCCP-SOCP	1.05	0.096	0.11	0.108
DRCCP-QM	1.02	0.094	0.08	0.107
DRCCP-SO	1.02	0.094	0.08	0.107
DRCCP-I	1.03	0.080	0.07	0.099

(b) Considering normal distribution for $\tilde{d}_i$

Approach	Target		OAR	
	Mean	SD	Mean	SD
CCP-U	0.91	0.089	0.09	0.128
DRCCP-SOCP	1.07	0.078	0.07	0.121
DRCCP-QM	1.05	0.071	0.05	0.113
DRCCP-SO	1.05	0.071	0.05	0.113
DRCCP-I	1.03	0.075	0.05	0.105

This indicates that the data points were spread over a wider range of values around the mean. Moreover, the mean dose of the plans generated by CCP-N was 0.92, which is a sign of underdose to the target. The same result was observed when the assumed distribution for the random dose was uniform. As shown in Table 4.2b, CCP-U with $\sigma_{CCP-U} = 0.089$ was more sporadic than was DRCCP-SOCP with $\sigma_{SOCP} = 0.078$, and 0.91 Gy, as an average dose deposited to the tumor, was not sufficient to cover the tumor. Hence, we can conclude that the distributionally robust CCP approach will give us a more realistic result, even if there is not enough information about the distribution for the uncertain parameter.

We evaluated the robustness of the DRCCP approaches and compared them with the distributional CCP approach. Figure 4.3 shows the differences in the average dose for voxels in the tumor and OARs.

The computational results generated some important insights. First, the effectiveness of the DRCCP-I and DRCCP-SOCP approaches were evaluated on the basis of the distribution assumption of the generated random parameter. The DRCCP approaches performed better than did CCP-N while the random parameter followed uniform distribution. This is

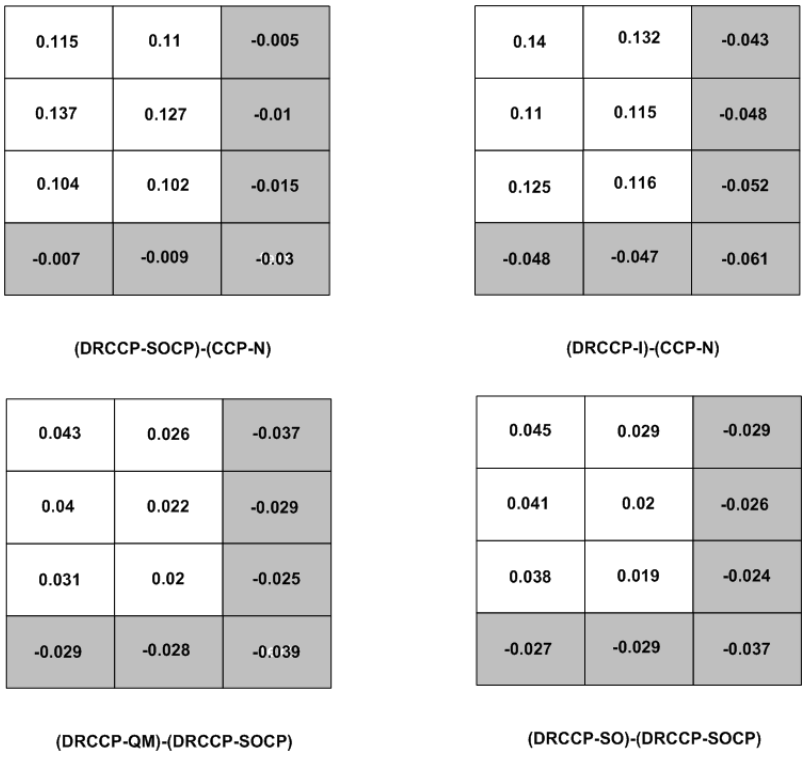

Figure 4.3: Differences between the mean-dose per voxel

probably because of the increase in the delivered mean-dose by the target and the decrease in the toxic effect on normal cells. Accordingly, we infer that the interval-based method is more efficient than is the SOCP approach because of the uniformity assumption.

We compared the abstract values, which refer to each voxel in the OARs and the target, and found that DRCCP-I had a higher gap with CCP-N than with SOCP (Figure 4.3). Thus, the dosage received by the normal cells around the tumor was reduced to protect them from damage; in addition, the average dosage given to kill the cancer cells was increased. This indicates that the optimal solution is critically dependent on the exact description of the distribution. We next compared the relative improvement with the DRCCP-QM and DRCCP-SO approaches with that of the DRCCP-SOCP approach when our random parameter followed a uniform distribution. The average dose delivered to the tumor was higher with these new approaches. QM and SO were also more effective at sparing healthy tissues than was SOCP.

The result shown in Figure 4.3 is also shown in Figure B.1 (Appendix) under the normality assumption of the random parameter.

4.4.2 Clinical case

We demonstrated our approach in a clinical prostate cancer case. The target volume and normal structures were manually contoured on the axial slices of the planning Computed Tomography (CT) scan by a radiation oncologist. The anatomy was discretized into 2.5 mm $\times$2.5 mm $\times$2.5 mm voxels. Treatments were delivered with six fixed coplanar photon beams at $30°, 90°, 120°, 150°, 240°$, and $270°$ angels. Note that the beam angles were optimized in advance (Lim et al. (2014)) and confirmed by a clinician. A prescription dose of 76 Gy was used. Table 6.2 lists patient information and the specific treatment planning parameters of the case.

Table 4.3: Patient information and treatment planning parameters.

Cancer case	Volume	Number of Beams	Constraints
Prostate I (IMRT)	Target: 1000	6	Prescription: 76 Gy Receiving $\geq$ 96% of θ_L Receiving $\leq$ 105% of θ_U
	OAR (Rectum): 5848		
	OAR (Bladder): 10603		

We assumed that the setup uncertainty ranged between -5 mm and $+5$ mm (Manning et al. (2001); Wong et al. (2005)), and generated four representative scenarios in addition to the nominal scenario for the patient setup uncertainty; we then calculated the values of the mean, variance, and bounded intervals of the random dose distribution to generate different plans from the DRCCP approaches. The treatment plans were compared in terms of plan quality, robustness, and the chance constraint confidence level. The computational efficiencies of different approaches were also evaluated and compared.

4.4.3 Plan quality and robustness

We compared the quality and robustness of the plans developed using the different approaches. For the sake of comparison, all plans were normalized so that at least 95% of the target was covered by the prescribed dose in the nominal dose distribution. Dose-volume indices (D_v and V_d) were used to evaluate the quality of the plans, where D_v denotes the amount of dosage received by more than v percent of the organ, and V_d denotes the percentage volume of the organ receiving a dose greater than d Gy.

To compare the robustness of different treatment plans, we plotted families of Dose Volume Histogram (DVH) that corresponded to different shifted setup scenarios, along with the nominal DVH. The resulting envelopes were used to assess the sensitivity of the plans under the setup uncertainty. To further improve the accuracy of our evaluation and compare the robustness of the different methods, we used the DVH family band width method (Trofimov et al. (2012)). The width of the DVH band (Δ) was inversely proportional to the robustness of the method. Here, $\Delta(D_v)$ denotes the width of the DVH band at volume v, and $\Delta(V_d)$ denotes the width of the DVH band at dose d.

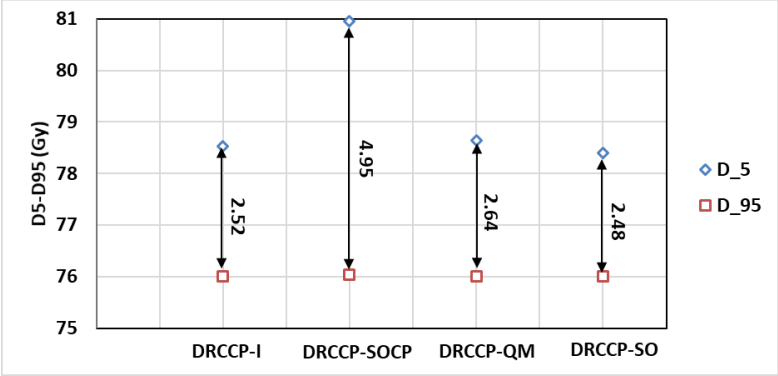

Figure 4.4: Homogeneity comparison: $D_5 - D_{95}$ statistics for nominal dose distributions

The homogeneity index is an objective measure to assess the uniformity of the dose distribution in the target volume. There are various ways to measure the homogeneity index. In this paper, we used D_{95} to assess target coverage and D_5 to measure the hot spot of the target. Thus, the target homogeneity can be measured by $D_5 - D_{95}$. Figure 4.4 shows

the intervals $[D_{95}, D_5]$ from all proposed approaches. The smaller $D_5 - D_{95}$ bar corresponds to a more homogeneous dose distribution within the target. As seen in Figure 4.4, DRCCP-I, DRCCP-QM, and DRCCP-SO provided plans with more homogeneous dose distribution than did DRCCP-SOCP. DRCCP-SO had the most homogeneous dose distribution.

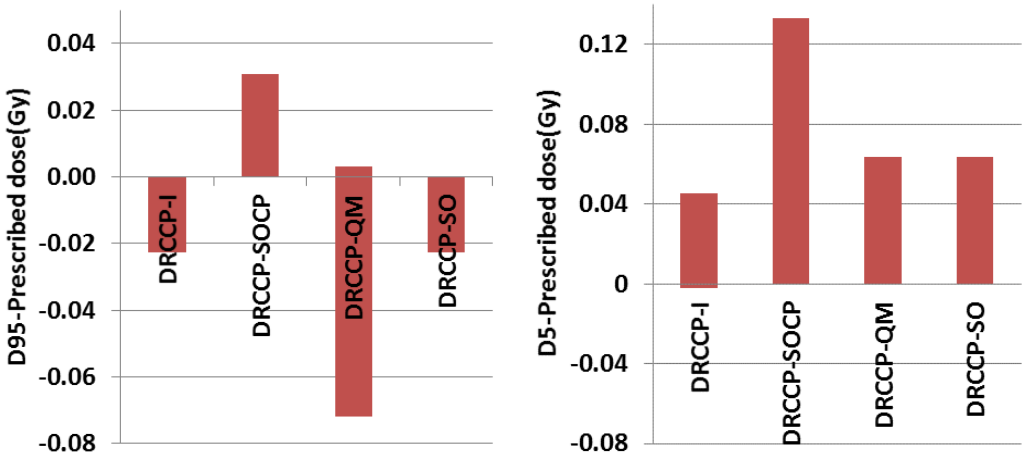

Figure 4.5: (a) D_{95} minus the prescribed dose and (b) D_5 minus the prescribed dose for shifted dose distributions from all DRCCP approaches. The height of the boxes shows the band width, i.e., $\Delta(D_{95})$ and $\Delta(D_5)$ in the DVH family of shifted setup scenarios are illustrated in (a) and (b), respectively. Zero on the vertical axis of (a) and (b) corresponds to D_{95} and D_5 for nominal dose distributions, respectively.

We next compared the robustness of the plans; Figure 4.5 shows plots of the DVH family band widths at $(a)D_{95}$ and $(b)D_5$ from all approaches. As seen in Figure 4.5a, both the DRCCP-I and DRCCP-SO approaches produced plans that were more robust at controlling cold spots than were the other two plans under various uncertainty scenarios. In terms of limiting hot spots in the target volume, DRCCP-I outperformed the others by having the smallest deviation as seen in Figure 4.5b. Figure 4.5b also shows that plans created by DRCCP-SOCP were notably less robust at controlling hot spots on the target.

4.4.4 Confidence levels

In this section, we discuss the use of confidence levels for satisfying treatment planning constraints when developing treatment plans. All plans developed using DRCCP approaches were compared with those of CCP approaches with a specific distributional assumption.

Table 4.4: Confidence levels $(1-\alpha)$ of plans generated by all DRCCP approaches versus distribution specific CCP

(a) Comparison under CCP-U

Approach	Target		Rectum	Bladder
	Under-dose	Over-dose		
CCP-N	0.86	0.82	0.82	0.82
DRCCP-I	0.92	0.91	0.92	0.9
DRCCP-SOCP	0.86	0.85	0.85	0.85
DRCCP-QM	0.91	0.91	0.9	0.9
DRCCP-SO	0.93	0.9	0.9	0.9

(b) Comparison under CCP-N

Approach	Target		Rectum	Bladder
	Under-dose	Over-dose		
CCP-U	0.85	0.86	0.85	0.85
DRCCP-I	0.92	0.9	0.9	0.9
DRCCP-SOCP	0.93	0.93	0.88	0.85
DRCCP-QM	0.99	0.97	0.92	0.92
DRCCP-SO	0.95	0.93	0.91	0.91

Our experiments were designed to test the performance of the proposed methods when the assumed dose distribution for planning was different from the true distribution, which is not known in advance. One of the many reasons why these distributions may differ is because of an insufficient number of sampled data points for developing a treatment plan. For example, treatment plans may have been developed on the basis of CCP-N when the data follow a uniform distribution. The confidence levels of the chance constraints that resulted from those experiments are shown in the first row of Table 4.4a. The DRCCP approaches were designed to address any realization of the probability distribution for random data. Thus, the confidence levels of DRCCP based treatment plans are also presented in Table 4.4a.

As expected, all DRCCP based plans resulted in consistently higher confidence levels than did CCP-N plans (Table 4.4a). Thus, DRCCP approaches provide more reliable treatment plans, in terms of satisfying constraints where there is an unknown probability distribution of the random parameter.

Of the three different DRCCP approaches we evaluated (SOCP, QM, and SO), the performance of the SOCP-based model was the poorest. This is because DRCCP-SOCP

uses affine dependence of the random radiation dose contribution, while both the QM and SO-based models inherently incorporate better approximations of dose contribution by using the quadratic format of the dose calculation. Such approximations include more information on the uncertain parameter, which makes the deterministic equivalence of CCP problems more precise. Note that the strength of the SOCP model is that it can be solved much faster than can the other two. This is explored further in Section 4.4.5, where we describe a two-phase algorithm that gives a better quality solution with less computational effort.

To test the robustness of the proposed approaches, a similar study was conducted under a different configuration. The treatment plan was developed on the basis of CCP-U. The first row in Table 4.4b shows the confidence levels optimized by CCP-U, and the subsequent rows show the optimized results of the DRCCP approaches. The optimized confidence levels from the CCP-U models were 85% for target under dose (cold spot) 86% for target over dose (hot spot) and 85% for both the rectum and bladder. Again, all DRCCP based models outperformed these benchmark confidence levels. Among the approaches, DRCCP-QM had the highest confidence levels on all measures for the three organs.

On the basis of these experiments, we observed that the DRCCP approaches were more efficient than was the CCP approach (both CCP-U and CCP-N), with an assumed probability distribution when only partial information about the uncertain parameters was available. In reality, it is rare to have full knowledge about the probability distribution of an uncertain parameter in RT planning. Under these circumstances, DRCCP approaches can better address uncertainties than can CCP approaches because DRCCP does not assume a known probability distribution function. Instead, it only uses partially known statistics about random data and provides a conservative solution that works well under various distribution scenarios.

4.4.5 Computational efficiency and a warm-start strategy

In this section, we discuss the computational efficiency of the four DRCCP approaches. DRCCP-SOCP quickly converged to a local optimal solution, but the quality and robustness

of the generated plan were not as good as were those of the other approaches as shown in Figures 4.4 and 4.5. Although the other three approaches (DRCCP-I, DRCCP-QM, and DRCCP-SO) require more time to solve, they provided treatment plans that were more homogeneous and robust under uncertainty.

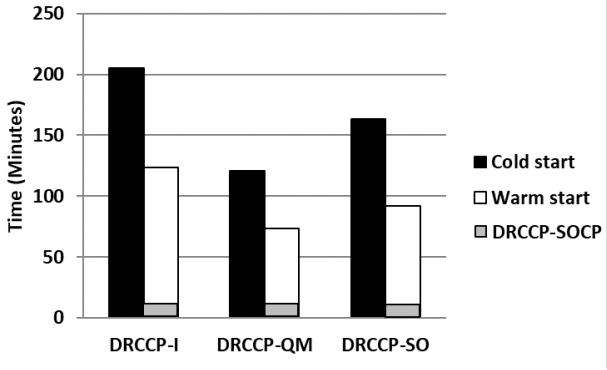

Figure 4.6: Computational time of all DRCCP approaches.

However, we found that a good starting solution to these approaches also improved convergence. Therefore, we considered a hybrid approach in which each of the three optimization techniques used a solution from DRCCP-SOCP as a warm start approach for DRCCP-I, DRCCP-QM, and DRCCP-SO.

In this approach, the DRCCP-SOCP approach is solved to generate a feasible solution within a short amount of time. Second, the DRCCP-I, DRCCP-QM, or DRCCP-SO approach is solved, using the SOCP solution as a starting point, to identify a higher quality optimal solution in less time. This warm start approach significantly reduced the computational time of the DRCCP approaches, as shown in Figure A.1. It also improved the computation time by 42%, 44%, and 47% for SRCCP-I, DRCCP-QM, and DRCCP-SO, respectively. Note that the total time of the warm-start approach includes the time needed to solve DRCCP-SOCP, which was approximatively 6 minutes.

4.5 Conclusion

The inclusion of uncertainties in RT planning optimization has been widely recognized as essential. For situations in which the only information about the random parameter

is the first moment, covariance, or support of the uncertain data, a DRCCP framework can be used to address uncertainty. We proposed the use of confidence levels for satisfying treatment planning constraints as a performance metric. Under those assumptions, SO cone counterparts of the distributionally robust chance constraints were explored to identify a more rapid solution, and two quadratic approximations of these constraints were developed to provide more precise deterministic equivalents. On the basis of these findings, we propose a CCP framework in which clinically relevant, locally optimal solutions can be identified consistently, in two sequential phases. The first phase is designed to quickly identify a feasible solution using DRCCP-SOCP. In the second, this solution is used as a starting point for DRCCP-I, and DRCCP-QM, or DRCCP-SO to identify a solution that is robust under uncertainty. Using both a small test case and a clinical case, we showed that the proposed models were effective for developing robust treatment plans under various uncertainty scenarios.

Chapter 5

Linear energy transfer incorporated intensity modulated proton therapy optimization

5.1 Introduction

In clinical practice, proton therapy treatments to date have been prescribed at physical doses 10% lower than those used in photon therapy. This paradigm is based on an assumption that doses deposited by protons are 10% more biologically effective than those by photons. In other words, the relative biological effectiveness (RBE) of protons versus photons is considered to have a constant value of 1.1. However, it is known that RBE is a complex variable dependent on many factors, including dose per fraction, linear energy transfer (LET), tissue type, biological endpoint, etc. Nevertheless, proton therapy practitioners continue to use the simplistic constant RBE due, in part, to the lack of reliable and accurate predictive RBE models (Paganetti et al. (2002)).

The LET, defined as the average energy transfer (ionization) per unit distance traveled by charged primary particles (ICRU (2011)), increases slowly at first and then exponentially near the end of proton range. It is shown that increased LET leads to increased RBE, especially at the end of range of protons (Wilkens and Oelfke (2004); Guan et al. (2015b)), where the RBE value can be 1.3 or higher at the Bragg peak and 1.6 or higher in the fall off region (in a few millimeters). Precautions in this respect have been taken into account in current proton treatment planning by avoiding the use of beams whose distal edge may end up in or close to a critical structures. In this way, the possible overshooting due to uncertainties in dose distributions and the resulting damage of high LET/RBE protons to healthy tissues could be prevented. However, this measure may prevent the selection

of potentially beneficial beam angles and could diminish the therapeutic value of proton therapy.

In passively scattered proton therapy (PSPT) and single field optimized intensity modulated proton therapy (SFO-IMPT), high LET protons at the distal edge of each beam are unavoidably placed in normal tissues just beyond the distal edges of target volumes. In multiple field optimized intensity modulated proton therapy (MFO-IMPT), denoted as IMPT hereafter, intensities of beamlets from all incident beams are simultaneously optimized to meet dosimetric requirements. IMPT thus has much higher degree of freedom for modulation than PSPT and SFO-IMPT. Previous studies have shown that highly modulated fields in IMPT can produce equivalent physical dose distributions but greatly different LET distributions (Grassberger and Paganetti (2011); Giantsoudi et al. (2013)). Therefore, in theory it is feasible for IMPT to produce satisfactory dose distributions while achieving desirable LET distributions, e.g., placement of high LET protons inside target volumes and away from critical normal tissues, guided by innovative planning or optimization techniques.

Although treatment planning and optimization methods that incorporate variable RBE of protons have been explored (Wilkens and Oelfke (2004); Frese et al. (2011)), they have not yet been implemented clinically. This may be due to the reluctance to accept the resulting physical dose (i.e., RBE of 1.1) distributions from such methods, which may not be consistent with conventional practice. However, recent clinical data have reported unforeseen normal tissue complications from proton treatments (Sabin et al. (2013); Gunther et al. (2015)) and their positive correlation with high LETs (Peeler et al. (2016)). Subsequently, considering the RBE dependence on LET in treatment planning while preserving the physical dose prescribed in current practice has been focused in recent studies (Bassler et al. (2010); Giantsoudi et al. (2013); Bassler et al. (2014); Fager et al. (2015); Unkelbach et al. (2016)). We will discuss these methods in the Discussion section.

The present study aimed to investigate the impact of incorporating LET criteria directly into IMPT optimization. Both dose and LET distributions could be optimized simultaneously in the proposed approach. Dose-averaged LET was used to indicate LET values in

this study. The goal of this optimization was set to not only produce satisfactory dose distributions but also to achieve reduced LET distributions (thus lower biologically effective dose distributions) in critical structures and increased LET in target volumes compared to plans created using conventional objectives.

5.2 Materials and Methods

5.2.1 LET-incorporated Optimization

The goal of LET-incorporated IMPT optimization in this study was to optimize dose and LET distributions simultaneously. The objectives and constraints on doses were consistent with those used in conventional IMPT optimization. The calculation and planning criteria of dose here implicitly included a RBE of 1.1, as in current clinical practice. The optimization of variable RBE was not within the scope of this study. The additive objectives of LET were, straightforwardly, maximization of LET in tumor targets and minimization of LET in critical tissues and normal tissues.

Given that $\mathbf{D}_{ij}$ and L_{ij} indicate the dose and LET contribution, respectively, from beamlet j to voxel i in unit intensity and w_j indicates the intensity of beamlet j, the total dose $\mathbf{D}_i$ and dose-averaged LET (LETd)L_i in voxel i are calculated as

$$\mathbf{D}_i = \sum_{j \in \mathcal{J}} D_{ij} w_j, \ \forall i \in \{\mathcal{T} \cup \mathcal{O}\},$$

$$L_i = \frac{\sum\limits_{j \in \mathcal{J}} D_{ij} L_{ij} w_j}{\sum\limits_{j \in \mathcal{J}} D_{ij} w_j}, \ \forall i \in \{\mathcal{T} \cup \mathcal{O}\}.$$

The calculation of $\mathbf{D}_{ij}$ and L_{ij} was carried out by a previously validated fast Monte Carlo system (Yepes et al. (2016)). Although LET is typically quantified in two averaging variants, i.e., track-averaged and dose-averaged LET (Grassberger and Paganetti (2011); Guan et al. (2015a)), only the latter was used in this study for consistency with most biological dosimetric analyses.

The general optimization model in radiation therapy including IMPT can be represented as follows in (5.2.1)-(5.2.3):

$$\min \quad f_D(\mathbf{w}) = ||\lambda_i(\mathbf{D}_i - \mathbf{D}_i^{pr})_+||_p \tag{5.2.1}$$

$$s.t.$$

$$LB_i \geq \mathbf{D}_i \leq UB_i \qquad \forall i \in \mathcal{T},\ and \tag{5.2.2}$$

$$\varphi, \mathbf{w} \geq \mathbf{0}. \tag{5.2.3}$$

The minimization cost function is formulated by the deviation between the delivered ($\mathbf{D}_i$) and prescribed ($\mathbf{D}_i^{pr}$) doses of each voxel. Also a priority factor (λ_i) is assigned to each voxel or structure in order to control the tradeoff between competing objectives. The lower and upper bounds of the doses are LB_i and UB_i, which are adjusted for different structures and specific applications. It has been established that quadratic (i.e., p=2) and linear (i.e., p=1) forms of the cost function (5.2.1) are effective in optimizing dose distributions for radiation therapy (Bortfeld (1999); Chan et al. (2006); Jia et al. (2011); Cao et al. (2013)). In this study, a linear cost function (5.2.4) was used for performing the conventional dose-based optimization (DoseOpt):

$$\begin{aligned} f_D(\mathbf{w}) = \frac{\lambda_T^+}{|\mathcal{T}|}||(\mathbf{D}_{i\in\mathcal{T}} - \mathbf{D}_{i\in\mathcal{T}}^{pr})_+||_1 + \frac{\lambda_T^-}{|\mathcal{T}|}||(\mathbf{D}_{i\in\mathcal{T}}^{pr} - \mathbf{D}_{i\in\mathcal{T}})_+ \\ ||_1 + \frac{\lambda_O}{|\mathcal{O}|}||(\mathbf{D}_{i\in\mathcal{O}} - \mathbf{D}_{i\in\mathcal{O}}^{max})_+||_1 + \frac{\lambda_N}{|\mathcal{N}|}||\mathbf{D}_{i\in\mathcal{N}}||, \end{aligned} \tag{5.2.4}$$

where $\mathcal{T}$, $\mathcal{O}$, $\mathcal{N}$ are the set of voxels in target volumes, organs at risk (OARs), and normal tissues, respectively. Optimization priority factors for penalizing over-dosing and under-dosing on target, OAR doses over the limit $\mathbf{D}_{i\in\mathcal{O}}^{max}$, and normal tissue doses are λ_T^+, λ_T^-, λ_O, and λ_N, respectively.

By adding two terms for maximizing dose-averaged LET in the target and minimizing it in OARs, the cost function for LET-incorporated optimization (LETOpt) was formulated

as shown in (5.2.5). The optimization priority factors for the two objectives are θ_T and θ_O.

$$f_L(\mathbf{w}) = f_D(\mathbf{w}) + \frac{\theta_T}{|\mathcal{T}|}||L_{i\in\mathcal{T}}||_1 + \frac{\theta_O}{|\mathcal{O}|}||L_{i\in\mathcal{O}}||_1. \tag{5.2.5}$$

Note that threshold LET values and objectives for normal tissue LETs were not used in this study, but they can be easily added for applications. Constraints on doses were identical in DoseOpt and LETOpt.

Solving the LET-incorporated optimization problem as formulated above essentially requires linear fractional programming (LFP) techniques, because the LET component in the cost function is a ratio of two linear questions, i.e., $\sum_{j\in\mathcal{J}} D_{ij}L_{ij}w_j$ and $\sum_{j\in\mathcal{J}} D_{ij}w_j$, with regard to the optimization variable w_j. Due to the linearity, the problem is quasiconvex and can be conveniently reformulated to a linear programming (LP) problem. Here we apply the Charnes and Cooper variable transformation (Charnes and Cooper (1962)) by defining the original variable w_j with two new variables x_j and t, e.g., $w_j = \frac{x_j}{t}$. Assuming $\mathbf{x} = \frac{\mathbf{w}}{(\mathbf{D}_i^T\mathbf{w})}$ and $t = \frac{1}{(\mathbf{D}_i^T\mathbf{w})}$ for our problem analogically, where $\mathbf{D}_i^T$ is the transposed dose contribution vector for voxel i for computing one objective term in a cost function like (5.2.5), an equivalent linear cost function can be formed as

$$f_L(\mathbf{x}) = f_D(\mathbf{x}) + \frac{\theta_T}{|\mathcal{T}|}||\sum_{j\in\mathcal{J}} D_{ij}L_{ij}x_j||_1 + \frac{\theta_O}{|\mathcal{O}|}||\sum_{j\in\mathcal{J}} D_{ij}L_{ij}x_j||_1. \tag{5.2.6}$$

The reformulated LP model of LETOpt thus has an optimization variable x_j, instead of the original beamlet intensity w_j, and an auxiliary variable t. Meanwhile, the dose constraints defined by w_j are changed to ones such as

$$tLB_i \leq \sum_{j\in\mathcal{J}} D_{ij}x_j \leq tUB_i, \forall i \in \mathcal{T} \text{ and} \tag{5.2.7}$$

$$x_j \geq 0. \tag{5.2.8}$$

After solving the reformulated LP for LETOpt, i.e., (5.2.6)-(5.2.8), and obtaining the optimal solution of x_j, the beamlet intensity can be post-processed using $w_j = \frac{x_j}{t}$ for the final dose and LETd calculation. In this study, both DoseOpt and LETOpt models were solved by the interior point method using a commercial solver CPLEX v12.3 (IBM, NY, USA).

5.2.2 Patients and Treatment Planning

Five brain tumor patients that had been treated with proton therapy (PSPT or SFO-IMPT) at our institution were selected for this study, including one glioblastoma, one anaplastic astrocytoma and three ependymoma cases. Although the tumor size and location varied from one patient to another, in all cases, one or more critical structures, e.g., brainstem or optic chiasm, were adjacent to or overlapped with gross target volumes (GTVs) and clinical target volumes (CTVs). The prescriptions to target volumes and field arrangements were the same as those used in the clinical treatments. The doses prescribed to all OARs are set to zero in optimization. Table 5.1 lists patient information and specific treatment planning parameters for the five patient cases.

Table 5.1: Patient information and treatment planning parameters.

Patient #	Type of Cancer	Prescription Dose (Gy/fx)	Number of Fractions	Number of Beams (non-coplanar)	OARs included in Optimization
1	Glioblastoma	2 (GTV) 1.67 (CTV)	30	2	Brainstem, Optic Chiasm, Rt Cochlea, Rt Optic Nerve, Brain
2	Anaplastic Astrocytoma	1.8 (GTV) 1.6 (CTV)	30	3	Brainstem, Optic Chiasm, Lt Cochlea, Lt Optic Nerve, Brain
3	Ependymoma	1.8 (GTV)	30	3	Brainstem, Optic Chiasm, Brain
4	Ependymoma	1.8 (GTV)	28	3	Brainstem, Optic Chiasm, Rt Cochlea, Rt Temp Lobe, Brain
5	Ependymoma	1.8 (GTV)	30	3	Brainstem, Rt Hippocampus, Spinal Cord, Brain

Two IMPT plans were created for each patient case, one using the conventional dose-based optimization and the other using the proposed LET-incorporated optimization. Each plan was based on 3D modulation delivery (Lomax (1999)). The intensities of all beamlets from all treatment fields were simultaneously and independently optimized, that is, MFO was applied. The simulation of plan delivery and dose/LET distributions was based on a discrete pencil beam scanning system commissioned at our institution (Gillin et al. (2010)).

It should be noted that all plans optimized by either DoseOpt or LETOpt were tailored to produce dose distributions as similar as possible to those of the previous clinical plans. If necessary, multiple optimization runs were performed as trial and error, with adjustment to criteria or priority factors, until the plans were reviewed and found to be acceptable. Our goal in this study was to investigate the impact of LET-incorporated optimization on the ability to manipulate LET distributions, not to improve dose distributions. The detailed results of the patient studies, i.e., primarily the dosimetric data, are discussed in the next section.

5.3 Results

Table 5.2 summarizes six key indices each of dose and LETd based on the IMPT plans optimized by DoseOpt and LETOpt for the five patient cases: dose and LETd for 1% and 99% of the GTV, the maximum of dose and LETd for the brainstem, dose and LETd that are exceeded in 0.1 cc of the brainstem, and the maximum and minimum of dose and LETd for the optic chiasm. There were only minor differences (at most 4% averaged over all five patients) in all dose indices between the DoseOpt and LETOpt plans. Meanwhile, there were pronounced differences in LETd. The maximum LETd and LETd to 0.1cc of the brainstem were reduced from DoseOpt to LETOpt by an average of 19.4% and 23.7%, respectively. The maximum and mean LETd for the optic chiasm were reduced by 21.1% and 21.9%, respectively, and the LETd for 1% and 99% of the GTV were increased by 27.2% and 18.4%.

Table 5.2: Dose (Gy) and Dose-averaged LET, i.e., LETd, ($keV/\mu m$) indices of the IMPT plans optimized by DoseOpt and LETOpt for five brain tumor patients. Max and mean values for dose and LETd are based on all voxels in corresponding structures, and the dose and LET to 0.1cc of the brainstem are reported. Dose and LETd to 1% and 99% of the GTV are also reported.

Patient #		Dose Optimization						LET Optimization					
		Brainstem		Chiasm		GTV		Brainstem		Chiasm		GTV	
		Max	0.1cc	Max	Mean	1%	99%	Max	0.1cc	Max	Mean	1%	99%
1	Dose	2.0	1.9	1.8	1.3	2.2	2.0	1.9	1.9	1.8	1.3	2.2	1.9
	LET	8.1	7.1	6.8	4.9	3.5	1.4	7.9	6.2	1.8	1.4	3.7	1.6
2	Dose	2.0	1.8	2.0	1.2	2.1	1.8	1.9	1.8	2.0	1.2	2.1	1.8
	LET	10.0	8.9	8.2	5.8	5.1	2.0	8.5	7.5	8.2	5.8	5.1	2.8
3	Dose	2.0	1.9	0.1	0.1	2.0	1.8	2.0	1.9	0.1	0.1	2.0	1.9
	LET	9.3	9.0	5.1	3.6	4.2	2.6	6.8	6.3	4.5	3.3	7.0	3.0
4	Dose	2.0	1.9	0.2	0.1	2.0	1.8	2.0	1.9	0.3	0.2	2.0	1.8
	LET	5.1	4.7	4.4	3.0	3.8	2.3	4.6	4.3	3.5	2.1	5.1	2.3
5	Dose	2.0	1.9	-	-	2.0	1.7	2.0	1.9	-	-	2.0	1.7
	LET	13.5	12.4	-	-	4.7	2.2	7.7	6.0	-	-	6.1	2.7

Plans optimized by DoseOpt and LETOpt for one glioblastoma case (Patient 1), are compared in Figure 5.1. Both the dose distributions and dose volume histograms (DVHs) confirmed that the doses generated by the DoseOpt and LETOpt plans were comparable for this case. In terms of LETd, as shown by LETd distributions and LETd volume histograms (LVHs), the sparing of the brainstem and the optic chiasm was significantly improved. For the optic chiasm, the max LETd was reduced from 6.8 $keV/\mu m$ to 1.8 $keV/\mu m$. However, the magnitude of the LETd increase in the GTV was not as pronounced as that of the LETd decrease in the brainstem or the optic chiasm. Another comparison is shown in Figure 5.2 for one of the ependymoma cases (Patient 3). The DoseOpt and LETOpt plans again had similar doses, although the DoseOpt plan was worse for sparing of the brainstem in the low-dose region than the LETOpt plan was. LETd hotspots in normal tissues and the brainstem were greatly reduced by LETOpt, and LETOpt plans had a larger area with high LETd distributed in the GTV and CTV than did DoseOpt plans. The DVHs and LVHs for three other patient cases are included in Appendix C.

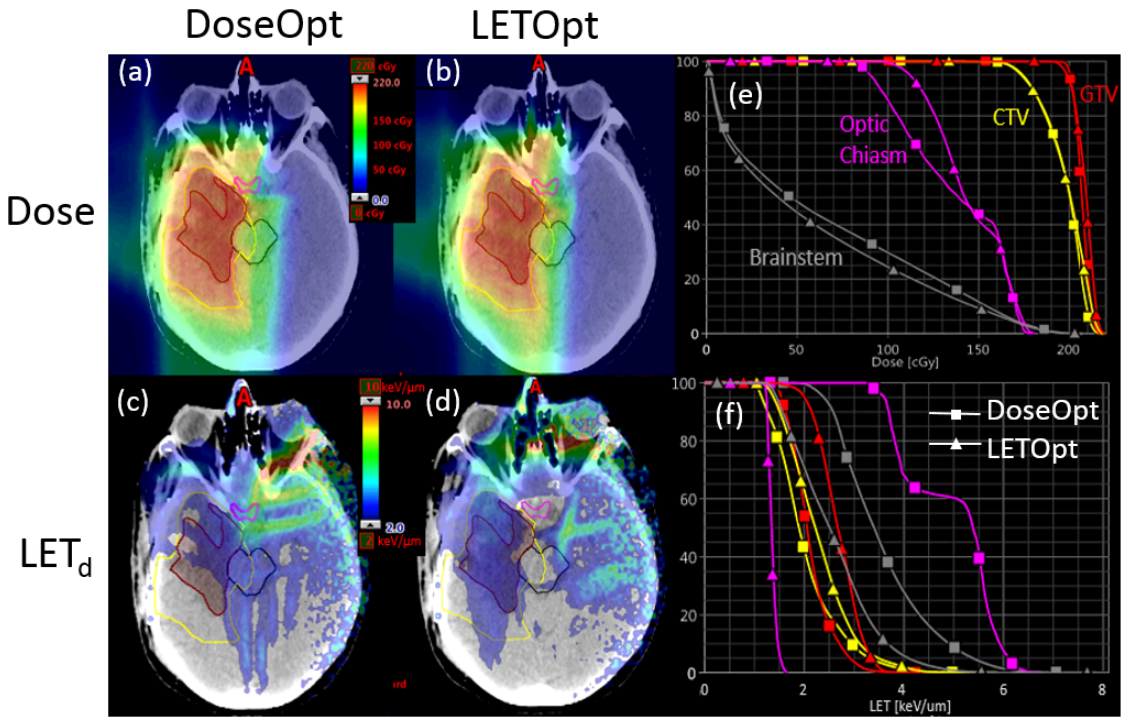

Figure 5.1: Comparison of DoseOpt and LETOpt plans for Patient 1. Panels (a) and (b) show dose distributions (based on a constant RBE of 1.1) for the DoseOpt and LETOpt plans. Panels (c) and (d) show dose-averaged LET distributions for the DoseOpt and LETOpt plans. Panels (e) and (f) are dose- and LET-volume histograms for the GTV (red contour), CTV (yellow contour), brainstem (black contour), optic chiasm (magenta contour).

Optimized plans for the Patient 3 as a representative case are further compared in DVHs and LVHs in Figure 5.2. One DoseOpt plan and two LETOpt plans (1 and 2) are shown and compared. The ratio of the optimization priority factor of the dose and LET objectives was set at one for the LETOpt plan 1 and ten for LETOpt plan 2. In other words, plan 1 was optimized with ten times less priority given to dose objectives, including ones for target volumes and critical normal tissues, than plan 2. For plan 1, although the brainstem was not well spared at low doses by LETOpt compared to DoseOpt, its exposure to high LETs was greatly reduced with a decrease of 3 $keV/\mu m$ from the maximum LETd. Note that the similar behavior was observed in Patient 4 and 5. For plan 2, the dose sparing of the brainstem was similar for LETOpt and DoseOpt, but the benefit of LET sparing could not be achieved as it was in plan 1. Pronounced increases of LETd in target volumes were

achieved by both LETOpt plans. However, the magnitude of increase was modestly lower for plan 2 than for plan 1 because higher optimization priority was given to dose instead of LET in plan 2. The choice between plan 1 and 2 in clinic should be determined by physician's preference on different metrics such as maximum or mean dose to brainstem, and boost in target dose, etc. We should note that the tradeoff effect between dose and LET metrics was observed in all patient cases, while its magnitude and sensitivity to changing optimization priorities varied among cases (as seen in examples shown in Figure 5.1, 5.2 and C.1).

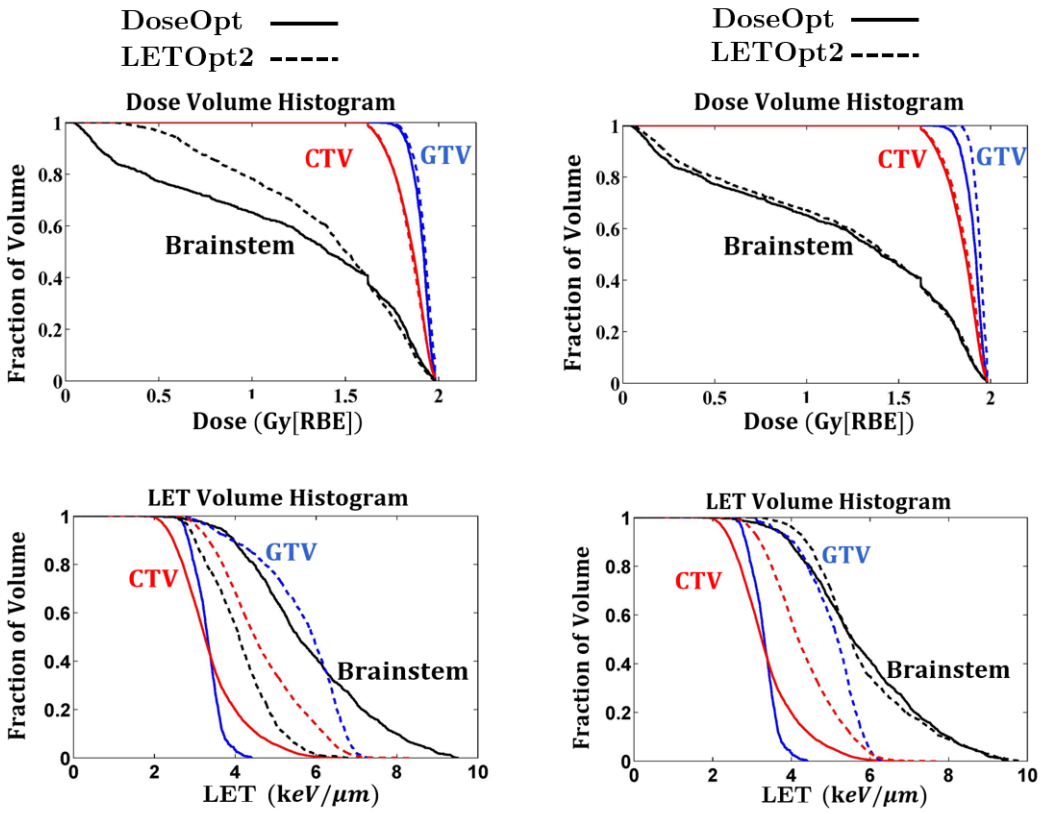

Figure 5.2: Dose (RBE=1.1) and dose-averaged LET volume histograms of the IMPT plans optimized by DoseOpt (solid lines) and LETOpt (dashed lines) for Patient 3. Two LETOpt plans (1 and 2) are shown here to illustrate the trade-off effect between dose and LET objectives. Each LETOpt plan is compared to the DoseOpt plan. The ratio of the optimization priority factor between the dose and LET objectives is 1 for the LETOpt plan 1 and 10 for the LETOpt plan 2.

5.4 Discussion

Proton therapy is increasingly accessible to cancer patients (Chang et al. (2014); Schuemann et al. (2014)). Continuous improvement of this cutting-edge technology, including treatment planning, will allow its theoretical benefits to be fully realized and its associated risks to be minimized. Currently, the biological uncertainties of protons remain a significant challenge to realize the full potential of proton therapy (Mitin and Zietman (2014)). Despite extensive ongoing research to better understand the biological effectiveness of protons and other heavy particles, including in vitro and in vivo animal studies as well as patient response analyses, a variable RBE model, especially one dependent on tissue type and clinical endpoint, has yet not been agreed upon for use in clinical treatment planning. From an alternative perspective, incorporation of LET in treatment planning assuming the dependence of RBE on LET, while ensuring no or minimal changes to the dose distributions used in current practice (with its simplistic constant RBE of 1.1), can be implemented straightforwardly and immediately in the clinic to benefit patients. At our center, we have begun evaluating the LET-incorporated optimization presented here in a clinical setting for selected patients and expect to generate LET-optimized plans together with conventionally optimized plans in the clinical routine for physicians to choose.

The present study demonstrated that the LET-incorporated IMPT optimization can create preferred dose-averaged LET distributions while maintaining satisfactory dose distributions. Optimization of LET, i.e., maximization in target volumes and minimization in critical normal tissues as shown in our patient studies, is expected to boost the differential benefits of increasing the biological effect of protons in tumor and/or reducing it in healthy tissues compared to the current standard for brain tumor cases. Within dose-exposed volumes, evaluation of LET can be used as another measure of plan quality, in addition to dose. Moreover, one can also choose to use radiobiological models as additional indicators of plan quality, such as the linear quadratic (LQ) cell survival model, tumor control probability (TCP), normal tissue complication probability (NCTP), and RBE models. For example, Figure 5.3 shows the DVHs from variable RBE-weighted doses based on a recently

published RBE model (McNamara et al. (2015)) for a representative case (Patient 1). This demonstrates that the LET-incorporated optimization not only increased the variable RBE-weighted dose for target volumes but also reduced it for critical structures compared to a plan conventionally optimized using constant RBE. Similar DVHs for other patient cases can be found in Appendix C.

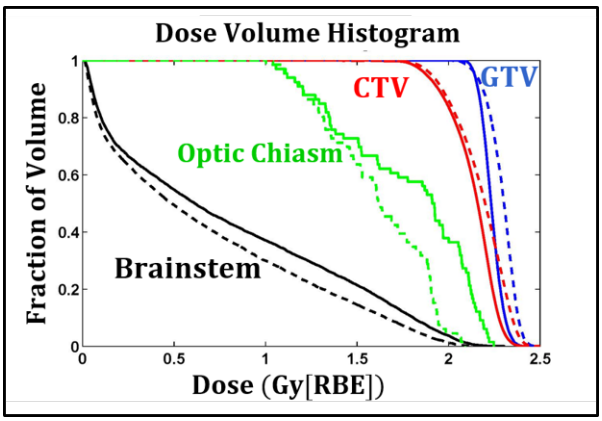

Figure 5.3: Dose volume histograms of the IMPT plans optimized by DoseOpt (solid lines) and LETOpt (dashed lines) for Patient 1. The RBE here is variable and calculated based on a recently published RBE model (McNamara et al., 2015). The required tissue parameters are obtained from literature (Frese et al., 2011).

LET painting approaches have been investigated for ion (Bassler et al. (2010, 2014)) and proton (Fager et al. (2015)) therapies, in which planning methods such as splitting targets or adopting opposite beam arrangements are used to allocate the high LET protons within target instead of normal tissues. However, those techniques may require greater effort in planning, quality assurance, and delivery than does the current practice because they use more planning volumes and beam angles. In contrast, incorporating LET directly into the optimization process may have certain practical advantages over the LET painting techniques and it could be easily implemented in clinical settings. Such an approach as presented in this work can adopt the same target volumes and beam arrangements that are used in conventional PSPT and IMPT treatment plans. Meanwhile, ideas in LET painting such as avoiding the distal edge in target boundary regions could be used to improve the benefits of LET-incorporated optimization.

One recent study discussed a multi criteria optimization approach in which a set of

IMPT plans were created using various dose based objectives and constraints, then plans with superior dose and LET distributions were selected (Giantsoudi et al. (2013)). While the advantage of this method is that multiple competing plans can be generated, the disadvantage is that the performance on finding improved LET distributions may be compromised because LET criteria are not included in optimization.

In another recent study, a two-step prioritized optimization approach was proposed: first a plan was optimized using conventional dose criteria, and, in the second step, the plan was optimized solely based on the product of LET and dose as a surrogate of variable RBE weighted dose with constraints to limit the change to physical dose distribution from the first step (Unkelbach et al. (2016)). Prioritized optimization may be an effective approach to managing the trade-off effect between dose and LET. However, the optimality of LET optimization may be affected by the local minimum problem in nonconvex optimization, as the second round of prioritized optimization uses a warm start. This is less of a problem for simultaneous optimization approaches such as the one proposed in this study. However, our approach has the drawback of requiring determination of good optimization priority factors to balance gains in dose and LET. The comparison of the effectiveness and efficiency of different optimization strategies is also of interest and will be an area of future study.

Our study confirms that the redistributed LET maps may compensate the cut of quality dose distributions achieved by IMPT (Unkelbach et al. (2016)). This was seen in Patient 3 and 5 where brainstem dose was increased in the LET optimized plans at the low dose region compared to the dose optimized plan. However, this is not always the case. For example, the LET optimized plan for Patient 1 in this study achieved a greatly improved LET distribution without degrading the physical dose distribution. The varying magnitude of the benefit of LET optimization may be attributed to patient anatomies and beam arrangements. The trade-off effect between dose and LET merits should be thoroughly investigated in future research. Methods such as multi-criteria optimization and beam angle optimization can be highly helpful in the search for superior dose and LET distributions.

5.5 Conclusion

In this study, a LET-incorporated IMPT optimization method was introduced. This method was able to produce clinically satisfactory dose distributions while increasing dose-averaged LET in target volumes and reducing it in critical normal tissues for five selected brain tumor patient cases. The clinical application of this method requires no changes to the current treatment protocols using a constant RBE and therefore has a potential to bring an immediate improvement to IMPT in enhancing tumor control and reducing normal tissue toxicities.

Chapter 6

Understanding Impacts of Radiobiological Parameters in Adaptive Radiation Treatment Planning under Setup Uncertainty

6.1 Introduction

Radiation therapy (RT) is administered to cancer patients to destroy cancer cells with minimum damage to healthy cells. Clinically, radiotherapy is usually delivered in multiple fractions over several weeks in such a way that achieves tumor control while enabling the repair of damage to normal tissues within the treatment area. In conventional RT, the treatment dose has been designed based on digital images acquired before the treatment begins. However, those treatment plans mostly ignore the dynamic nature of the inherent biological processes that take place during the course of treatment. With normal anatomical changes of both the tumor and healthy tissue during a 5- to 7-week course of radiation, relying solely on those images could lead to (1) underdosing the tumor and/or (2) unnecessary exposure of organs-at-risk (OARs) to higher radiation doses. Also, due to the uncertainties, the determination of radiation treatment plans for individual patients becomes a very complicated task. The effect of these uncertainties on the dose distribution should be mitigated appropriately to ensure that the right amount of dose is actually deposited in the tumor region and patients are treated safely.

One of the significant efforts in adaptive radiation radiotherapy (ART) has been to reduce the effects of treatment variations, such as beam placement errors and geometric variation of the therapy target and critical normal organs incurred in previous fractions

(Trofimov et al. (2005); Wu et al. (2008); Mohan et al. (2005); de la Zerda et al. (2007); Lu et al. (2006)). Recent advances have centered on using image guidance for ART to allow for treatment changes in radiation planning. The ART technique aims to customize each patient's treatment plan to patient-specific variation by evaluating and characterizing the systematic and random variations through image feedback and including them in adaptive planning. As a result, the overall patient outcome is improved by fractionating radiation treatments. This improvement may be explained in the case of the biological responses of tissue. The five R's (repair, repopulation, redistribution, reoxygenation, and radiosensitivity) are well-documented biological factors influencing the responses of tumors and normal tissues to fractionated treatment (Withers (1975); Steel et al. (1989)). Determining the response of cells and tissues to radiation and balancing them against one another has become one of the pillars of fractionation radiotherapy because it helps to maximize the therapeutic gain. Yet, the complexities of how radiation affects the underlying biological processes make it difficult to determine how, if at all, treatment planning should be redesigned. In fact, the potential for improvement of any fractionation scheme employing the impact of radiobiological factors on the outcome of treatments could be evaluated.

To this point, the theoretical advantage of ART for dosimetric and clinical parameters has been established in multiple studies (Juloori et al. (2015); Ghilezan et al. (2010); Wu et al. (2008); van de Schoot et al. (2017)). Within this line of research, various models have been developed in an attempt to describe and predict how the treatment plan will be adjusted to the biological changes (Ghate (2011); Hernández et al. (2013); Bortfeld et al. (2015); de la Zerda et al. (2007)). Ghate (2011) proposed a stochastic control framework to utilize the biological images and tumor response models in order to design an adaptive radiation treatment strategy. They attempted to incorporate response-uncertainties into the planning process to deliver the right dose to the right location at the right time. However, to effectively guide decisions their approach relies on how accurately the biological information can be gleaned from biological images. Bortfeld et al. (2015) provided a dynamic programming framework to determine the optimal fractionation schedule in the presence of

accelerated repopulation. Another study by de la Zerda et al. (2007) performed dynamic closed-loop control algorithms for ART to adjust the treatment plan to the changing geometry and delivered dose. Recently, Nohadani and Roy (2017) provided a general robust optimization framework that incorporates changes in cell oxygenation due to the radiation during the treatment. In these studies, the normal tissue response and its effects on designing a treatment plan have not been well addressed, since the main goal of their model was to remove the tumor cells with certainty. Moreover, the patient needs to be set up on the treatment couch in the exact same position for each treatment session. Due to the repeated positioning of patients, the actual and planned position of the patient with respect to the treatment can differ between each visit. So, uncertainties inherent in setting up the treatment plans is also another factor that needs to be considered while adapting the plans.

Therefore, there is a need to determine the adapted treatment plan considering the biological responses of the tumor and normal tissues to radiation. This study focuses on the tumor repopulation and repair of normal cells during treatment among those five radiaobiological factors. In particular, repair is a major factor in the response of nearly all tissues. Studies show that such tissues appear to have a higher repair capacity than tumors (Khaled and Held (2012)), which supports the fractionated treatments scheme. However, prolonging treatments over a long interval may be counterproductive since proliferation and repopulation of the surviving tumor cells will occur during the treatment.

In this research, the biological response of the tumor and healthy cells (repopulation and repair) are characterized by volume changes, since this is the important predictor of the treatment outcome (Bralcet et al., 2009). Many applications of the mathematical modeling of tumor growth as a function of time have been proposed. A simple linear model for describing the tumor growth was developed by Nieves and Ubriaco (2015) under the assumption that the tumor is in untreated environments. They show the importance of considering tumor growth or shrinkage in the radiation therapy treatment planning. Furthermore, Huang et al. (2010) presented the details of the kinetic model, and they utilized it to analyze the tumor regression data, estimate the tumor radiosensitivity, and

time for resolving dead cells for individual patients.

We present a biologically-based treatment planning model to examine the biological effects in terms of changes in size of the tumor and organs-at-risks (OARs) under setup uncertainty. We optimize the prescribed dose in each treatment considering those two important factors. One indicates a relationship between the biological effects of tumor repopulation that occurs during the treatment and an appropriate target dose. Meanwhile, by incorporating the biological effects of healthy cells, another relationship between a safe treatment dose and the repair of radiation damage during a treatment can be obtained. In this regard, a deformation in size of the target and surrounding healthy tissues are determined, and the next treatment is optimized by incorporating the updated volumetric changes and the clinical dose requirements.

To handle the setup uncertainty in our study, we use the chance-constrained programming (CCP) approach developed for radiation therapy framework (Zaghian et al. (2018)) in a biologically-based treatment planning optimization model to overcome the conservativeness of worst-case robust optimization model (Casiraghi et al. (2013); Fredriksson and Bokrantz (2014)) that are commonly used for incorporating uncertainties in treatment planning optimization problems (Pflugfelder et al. (2008); Liu et al. (2012b); Fredriksson et al. (2011)). Using this method, we design the fractionation radiation scheme under setup uncertainty in which the treatment plan can be optimized considering the best compromise between the radiobiological effects on the tumor and healthy tissues over time in a treatment planning process. Accordingly, for each treatment, reasonable confidence levels can be determined according to the decision preference on a specific cancer case. Our goal is to investigate whether the current fractionation scheme for the treatment of clinical cancer cases with radiation is optimal or could be improved. We investigate the circumstances under which these optimal schedules result in a significant improvement over current treatments for three clinical prostate cases.

The main contributions of the following methodology are summarized bellow:

- We propose a biologically-based treatment planning model that not only allows for

the correction of patient setup error, but also allows dose recalculation and adaptive radiation therapy (ART) using the volumetric information to adjust the treatment plan of each fraction to the updated patient anatomy.

- In this study, a direct re-optimized treatment plan can be determined on a slower time-scale than employing imaging information for clinical implementation of on-line and off-line ART. Thus, considering the patient wait time and treatment duration limitations, our model performs well.

- To make the treatment planning process clinically practical, the tumor volume was modified every few fractions (in 7 fractions or once a week).

- Using real patient data, we analyze the CCP biologically-based treatment planning model to determine whether there is a dosimetric advantage in adapting the treatment delivery to compensate for the reduction in the tumor volume.

6.2 Proposed methodology and formulations

In treatment planning, we aim to deliver the prescribed dose to the target while minimizing the dose to adjacent healthy tissue. Within this goal, ART plan refers to a method of treating cancer when the total dose of radiation is divided into several smaller doses over a period of several days. Table 6.1 summarizes the parameters and variables definitions.

The total amount of dose delivered to voxel i in fraction k can be calculated as

$$\mathbf{D}_i^k(\mathbf{w}) = \sum_{j \in \mathcal{J}} d_{ij}^k w_j^k = (\mathbf{d}_i' \mathbf{w})^k, \ \forall i \in \{\mathcal{T} \cup \mathcal{OAR}\}, \forall k \in \mathcal{K},$$

where $\mathbf{d}_i$ represents the dose contribution from all beamlets to voxel i and $\mathbf{w}$ illustrates the intensity of beamlets.

Table 6.1: Input parameters and variables for radiation treatment planning models

Parameter	Definition[1]
$\mathcal{T}$	A set of voxels in the planning target volume (PTV or target)
$\mathcal{OAR}$	A set of voxels in the organ-at-risk
$\mathcal{J}$	A set of all beamlets
$\mathcal{K}$	Number of fractions
θ_L ,θ_U	Lower (L) and Upper (U) control limit on the target
φ	Upper control limit on the organ-at-risk
λ_T^+	Penalty coefficient for hot spots on the target
λ_T^-	Penalty coefficient for cold spots on the target
λ_{OAR}	Penalty coefficient for hot spots on the organs-at-risk
λ_T	Penalty coefficient for survival rate of the target
λ_H	Penalty coefficient for survival rate of the organs-at-risk
α_T^+	Risk level for having hot spots on the target
α_T^-	Risk level for having cold spots on the target
α_{OAR}^+	Risk level for having hot spots on the organs-at-risk
α_T^-	Risk level for controlling the survival rate of the target
α_H^+	Risk level for controlling the survival rate of the organs-at-risk
d_{ij}^k	Dose contributed by the j^{th} beamlet to voxel i per unit weight in fraction k
t_k	Resting time between each fraction
τ_g	Tumor repoulation time (doubling time)
τ_o	Time for normal cells to repair
Variables	**Definition**
w_j^k	Intensity of beamlet $j \in \mathcal{J}$ in fraction k
θ_L^k, θ_U^k	Lower and upper control limit on the target in fraction k
φ^k	Upper control limit on the organs-at-risk in fraction k
$\mathbf{D}_i^k(\mathbf{w})$	Total amount of dose delivered in fraction k by voxel i

6.2.1 The radiobilogical basis for the development of treatment

The idea of dividing a treatment into multiple stages with a rest period of typically one day between two sessions has been around for a long time, as it is called the fractionation radiotherapy. The most common argument for this method is the better preservation of healthy tissue due to faster regeneration capability compared to tumors in the rest period. Thus, to accurately quantify the relative amount of dose observed in each fraction of RT, it is important to biologically adapt the treatment plan to the cell survival models for tumors and normal tissues. In this section, we developed a model not only to control the significant

[1] A cold spot is a portion of tissue that receives less than the desired radiation dose, and a hot spot is a portion of tissue that receives a dose higher than the desired dose

tumor shrinkage or proliferation during the gap period but also to take advantage of the repair capability of healthy cells during the treatment.

6.2.1.1 Tumor Repopulation

Let $|\mathcal{K}|$ be the number of the entire treatment sessions and $k \in \mathcal{K}$ is an index representing individual treatment sessions, and s_k denotes the number of viable tumor cells at the beginning of therapy stage k. Thus, the number of viable tumor cells at the next stage is given by (Unkelbach et al. (2014)):

$$r_{k+1} = \frac{s_{k+1}}{s_k} = e^{(-\delta_i^k \mathbf{D}_i^k(\mathbf{w}))}\, e^{(t_k/\tau_g)}, \quad \forall k \in \mathcal{K}, \forall i \in \mathcal{T}, \tag{6.2.1}$$

in which $\delta_i^k = \alpha_0(1 + \mathbf{D}_i^k(\mathbf{w})/(\alpha_0/\beta_0)), \forall k \in \mathcal{K}, \forall i \in \mathcal{T}$, is an effective radio-sensitivity parameter.

The first part of equation (6.2.1) refers to the radiation effect on the tumor, which is described by exponential cell kill such that the surviving fraction of tumor cells after irradiation is given by $e^{\delta^k \mathbf{D}_i^k}, \forall i \in \mathcal{T}$. The second exponential function ($e^{(t_k/\tau_g)}$) describes the proliferation of the surviving tumor cells after the k^{th} treatment session. It means that after a time t_k, the number of active tumor cells increases by a factor of $e^{(t_k/\tau_g)}$, where τ_g is the time constant for tumor repopulation. Differences in fractionation response between tissues (Withers et al. (1983)) are quantified through differences in the ratio of parameters α_0 and β_0, and this ratio (α_0/β_0) can be obtained from clinical data (Pedicini et al. (2013)), which is beyond the scope of this paper.

In general, for tumors with a high α/β ratio, fractionated radiation therapy (FRT) results in a better therapeutic ratio than the single session therapy, because it spares more healthy tissues through repair of sublethal damage, because of the repopulation of cells between fractions, and because of increased tumor damage through reoxygenation and redistribution of tumor cells.

6.2.1.2 Repair of healthy cells

In addition to the repopulation, the repair of cellular damage between treatment sessions is the primary mechanism underlying the clinical observation that a larger total dose can be tolerated when the radiation dose is fractionated. During the resting time of fractionation treatment planning, healthy tissues can repair themselves. Repair of radiation damage is a complex mechanism which is a function of radiation dose and resting time. The continuous increase of cell survival with declining dose rate is consistent with the role of time in repair. Accordingly, maximizing sparing of healthy cells around the target could beneficially prevent patients from having side effects. Equation (6.2.2) shows the ratio of active cells after the k^{th} treatment session.

$$h_{k+1} = \frac{o_{k+1}}{o_k} = \ e^{(-\delta_i^k \mathbf{D}_i^k(\mathbf{w}))}\ e^{(t_k/\tau_O)}, \quad \forall k \in \mathcal{K}, \forall i \in \mathcal{OAR}, \tag{6.2.2}$$

in which, τ_O is the parameter showing time for healthy tissues recovery, and o_k denotes the number of healthy cells that survive radiation. The radio sensitivity parameter δ_i^k is:

$$\delta_i^k = \alpha_0^{'}(1 + \mathbf{D}_i^k(\mathbf{w})/(\alpha_0^{'}/\beta_0^{'})), \quad \forall k \in \mathcal{K}, \forall i \in \mathcal{OAR}.$$

In fact, $\mathbf{D}_i^k(\mathbf{w}), \forall i \in \{\mathcal{T} \cup \mathcal{OAR}\}$ is a random variable ($\tilde{\mathbf{D}}_i^k(\mathbf{w})$) which makes the constraints (6.2.1) and (6.2.2) probabilistic constraints. As a result, in order to simplify the inequalities (6.2.1) and (6.2.2), we apply the logarithm of each side of the equations as:

$$\ln r_{k+1} = -\delta_i^k \tilde{\mathbf{D}}_i^k(\mathbf{w}) + (t_k/\tau_g), \quad \forall k \in \mathcal{K}, \forall i \in \mathcal{T} \ and \tag{6.2.3}$$

$$\ln h_{k+1} = -\delta_i^k \tilde{\mathbf{D}}_i^k(\mathbf{w}) + (t_k/\tau_O), \quad \forall k \in \mathcal{K}, \forall i \in \mathcal{OAR}. \tag{6.2.4}$$

6.2.1.3 Dose escalation and tumor volumetric changes

The problem of interest then is to determine the amount of prescribed dose required for the next treatment that counters the effects of volumetric changes in tumor and healthy cells due to the radiation.

In this regard, expressions (6.2.3) and (6.2.4) could be used to update the plan for the next treatment. We assume that there is a linear relation between the amount of dose that needs to be delivered for the rest of treatment and the number of cancer cells that are remained in situ ($\sum_{n=k}^{|\mathcal{K}|}\theta^n \sim s_k$). Having the same relation for each fraction:

$$\begin{aligned}
\sum_{n=2}^{|\mathcal{K}|}\theta^n &= \nu\sum_{n=1}^{|\mathcal{K}|}\theta^n\ (\frac{s_2}{s_1}),\\
&\vdots\\
\sum_{n=k}^{|\mathcal{K}|}\theta^n &= \nu\sum_{n=k-1}^{|\mathcal{K}|}\theta^n\ (\frac{s_k}{s_{k-1}}), \quad \forall k\in\mathcal{K},\\
&\vdots\\
\sum_{n=K-1}^{|\mathcal{K}|}\theta^n &= \nu\sum_{n=|\mathcal{K}|}^{|\mathcal{K}|}\theta^n\ (\frac{s_{|\mathcal{K}|}}{s_{|\mathcal{K}|-1}}).
\end{aligned}$$

By putting all of the above equations together, the amount of prescribed dose in each stage k can be achieved by:

$$\sum_{n=k+1}^{|\mathcal{K}|}\theta^n = \nu\sum_{n=k}^{|\mathcal{K}|}\theta^n\ (\frac{s_{k+1}}{s_k}), \quad \forall k\in\mathcal{K}, \tag{6.2.5}$$

where ν is a relative coefficient. We obtain parameter ν from Equation (6.2.5) and consider the same amount of prescribed dose for each treatment ($\theta^0 = \theta^1 = ... = \theta^{|\mathcal{K}|}$) as the conventional treatment planning which means that for the two consecutive fractions, k and $k+1$, $\frac{\sum_{n=k+1}^{N}\theta^n}{|\mathcal{K}|-k+1} = \frac{\sum_{n=k}^{|\mathcal{K}|}\theta^n}{|\mathcal{K}|-k}$. Thus, Equation (6.2.5) can be reformulated as

$$\frac{|\mathcal{K}|-k+1}{|\mathcal{K}|-k} = \nu(\frac{s_{k+1}}{s_k}), \quad \forall k\in\mathcal{K}.$$

Using the survival rate equation (6.2.1) we can obtain parameter ν and update Formulation (6.2.5) as:

$$\sum_{n=k+1}^{|\mathcal{K}|}\theta^n = e^{(\sum_k \delta'\mathbf{d}')-\sum_k(t_k/\tau_g)}(\frac{|\mathcal{K}|-k}{|\mathcal{K}|-k+1})\sum_{n=k}^{|\mathcal{K}|}\theta^n\ (\frac{s_{k+1}}{s_k}), \quad \forall k\in\mathcal{K},$$

in which d' is a constant 2 Gy amount of dose and δ' can be calculated from $\delta' = \alpha_0 + 2\beta_0$.

6.2.2 Biologically-based plan optimization model

To optimize the amount of prescribed dose in each fraction of multi-stage treatment planning, we will have:

$$\min_{w_j^k, \theta_L^k, \theta_U^k, \varphi^k, r_k, h_k} \quad -\lambda_T^- \theta_L^k + \lambda_T^+ \theta_U^k + \lambda_{OAR}^+ \varphi^k + \lambda_T \sum_{k \in \mathcal{K}} r_k - \lambda_H \sum_{k \in \mathcal{K}} h_k \tag{6.2.6}$$

$s.t.$

$$\mathbf{D}_i^k(\mathbf{w}) \geq \theta_L^k, \qquad \forall k \in \mathcal{K}, \forall i \in \mathcal{T}, \tag{6.2.7}$$

$$\mathbf{D}_i^k(\mathbf{w}) \leq \theta_U^k, \qquad \forall k \in \mathcal{K}, \forall i \in \mathcal{T}, \tag{6.2.8}$$

$$\mathbf{D}_i^k(\mathbf{w}) \leq \varphi^k, \qquad \forall k \in \mathcal{K}, \forall i \in \mathcal{OAR}, \tag{6.2.9}$$

$$-\delta_i^k \mathbf{D}_i^k(\mathbf{w}) + (t_k/\tau_g) \leq \ln r_{k+1}, \qquad \forall k \in \mathcal{K}, \forall i \in \mathcal{T}, \tag{6.2.10}$$

$$-\delta_i^k \mathbf{D}_i^k(\mathbf{w}) + (t_k/\tau_O) \geq \ln h_{k+1}, \qquad \forall k \in \mathcal{K}, \forall i \in \mathcal{OAR}, \tag{6.2.11}$$

$$\delta_i^k = \beta_0 \, \theta^K + \alpha_0, \qquad \forall k \in \mathcal{K}, \forall i \in \mathcal{T}, \tag{6.2.12}$$

$$\delta_i^k = \beta_0^{'} \, \varphi^K + \alpha_0^{'}, \qquad \forall k \in \mathcal{K}, \forall i \in \mathcal{OAR}, \tag{6.2.13}$$

$$\theta^k = \nu \sum_{n=k}^{|\mathcal{K}|} \theta^n \ (r_{k+1}), \tag{6.2.14}$$

$$\theta_L^k \leq \theta^k \leq \theta_U^k, \qquad \forall k \in \mathcal{K}, \tag{6.2.15}$$

$$\sum_{k=1}^{|\mathcal{K}|} \theta_L^k \geq \theta_L \ , \ \sum_{k=1}^{|\mathcal{K}|} \theta_U^k \leq \theta_U \ , \ \sum_{k=1}^{|\mathcal{K}|} \varphi^k \leq \varphi, \ and \tag{6.2.16}$$

$$r_{k+1}, h_{k+1}, \mathbf{w} > 0, \tag{6.2.17}$$

where, λ_T^-, λ_T^+, λ_{OAR}, λ_T, and λ_H are penalty coefficients for cold spots on the target, hot spots on the target, hot spots on the organs-at-risk (OARs), ratio of viable tumor cells and healthy cells in each stage k, respectively. θ_L^1, θ_U^1, and φ^1 are given for the first stage.

Our strategy heavily exploits the following facts:

Theorem 6.2.1. Let s_k and $s_k^{'}$ be the tumor volume after k number of equal dose fractionation $\hat{d}$ and variable dose fractionation $\hat{d} + \theta_i, |\theta_i| \leq \hat{d}, k = \{0, \cdots, |\mathcal{K}|\}$. If $\sum_{i=1}^{|\mathcal{K}|} \hat{d} + \theta_i =$

$\sum_{i=1}^{|\mathcal{K}|} \hat{d}$, then

$$\frac{s_k^{'}}{s_k} = e^{-\beta_0(\sum_i^{|\mathcal{K}|} \theta_i^2)} \leq 1, \forall k \in \mathcal{K}, \forall i \in \mathcal{T},$$

which means that the variable dose fractionation performs better than the equal dose fractionation in terms of tumor coverage.

Proof. Let $\hat{d} + \theta_i \geq 0$ be the variable dose fractionation, where $\sum_i^{|\mathcal{K}|} \theta_i = 0$. From the survival rate equation, (6.2.1), the volume of the tumor at the end of the treatment ($|\mathcal{K}|$ fractions) can be calculated as:

$$s_{|\mathcal{K}|}^{'} = s_0 \; e^{-\sum_{i=1}^{|\mathcal{K}|}(\alpha_0(\hat{d}+\theta_i)+\beta_0(\hat{d}+\theta_i)^2)} \; e^{|\mathcal{K}|(t_k/\tau_g)},$$

where

$$\sum_{i=1}^{|\mathcal{K}|}(\alpha_0(\hat{d}+\theta_i)+\beta_0(\hat{d}+\theta_i)^2) = \alpha_0 \sum_i \hat{d} + \alpha_0 \sum_i \theta_i + \beta_0 \sum_i \hat{d}^2 + \beta_0 \sum_i \theta_i^2 + 2\beta_0 \sum_i \hat{d}\theta_i.$$

Considering $\sum_i^{|\mathcal{K}|} \theta_i = 0$, equation above can be reformulated as:

$$\sum_{i=1}^{|\mathcal{K}|}(\alpha_0(\hat{d}+\theta_i)+\beta_0(\hat{d}+\theta_i)^2) = \alpha_0 \sum_i \hat{d} + \beta_0 \sum_i \hat{d}^2 + \beta_0 \sum_i \theta_i^2,$$

$$= |\mathcal{K}|\alpha_0\hat{d} + |\mathcal{K}|\beta_0\hat{d}^2 + \beta_0 \sum_i \theta_i^2.$$

So, we will have:

$$s_{|\mathcal{K}|}^{'} = s_0 e^{-|\mathcal{K}|(\alpha_0\hat{d}+\beta_0\hat{d}^2)} e^{-\beta_0(\sum_i^{|\mathcal{K}|} \theta_i^2)} e^{|\mathcal{K}|(t_k/\tau_g)},$$

which arrives at the relation:

$$\frac{s_{|\mathcal{K}|}^{'}}{s_{|\mathcal{K}|}} = e^{-\beta_0(\sum_i^{|\mathcal{K}|} \theta_i^2)} \leq 1.$$

Theorem 6.2.2. Consider $\hat{d}+\theta_i, |\theta_i| \leq \hat{d}, i = \{0, \cdots, |\mathcal{K}|\}$ to be the amount of dose received

in each fraction of RT, such that

$$\hat{d} + \theta_i \geq 0, \sum_{i}^{|\mathcal{K}|} \theta_i = 0,$$

then, the equal amount of dose fractionation to produce either approximately the same final results as the variable dose fractionation, $\hat{d} + \theta_i$, with regard to the surviving tumor will be:

$$\hat{d}^{'} = \frac{-\alpha_0 + \sqrt{\Delta}}{2\beta_0},$$

where

$$\Delta = \alpha_0^2 + 4\beta_0(\alpha_0 + \beta_0 \hat{d}^2 + \beta_0 \frac{\sum_i \theta_i^2}{N}).$$

Proof. Let $d + \theta_i \geq 0$ be the variable dose fractionation and $d^{'}$ be the amount of equal dose fractionation resulting in a same tumor coverage as variable dose fractionation. Thus, we have:

$$s_N = s_N^{'}.$$

From equation (6.2.1):

$$s_0 \ e^{-N(\alpha_0 \hat{d}^{'} + \beta_0 {d^{'}}^2)} \ e^{N(t_k/\tau_g)} = \ s_0 \ e^{-N(\alpha_0 \hat{d} + \beta_0 \hat{d}^2)} e^{-\beta_0 (\sum_i^N \theta_i^2)} \ e^{|\mathcal{K}|(t_k/\tau_g)}. \quad (6.2.18)$$

We can simplify Equation (6.2.18) by removing the similar parameters from each side of the equality:

$$e^{-|\mathcal{K}|(\alpha_0 \hat{d}^{'} + \beta_0 \hat{d}^{'2})} = \ e^{-|\mathcal{K}|(\alpha_0 \hat{d} + \beta_0 \hat{d}^2)} e^{-\beta_0 (\sum_i^{|\mathcal{K}|} \theta_i^2)}.$$

By making Logarithm from each side of the equality, we have:

$$|\mathcal{K}|(\alpha_0 \hat{d}^{'} + \beta_0 \hat{d}^{'2}) = \ |\mathcal{K}|(\alpha_0 \hat{d} + \beta_0 \hat{d}^2) + \beta_0 (\sum_{i}^{|\mathcal{K}|} \theta_i^2),$$

which could be simplified as the following equation:

$$\alpha_0 \hat{d}' + \beta_0 \hat{d}'^2 = \alpha_0 \hat{d} + \beta_0 \hat{d}^2 + \beta_0 \frac{\sum_i^{|\mathcal{K}|} \theta_i^2}{|\mathcal{K}|}.$$

Thus, we will have the quadratic formulation as:

$$\beta_0 \hat{d}'^2 + \alpha_0 \hat{d}' - (\alpha_0 \hat{d} + \beta_0 \hat{d}^2) - \beta_0 \frac{\sum_i^{|\mathcal{K}|} \theta_i^2}{|\mathcal{K}|} = 0.$$

Considering that $\hat{d}' \geq 0$, the solution to the quadratic equation above will be:

$$\hat{d}' = \frac{-\alpha_0 + \sqrt{\Delta}}{2\beta_0},$$

where $\Delta = \alpha_0^2 \hat{d}' + 4(\beta_0)((\alpha_0 \hat{d} + \beta_0 \hat{d}^2) + \beta_0 \frac{\sum_i^{|\mathcal{K}|} \theta_i^2}{|\mathcal{K}|}) \geq 0$.

Theorem 6.2.3. Let $O_{|\mathcal{K}|}$ and $O'_{|\mathcal{K}|}$ be the number of voxels in OARs after N number of equal dose fractionation $\hat{d}$ and variable dose fractionation $\hat{d} + \theta_i, i = \{0, \cdots, |\mathcal{K}|\}$, respectively. If $\sum_{i=1}^{|\mathcal{K}|} \hat{d} + \theta_i = \sum_{i=1}^{N} \hat{d}$, then

$$\frac{O'_{|\mathcal{K}|}}{O_{|\mathcal{K}|}} = e^{-\beta_0'(\sum_i^{|\mathcal{K}|} \theta_i^2)} \leq 1,$$

which shows that the outcome of a treatment plan with an equal amount of fractionation dose will be better in terms of sparing the healthy cells.

Proof. The proof of this theorem is a minor modification of the proof of Theorem 6.2.1.

The theorems above show that to have a successful treatment plan in terms of both tumor coverage and sparing of nearby healthy tissues, a strategy needs to be developed considering the trade-offs between an equal amount of dose and variable amount of radiation.

6.2.3 CCP biologically-based plan optimization

By putting the probabilistic equations under the limitations of RT treatment, the chance constraints for controlling the amount of dose in each fraction can be formulated. Next, we can express the physical dose constraints in a CCP framework by introducing a confidence level (α) and enforcing the constraint in probability as described in (Zaghian et al. (2018)):

$$P\{\tilde{\mathbf{D}}_i^k(\mathbf{w}) \geq \theta_L^k\} \geq 1 - \alpha_T^-, \qquad \forall k \in \mathcal{K}, \forall i \in \mathcal{T}, \tag{6.2.19}$$

$$P\{\tilde{\mathbf{D}}_i^k(\mathbf{w}) \leq \theta_U^k\} \geq 1 - \alpha_T^+, \qquad \forall k \in \mathcal{K}, \forall i \in \mathcal{T}, \ and \tag{6.2.20}$$

$$P\{\tilde{\mathbf{D}}_i^k(\mathbf{w}) \leq \varphi^k\} \geq 1 - \alpha_{OAR}^+, \quad \forall k \in \mathcal{K}, \forall i \in \mathcal{OAR}, \tag{6.2.21}$$

where $1 - \alpha_T^-$, $1 - \alpha_T^+$, and $1 - \alpha_{OAR}^+$ are the confidence levels for avoiding cold spots and hot spots on target voxels and sparing the organs-at-risk, respectively.

Similarly, we can convert the biological dose constraints to the following chance constraints:

$$P\{-\delta_i^k \tilde{\mathbf{D}}_i^k(\mathbf{w}) + (t_k/\tau_g) = \ln r_{k+1}\} \geq 1 - \alpha_T, \quad \forall k \in \mathcal{K}, \forall i \in \mathcal{T} \ and \tag{6.2.22}$$

$$P\{-\delta_i^k \tilde{\mathbf{D}}_i^k(\mathbf{w}) + (t_k/\tau_O) = \ln h_{k+1}\} \geq 1 - \alpha_H, \quad \forall k \in \mathcal{K}, \forall i \in \mathcal{OAR}, \tag{6.2.23}$$

where $1 - \alpha_T$ and $1 - \alpha_H$ are the confidence levels for the probabilistic constraints above.

Then, the CCP biologically-based treatment planning model can be formulated as follows:

$$\min_{w_j^k, \theta_L^k, \theta_U^k, \varphi^k, r_k, h_k} \quad -\lambda_T^- \theta_L^k + \lambda_T^+ \theta_U^k + \lambda_{OAR}^+ \varphi^k + \lambda_T \sum_{k \in \mathcal{K}} r_k - \lambda_H \sum_{k \in \mathcal{K}} h_k \tag{6.2.24}$$

$s.t.$

$$P\{\tilde{\mathbf{D}}_i^k(\mathbf{w}) \geq \theta_L^k\} \geq 1 - \alpha_T^-, \qquad \forall k \in \mathcal{K}, \forall i \in \mathcal{T}, \tag{6.2.25}$$

$$P\{\tilde{\mathbf{D}}_i^k(\mathbf{w}) \leq \theta_U^k\} \geq 1 - \alpha_T^+, \qquad \forall k \in \mathcal{K}, \forall i \in \mathcal{T}, \tag{6.2.26}$$

$$P\{\tilde{\mathbf{D}}_i^k(\mathbf{w}) \leq \varphi^k\} \geq 1 - \alpha_{OAR}^+, \qquad \forall k \in \mathcal{K}, \forall i \in \mathcal{OAR}, \tag{6.2.27}$$

$$P\{-\delta_i^k \tilde{\mathbf{D}}_i^k(\mathbf{w}) + (t_k/\tau_g) \leq \ln r_{k+1}\} \geq 1 - \alpha_T, \quad \forall k \in \mathcal{K}, \forall i \in \mathcal{T}, \tag{6.2.28}$$

$$P\{-\delta_i^k \tilde{\mathbf{D}}_i^k(\mathbf{w}) + (t_k/\tau_O) \geq \ln h_{k+1}\} \geq 1 - \alpha_H, \ \forall k \in \mathcal{K}, \forall i \in \mathcal{OAR}, \tag{6.2.29}$$

$$\delta_i^k = \beta_0 \, \theta^K + \alpha_0, \qquad \forall k \in \mathcal{K}, \forall i \in \mathcal{T}, \tag{6.2.30}$$

$$\delta_i^k = \beta_0^{'} \, \varphi^K + \alpha_0^{'}, \qquad \forall k \in \mathcal{K}, \forall i \in \mathcal{OAR}, \tag{6.2.31}$$

$$\theta^k = \nu \sum_{n=k}^{|\mathcal{K}|} \theta^n \ (r_{k+1}), \tag{6.2.32}$$

$$\theta_L^k \leq \theta^k \leq \theta_U^k, \qquad \forall k \in \mathcal{K}, \tag{6.2.33}$$

$$\sum_{k=1}^{|\mathcal{K}|} \theta_L^k \geq \theta_L \ , \ \sum_{k=1}^{|\mathcal{K}|} \theta_U^k \leq \theta_U \ , \ \sum_{k=1}^{|\mathcal{K}|} \varphi^k \leq \varphi, \tag{6.2.34}$$

$$\alpha_T^-, \alpha_T^+, \alpha_{OAR}^+, \alpha_T, \alpha_H \leq 0.2, \ \textit{and} \tag{6.2.35}$$

$$r_{k+1}, h_{k+1}, \mathbf{w} > 0. \tag{6.2.36}$$

We formulate the deterministic equivalence of Model (6.2.24) considering random dose follows a standard normal distribution (Zaghian et al. (2018)):

$$\min_{w_j^k, \theta_L^k, \theta_U^k, \varphi^k, r_k, h_k} \quad -\lambda_T^- \, \theta_L^k + \lambda_T^+ \, \theta_U^k + \lambda_{OAR}^+ \, \varphi^k + \lambda_T \sum_{k \in \mathcal{K}} r_k - \lambda_H \sum_{k \in \mathcal{K}} h_k \tag{6.2.37}$$

$s.t.$

$$E(\tilde{\mathbf{D}}_i^k(\mathbf{w})) - \Phi^{-1}(1 - \alpha_T^-)\sigma(\tilde{\mathbf{D}}_i^k(\mathbf{w})) \geq \theta_L^k, \qquad \forall k \in \mathcal{K}, \forall i \in \mathcal{T},$$

$$E(\tilde{\mathbf{D}}_i^k(\mathbf{w})) + \Phi^{-1}(1 - \alpha_T^+)\sigma(\tilde{\mathbf{D}}_i^k(\mathbf{w})) \leq \theta_U^k, \qquad \forall k \in \mathcal{K}, \forall i \in \mathcal{T},$$

$$E(\tilde{\mathbf{D}}_i^k(\mathbf{w})) + \Phi^{-1}(1 - \alpha_{OAR}^+)\sigma(\tilde{\mathbf{D}}_i^k(\mathbf{w})) \leq \varphi^k, \qquad \forall k \in \mathcal{K}, \forall i \in \mathcal{OAR},$$

$$\delta_i^k \Phi^{-1}(1 - \alpha_T)\sigma(\tilde{\mathbf{D}}_i^k(\mathbf{w})) - \delta_i^k E(\tilde{\mathbf{D}}_i^k(\mathbf{w})) \geq U, \qquad \forall k \in \mathcal{K}, \forall i \in \mathcal{T},$$

$$-\delta_i^k \Phi^{-1}(1 - \alpha_H)\sigma(\tilde{\mathbf{D}}_i^k(\mathbf{w})) - \delta_i^k E(\tilde{\mathbf{D}}_i^k(\mathbf{w})) \leq L, \qquad \forall k \in \mathcal{K}, \forall i \in \mathcal{OAR},$$

$$\textit{constraints} \ (6.2.33 - 6.2.36),$$

where τ_g and τ_O are considered as constant parameters, L is $(\ln h_{k+1} - (t_k/\tau_O))$ and U is $(\ln r_{k+1} - (t_k/\tau_g))$.

6.3 Experimental results

We evaluate the relative performance of Model (6.2.37) on the treatment plan information using three clinical prostate cases who received radiation therapy at the MD Anderson Cancer Center (MDACC), Houston, TX. Table 6.2 lists patient information and specific treatment planning parameters for the three prostate cases.

Table 6.2: Treatment planning parameters for prostate cancer cases.

Prescription Dose	Number of Fractions	OARs Included in Optimization	Dose Requirements
76 Gy	38		Target receiving $\leq 105\%$ of θ_U
			Target receiving $\geq 95\%$ of θ_L
		Rectum, Bladder	OARs receiving $\leq 105\%$ of φ

Two plans were created for each patient case, one using the conventional plan optimization and the other using the proposed CCP biologically-based optimization model. We assume the standard exponential tumor growth and OARs recovery with a constant duration of $\tau_g = 5.1$ days (95% CI 4.2-7.2 days) (Pedicini et al. (2013)) and $\tau_O = 2.0$ days, respectively, for a prostate cancer case. We use the realistic choice of radiobiological parameter (α_0, β_0) in order to assess the effect of variable dose in each fraction of RT on the radiosensitivity parameter δ. We use $\alpha_0 = 0.16$ (95% CI $0.14 - 0.18\ Gy^{-1}$), $\alpha_0/\beta_0 = 2.96$ (95% CI $2.41 - 3.53$ Gy) for target, and $\alpha_0^{'} = 0.0532$, $\alpha_0^{'}/\beta_0^{'} = 2.00$ for OARs parameter which are the appropriate standard values for the prostate case (Pedicini et al. (2013)). We consider a standard fractionated treatment as a reference, i.e., a dose of 76 Gy delivered to the target in 38 fractions of 2 Gy. The corresponding penalty coefficients in the objective were determined by manual adjustments and multiple experiments to achieve the best resulting treatment plan in terms of both target coverage and healthy tissues sparing.

We set up the experiment using ± 5 mm shift position from the original position of the patient (nominal position). In that case, five scenarios (0,± 2.5 mm, and ± 5 mm) were considered. The data were generated by sampling from a normal probability distribution

of a random error. We evaluate the quality of the optimized plans regarding dose analysis, tumor coverage and total damage to the healthy cells.

6.3.1 Dose fractionation analysis

Plans optimized by the proposed CCP adaptive model for three cancer cases, and the optimal amount of prescribed dose (θ^K) are listed in Table 6.3. The radiobiological parameters, α_0 and α_0/β_0, are set to be 0.16 Gy^{-1} and 2.96 Gy for prostate cancer, and the OARs radiobiological parameters, $\alpha_0^{'}$ and $\alpha_0^{'}/\beta_0^{'}$, are considered to be 0.05 Gy^{-1} and 2.00 Gy, respectively. During the first treatment, the patient is irradiated with a beamlet intensity vector obtained by Model (6.2.37) using the initial data acquired regarding the prescribed amount of radiation dose for any type of cancer. New data sets corresponding to different tumor volume instances will be generated and accordingly the prescribed amount of dose will be updated for the other fractions based on patient specific changes. This may lead to a different beamlet intensity values to be used on the next treatments. This procedure is optimized in Model (6.2.37), and to have a treatment plan clinically acceptable, we put two requirements bellow for the optimization algorithm:

1: A treatment plan designed to meet the minimum dose requirement that has to be delivered in multiple sessions of radiation therapy for a particular case. The amount of dose delivered in each treatment considered to be between a clinically acceptable rang of prescription (larger than 1.8 and lower than 2.0 Gy).

2: The remaining viable tumor cells can be adjusted to be less than a determined value. This threshold can be considered to diagnose whether the therapy is working or not.

For simulation of radiation therapy treatment planning procedure occurred in multiple weeks, treatment plans were adapted to the patient volumetric changes once a week. Our hypothesis was that tumor and healthy tissues nearby are both subject to geometrical changes over the course of the treatment. Therefore, the plan can be adjusted on the basis of the physician's preference and considering a trad-off between target coverage and healthy

tissue recovery over time to avoid overly conservative treatment plans. Table 6.3 shows the result of treatment plans for three cancer cases generated using the proposed methodology. The cumulative dose prescription based on the adapted plans were calculated and presented on the last column of that table. The result of our approach shows a reduction by at least 3.0% in cumulative dose prescription for a treatment (from 76.00 Gy to 73.12, 73.71, and 72.80 Gy). It can be seen that the biologically-based plans typically deliver less cumulative dose to the cancerous region than the conventional plan. Note that the developed plans essentially ensure that the target receives the required dose (by controlling the remaining viable tumor cells to be less than a determined value (see Figure 6.1)), while reducing the dose delivered to healthy tissue as compared to the conventional plan. This leads to an improvement in protecting more healthy cells affected by radiation and a better recovery of patient from radiotherapy.

Table 6.3: The prescribed doses optimized from adaptive planning model for three prostate cancer cases I-III.

	Optimized fractionated dose (Gy)							
No. Treatments	**1-8**	**9-13**	**14-18**	**19-23**	**24-28**	**29-33**	**34-38**	**Total Dose**
Patient 1	2.00	1.90	1.90	1.90	1.90	1.90	1.89	73.12
Patient 2	2.00	1.93	1.93	1.93	1.93	1.93	1.89	73.71
Patient 3	2.00	1.87	1.87	1.92	1.90	1.90	1.90	72.80

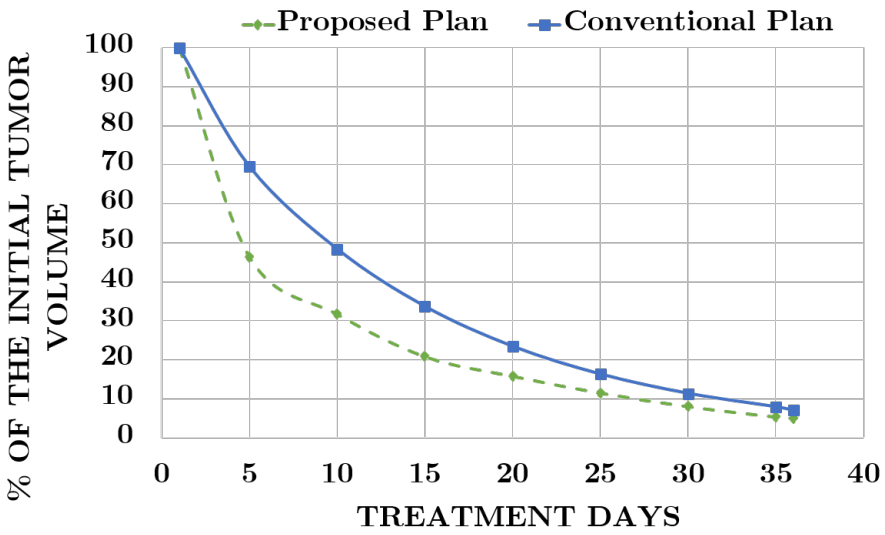

Figure 6.1: The comparison of surviving fraction of tumor volume through the course of treatment under the conventional and the proposed plan for prostate cancer cases I.

We conducted a series of experiments on the range of radiobilogical parameters for prostate cancer case I-III, and the optimal amount of radiation dose developed to be within a bound that is shown in Figure 6.2. In each experiment, different radiobilogical parameters were used having the same constant tumor population rate to estimate the changes in the tumor volume and its impact on a treatment plan. The maximum, minimum, and the average amount of radiation per week are plotted. Here, we consider the rate of tumor doubling (τ_g) to be constant value of 5.1 days.

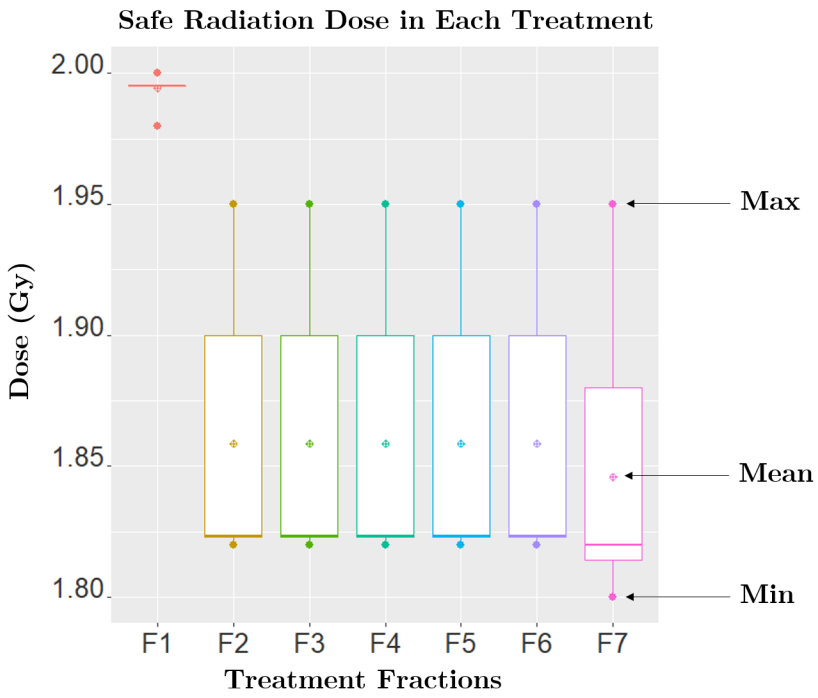

Figure 6.2: The safe range of prescribed doses in each treatment optimized from adaptive planning model under the given clinical interval of radiobilogical parameters for prostate cancer cases I-III.

From this Figure one can see how the range of radiation dose can be changed though the treatment. Reductions (from 2.0 Gy to 1.85 Gy) in some fractions may result in a better sparing of healthy tissues in some cancer cases. This shows the importance of understanding the radiobiological factors in designing a treatment plan for different types of cancer cases.

We also evaluate the effect of changes in tumor size on the amount of optimized fractionated dose by comparing two cases:

1) The limitation on the growth of tumor cell is considered in each update (Survival rate of tumor cells ≤ 1) .

2) No limitation on the growth of tumor cell in each update.

Table 6.4 presents the results of optimized plans for the two different assumptions above on three cancer cases. As it is shown from a treatment plan developed under first condition for Patient 1 (first column), the initial amount of radiation is set to be 2.0 Gy per treatment

in the first week and then drops to around 1.9 Gy for the rest of the treatments. However, a treatment plan that is developed for the same patient but under the second condition has more variability among doses optimized for each updated sessions of a treatment plan. It starts from 2 Gy during the first week and then is reduced to 1.8 Gy during the second and third weeks and then increased up to 2.17 Gy during the rest of the treatment. This can be explained from the fact that delivering a higher radiation dose in each treatment will cause more damage to the tumor cells and this will change the dose requirement for the next treatment to be lower. In this case, if we control the survival rate in each treatment from increasing ($r_k.up = 1$), the size of the tumor cells will not increase. So, the amount of dose required for the next treatment will be the same or less than the previous one. We can also conclude the same from the results for the other patients.

Table 6.4: The prescribed doses optimized from adaptive planning model under two different conditions.

		Optimized fractionated dose (Gy)					
		$r_k.up = 1$			$r_k.up \geq 0$		
		Patient 1	Patient 2	Patient 3	Patient 1	Patient 2	Patient 3
Fractions	**1-8**	2.00	2.00	2.00	2.00	2.00	2.00
	9-13	1.90	1.93	1.87	1.80	1.85	1.80
	14-18	1.90	1.93	1.87	1.80	1.85	1.80
	19-23	1.90	1.93	1.92	1.85	1.85	1.87
	24-28	1.90	1.93	1.90	1.90	1.93	1.95
	29-33	1.90	1.93	1.90	2.17	2.19	1.95
	34-38	1.89	1.89	1.89	2.05	2.08	2.05
Total Dose		73.12 Gy	73.71 Gy	72.80 Gy	73.85 Gy	74.75 Gy	73.10 Gy

This comparison demonstrates that by controlling the tumor size in each update, the total amount of dose prescribed for a treatment can be reduced (e.g. from 74.75 to 73.71 for Patient 2). This reduction in total radiation dose may not seem to be significant, but this will result in a better sparing of the normal tissues with a lower amount of radiation. Note that within this approach we can have different plans in which the best one can be determined in the clinic based on the physician's preference on different cancer cases.

6.3.2 Plan quality evaluation

We measured the maximum amount of dose delivered to OARs using two different plans to determine whether prescribing variable amount of dose in each treatment of radiotherapy could play a role in reducing the amount of cumulative radiation dose received by healthy cells near the tumor.

Figure 6.3 presents the maximum dose received by rectum and bladder based on the conventional plan and the new plan generated by the CCP adaptive model for three patient cases. It is shown that the maximum amount of dose which is critical in the serial organs, is reduced by the CCP adaptive model. Compared to the conventional plan, the CCP adaptive plan reduced the maximum dose on both the rectum and bladder by an average 2.5% and 1.8%, respectively.

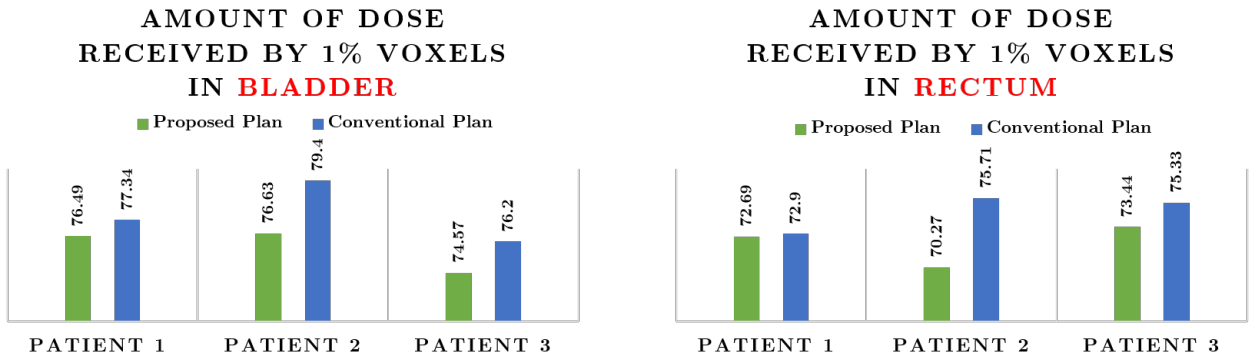

Figure 6.3: Comparison of the maximum amount of doses received by the healthy cells under the biologically-based optimization model and conventional treatment planning model.

6.3.3 Biological Effective Dose Comparison

To quantify the extent of potential therapeutic gain, the biological effective dose (BED) of the plans are further compared. The concept of BED has been widely used in the clinic for iso-effective dose calculation (Fowler (2010)). More specifically, different fractionation schemes with the same BED value in a given structure are expected to lead to the same biological damage in that structure. The BED associated with a fractionation scheme consisting of $|\mathcal{K}|$ treatment fractions, indexed by $k \in \mathcal{K} = \{1, ..., |\mathcal{K}|\}$, where a dose of $\mathbf{D}_i^k$

Gy is administered at fraction k is given by

$$BED(d;[\alpha/\beta]) = \sum_{k\in\mathcal{K}} \mathbf{D}_i^k(1+\frac{\mathbf{D}_i^k}{\alpha/\beta}),\ \forall i \in \{\mathcal{T}\cup\mathcal{OAR}\}, \forall k \in \mathcal{K}.$$

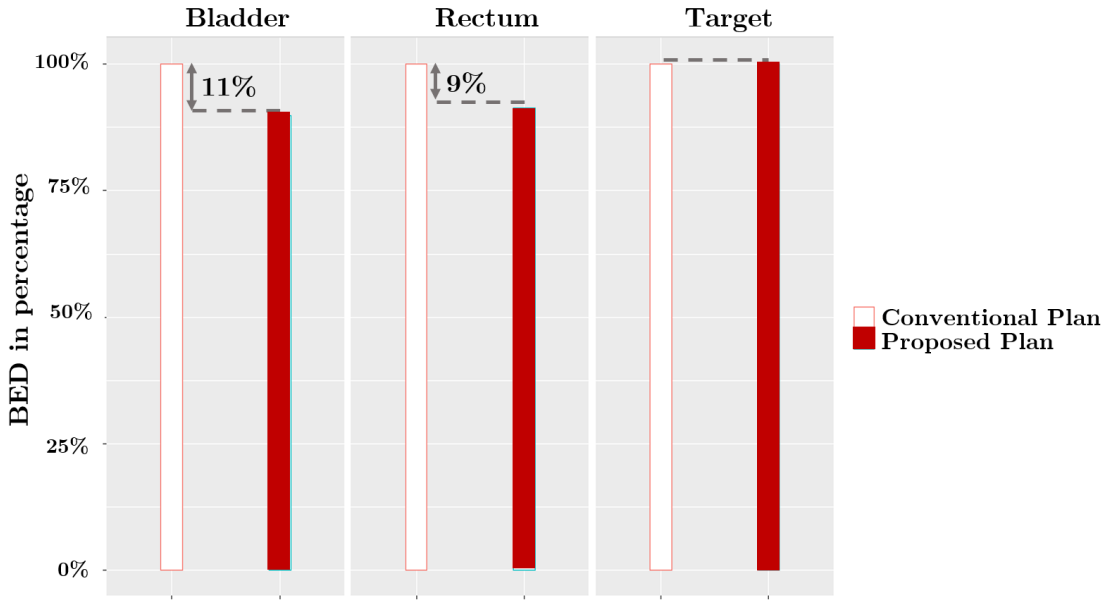

Figure 6.4: Comparison of the biological effective dose (BED) on organs-at-risk under the biologically-based optimization model and conventional treatment planning model (BED on target is assumed to be similar for both plans).

The goal of the biological-based treatment planning model is to obtain the optimal fraction-dependent fluence maps that minimize the BED on normal-tissue structures while limiting the BED in the target volume to a clinically desired level. In this experiment, we setup the treatment for both plans to have a similar biological effect on target (BED). Figure 6.4 compares the BED on OARs (rectum and bladder) associated with the conventional plan and biological-based model. The figure shows that the BED in target structure is similar between the two plans. However, the BED in the normal-tissue structures are substantially improved as a result of CCP biological-based treatment plan. This BED values were reduced by 9% in rectum and by 11% in bladder. The results shows the effectiveness of the proposed biologically-based model in preserving more healthy cells and improving the outcome of treatment.

6.3.4 Analysis based on different radiobiological parameters

We analyzed three clinical data sets on radiotherapeutic tumor control (α/β) for one prostate cancer (Patient 1), $\alpha/\beta = \{1.5, 3, 10\}$ (Hernández et al. (2013); Pedicini et al. (2013)), to assess the effects of various rates of tumor growth on the amount of dose per fraction. Table 6.5 shows that for $\alpha/\beta = 1.5$ there is no significant difference for the radiation dose in each fraction (at least 1.89, at most 2.00 Gy). However, for $\alpha/\beta = 3$ and 10 the amount of dose per fraction is lower and it is reduced until the end of the treatment (to 1.62 Gy and 1.29 Gy). Note that tumor cells with low α/β are more sensitive to large fraction doses and resistant to small fraction doses (Hernández et al. (2013)). Thus, for the higher radiobiological ratio of 3 and 10 the tumor cells become more sensitive to the radiation of 2 Gy at the beginning, which resulted in a big reduction in the number of the viable tumor cells remaining in situ. As a result, the model did not necessitate the large amount of dose for the following treatment and the total amount of dose for treating the cancer could be lower.

Table 6.5: The prescribed doses optimized from adaptive planning model under different assumption of the radiobiological parameters for prostate cancer (case 1).

Optimized fractionated dose (Gy)

Patient 1		**Radiobiological ratio**		
		$\alpha/\beta = 1.5$	$\alpha/\beta = 3$	$\alpha/\beta = 10$
Fractions	**1-8**	2.00	2.00	2.00
	9-13	1.90	1.85	1.70
	14-18	1.90	1.71	1.35
	19-23	1.90	1.71	1.35
	24-28	1.90	1.71	1.35
	29-33	1.90	1.71	1.35
	34-38	1.89	1.62	1.29
Total Dose		73.12 Gy	67.55	58.09 Gy

6.3.5 Treatment plans under different amount of initial dose

Next, we tested whether starting the treatment plan with the amount of dose higher or lower than the clinical prescribed dose (2 Gy) would affect the optimum radiation delivery for the other fractions.

Figure 6.5 compares the prescribed dose optimized by the CCP adaptive model for patient 1 with different amounts of initial dose given to the problem. For the treatment that starts with a higher amount of dose (2.1 Gy), there is a large reduction (at least 1.90 Gy) for the rest of the treatments. On the other hand, when the treatment starts with a lower amount of dose than usual (1.8 Gy), the higher amount of dose is delivered in most of the remaining fractions, and at the end this was reduced to 1.9 Gy. From this figure, it is shown that the total amounts of radiation vary depending on the initial amount of dose in the first fraction of radiotherapy. Hence, if the amount of dose delivered in the first treatment is less or more than the conventional equal fractionated dose, the total radiation required to remove the tumor cells for a specific rate will be increased with the rate of 0.05% (a) and 0.7%.

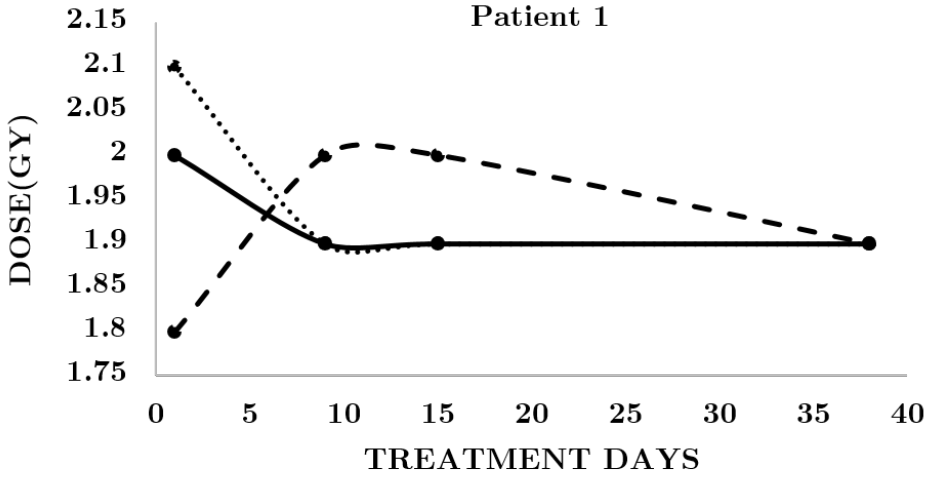

Figure 6.5: Optimized fractionation dose with different amount of initial radiation dose (2, less than 2, or more than 2)-Prostate cancer (case 1).

6.3.6 Worst Case Performance:

We study the sensitivity of the proposed model on the optimized amount of dose when the tumor re-population time is irregularly high and low. To determine whether the same optimal prescribed dose would result in the treatment plans with different tumor types growing, we optimized the plans when the tumor repopulation time is considered to be 5.1

days, a standard tumor growth rate, as well as faster and slower ones that are estimated to be 4.2 days and 7.2 days by deceasing and increasing the doubling time by 20%.

Figure 6.6 shows the results for the fractionated dose analysis in all three plans for prostate cancer (case 1).

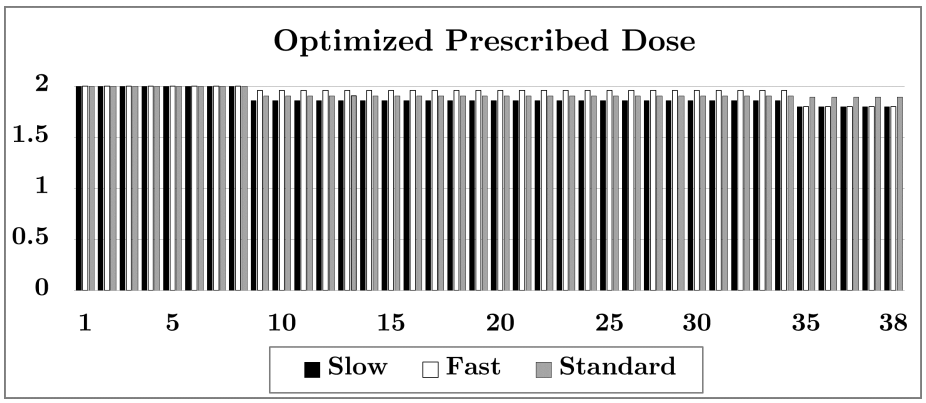

Figure 6.6: Dependence of the optimized prescribed dose for different choice of tumor growth rate. We set 5.1 *days* as the standard tumor growth rate, 7.2 *days* for slower growing tumor and 4.2 *days* for faster growing tumor.

Collectively, these results show that the treatment plan with a higher tumor growth rate (slower) has more variability among the amount of radiation dose for each treatment.

6.3.7 CCP Robustness Quantification

In this section, the quality and robustness of plans developed by deterministic, CCP, and robust optimization models are compared. In Figures 6.7(a), 6.7(b), and 6.7(c), the DVHs corresponding to the nominal dose distribution are displayed along with the DVH bands for the deterministic robust optimization, and chance-constrained models. Target coverage and OAR sparing provided by nominal plans were clinically acceptable for all plans. However, the target coverage provided by the plan based on the deterministic model was notably less robust than the target coverage of the plans generated using chance-constrained models. The DVH bands for the target were wider for the deterministic plan than for those of the chance-constrained models, indicating that CCP outperformed the deterministic model under setup uncertainty. In addition, the robustness of plans created

using CCP and robust optimization models was similar. Both the robust optimization model and the CCP approach were similarly robust in regard to normal tissue sparing.

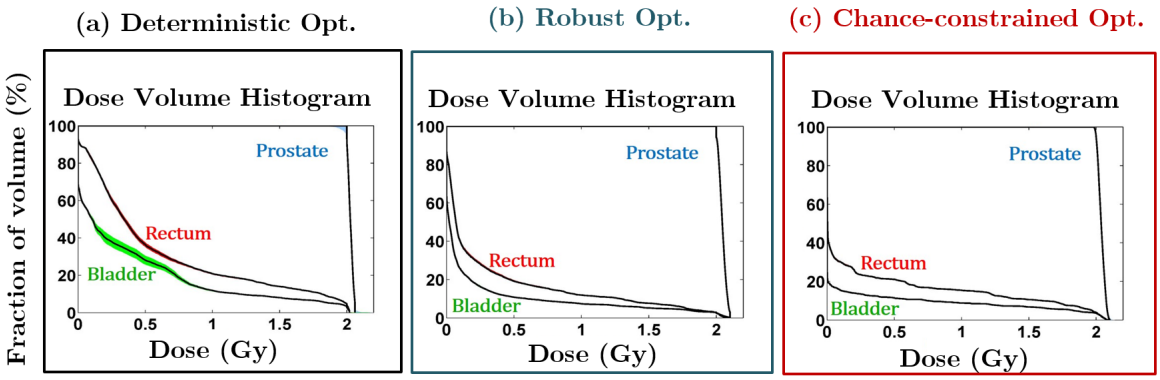

Figure 6.7: Prostate cancer (case 3) dose-volume histogram bands for target and organ-at-risk dose distributions covering all setup uncertainties in a single fraction, resulting from (a) the deterministic approach, (b) robust optimization, and (c) CCP under the normality assumption (c).

Looking at the DVH in Figure 6.7, the CCP adaptive plan achieved a significantly better results than the nominal plan (a). The CCP adaptive plan performs well not only in terms of tumor target coverage, but also in the sparing of sensitive structures. This is explained by the fact that the CCP approach can reduce the sensitivity of the optimization model to uncertain changes.

6.4 Conclusion

The use of ART is becoming more general in today's clinical practices. Multiple studies indicate the dosimetric benefits of ART when employed in particular subsets of patients, although clinical implications of this remain unclear. In this study, we evaluate the effects of radiobiological parameter in the dose optimization problem where the patient go through multiple treatments of radiotherapy. We emphasize that the proposed biologically-based treatment planning is not only dose based but also considers the most important radiobiological effects as they are clinically the most relevant. We analyze the proposed model with different assumptions on the clinical case to see the trade off in terms of tumor coverage

and OARs recovery. The current practice of delivering physical dose distributions across the tumor may potentially be improved by dose distributions guided by the biological responses of the tumor and healthy tissues. The biological-based optimization model developed and tested in this paper generate treatment plans reacting to the tumor and healthy structures biology prior to the treatment as well as the changing them throughout the treatment while satisfying both cumulative and fraction-size dose limit. In this study, we show that the standard fractionation schedule of around 2 Gy per day for five days a week is probably not optimal for all cases. Importantly, using the proposed model one can determine the overall efficacy of the treatment among multiple plans by evaluating their clinical benefits and consequences on a patient's body, and this could be valuable information in designing the clinical treatment plan.

Chapter 7

Future Work

7.1 Fractionation Scheduling Considering the Radio-biological Effects

A biologically-based chance-constrained treatment planning model is constructed to incorporate uncertainties in fractionated radiation therapy treatment planning problem, explained in **Chapter 6**. The biological changes of the proposed model compared to the traditional treatment plan for real cancer cases are evaluated. In this study, we assume constant tumor volume to produce treatments for a particular patient. However, it is shown that rate of tumor growth is not a constant parameter during a treatment. So, the probability of the instances of the tumor shrinkage or proliferation can be considered as the next steps of this study. In addition, further analysis and computational experiments using different clinical cancer cases need to be performed to understand the efficacy of this approach for other types of cancer and treatment modalities.

7.2 Fluence Map Optimization under Uncertainty Considering Energy Deposition

In **Chapter 5**, we propose an LET-based optimization problem to investigate the impact of including an additive linear energy transfer (LET)-dependent term in the objective function in intensity-modulated proton therapy (IMPT) optimization. As an extension to the current works can be optimizing the model under uncertainty using CCP approach. So, the performance of the LET-based model can be compared with the deterministic one regarding plan quality and robustness.

7.3 Including Relative Biological Effectiveness in a Fluence Map Optimization under Uncertainty

The future work is to develope a CCP model to optimize the intensity profile as well as the relative biological effectiveness (RBE) under uncertainty. This model can be compared to the CCP model with constant RBE regarding plan quality on a real patient. The CCP model considers a probability of constraint violations under shift uncertainty, and a planner can specify the level of conservatism for a particular patient. Within the flexibility that CCP provides, we can analyze the plan under the different expectation of physicians and provide more information on rejecting or approving a treatment plan.

References

21th Century Oncology (2019). Ct simulation. *www.21co.com radiation-therapy technologies ct-simulation*.

Acceletronics (2019). Linear accelerators. *www.acceletronics.com radiation therapy devices linear accelerators*.

Acharya, S., Fischer-Valuck, B. W., Kashani, R., Parikh, P., Yang, D., Zhao, T., Green, O., Wooten, O., Li, H. H., and Hu, Y. (2016). Online magnetic resonance image guided adaptive radiation therapy: first clinical applications. *International Journal of Radiation Oncology Biology Physics*, 94(2):394–403.

Alber, M. and Nüsslin, F. (2001). Optimization of intensity modulated radiotherapy under constraints for static and dynamic mlc delivery. *Physics in Medicine & Biology*, 46(12):3229.

Aleman, D. M., Wallgren, J., Romeijn, H. E., and Dempsey, J. F. (2014). A fluence map optimization model for restoring traditional fractionation in imrt treatment planning. *Optimization Letters*, 8(4):1453–1473.

AmericanCancerSociety (2019). Cancer facts and figures. *www.cancer.org research cancer-factsfigures acspc-031941*.

An, Y., Liang, J., Schild, S. E., Bues, M., and Liu, W. (2017). Robust treatment planning with conditional value at risk chance constraints in intensity-modulated proton therapy. *Medical Physics*, 44(1):28–36.

Bai, X., Lim, G. J., Grosshans, D. R., Mohan, R., and Cao, W. (2018). Robust optimization to reduce the impact of biological effect variation from physical uncertainties in intensity-modulated proton therapy. *Physics in medicine and biology*.

Bassler, N., Jäkel, O., Søndergaard, C. S., and Petersen, J. B. (2010). Dose-and let-painting with particle therapy. *Acta oncologica*, 49(7):1170–1176.

Bassler, N., Toftegaard, J., Lühr, A., Sørensen, B. S., Scifoni, E., Krämer, M., Jäkel, O., Mortensen, L. S., Overgaard, J., and Petersen, J. B. (2014). Let-painting increases tumour control probability in hypoxic tumours. *Acta Oncologica*, 53(1):25–32.

Baum, C., Alber, M., Birkner, M., and Nüsslin, F. (2006). Robust treatment planning for intensity modulated radiotherapy of prostate cancer based on coverage probabilities. *Radiotherapy and Oncology*, 78(1):27–35.

Beckham, W., Keall, P., and Siebers, J. (2002). A fluence-convolution method to calculate radiation therapy dose distributions that incorporate random set-up error. *Physics in Medicine & Biology*, 47(19):3465.

Bednarz, G., Michalski, D., Houser, C., Huq, M. S., Xiao, Y., Anne, P. R., and Galvin, J. M. (2002). The use of mixed-integer programming for inverse treatment planning with pre-defined field segments. *Physics in Medicine & Biology*, 47(13):2235.

Bentel, G. C. (1999). *Patient positioning and immobilization in radiation oncology*. McGraw-Hill.

Bertsekas, D. P. and Tsitsiklis, J. N. (2002). *Introduction to probability*, volume 1. Athena Scientific Belmont, MA.

Bertsimas, D. and Popescu, I. (2005). Optimal inequalities in probability theory: A convex optimization approach. *SIAM Journal on Optimization*, 15(3):780–804.

Birge, J. R. and Louveaux, F. (2011). *Introduction to stochastic programming*. Springer Science & Business Media.

Bortfeld, T. (1997). Clinically relevant intensity modulation opitimization using physical criteria. In *XII International Conference on the Use of Computers in Radiation Therapy, 1997*. Medical Physics Publishing.

Bortfeld, T. (1999). Optimized planning using physical objectives and constraints. In *Seminars in Radiation Oncology*, volume 9, pages 20–34. Elsevier.

Bortfeld, T., Chan, T. C., Trofimov, A., and Tsitsiklis, J. N. (2008). Robust management of motion uncertainty in intensity-modulated radiation therapy. *Operations Research*, 56(6):1461–1473.

Bortfeld, T., Ramakrishnan, J., Tsitsiklis, J. N., and Unkelbach, J. (2015). Optimization of radiation therapy fractionation schedules in the presence of tumor repopulation. *INFORMS Journal on Computing*, 27(4):788–803.

Bourhis, J., Overgaard, J., Audry, H., Ang, K. K., Saunders, M., Bernier, J., Horiot, J.-C., Le Maître, A., Pajak, T. F., and Poulsen, M. G. (2006). Hyperfractionated or accelerated radiotherapy in head and neck cancer: a meta-analysis. *The Lancet*, 368(9538):843–854.

Bral, S., Duchateau, M., De Ridder, M., Everaert, H., Tournel, K., Schallier, D., Verellen, D., and Storme, G. (2009). Volumetric response analysis during chemoradiation as predictive tool for optimizing treatment strategy in locally advanced unresectable nsclc. *Radiotherapy and Oncology*, 91(3):438–442.

Calafiore, G. C. and El Ghaoui, L. (2006). On distributionally robust chance-constrained linear programs. *Journal of Optimization Theory and Applications*, 130(1):1–22.

Cao, W., Khabazian, A., Yepes, P. P., Lim, G., Poenisch, F., Grosshans, D. R., and Mohan, R. (2017). Linear energy transfer incorporated intensity modulated proton therapy optimization. *Physics in Medicine and Biology*, 63(1):015013.

Cao, W., Lim, G., Li, X., Li, Y., Zhu, X. R., and Zhang, X. (2013). Incorporating deliverable monitor unit constraints into spot intensity optimization in intensity-modulated proton therapy treatment planning. *Physics in Medicine & Biology*, 58(15):5113.

Cao, W., Lim, G. J., Lee, A., Li, Y., Liu, W., Zhu, X. R., and Zhang, X. (2012). Uncertainty incorporated beam angle optimization for impt treatment planning. *Medical physics*, 39(8):5248–5256.

Carabe-Fernandez, A., Dale, R. G., and Jones, B. (2007). The incorporation of the concept of minimum rbe (rbe min) into the linear-quadratic model and the potential for improved

radiobiological analysis of high-let treatments. *International journal of radiation biology*, 83(1):27–39.

Casiraghi, M., Albertini, F., and Lomax, A. (2013). Advantages and limitations of the worst case scenario approach in IMPT treatment planning. *Physics in Medicine & Biology*, 58(5):1323.

Chan, T. C., Bortfeld, T., and Tsitsiklis, J. N. (2006). A robust approach to imrt optimization. *Physics in Medicine & Biology*, 51(10):2567.

Chan, T. C. and Mišić, V. V. (2013). Adaptive and robust radiation therapy optimization for lung cancer. *European Journal of Operational Research*, 231(3):745–756.

Chan, T. C., Tsitsiklis, J. N., and Bortfeld, T. (2009). Optimal margin and edge-enhanced intensity maps in the presence of motion and uncertainty. *Physics in Medicine and Biology*, 55(2):515.

Chan, T. C.-Y. (2007). *Optimization under uncertainty in radiation therapy*. PhD thesis, Massachusetts Institute of Technology.

Chang, A. L., Yock, T. I., Mahajan, A., Hill-Kaiser, C., Keole, S., Loredo, L., Cahlon, O., McMullen, K. P., Hartsell, W., and Indelicato, D. J. (2014). Pediatric proton therapy: patterns of care across the united states. *International Journal of Particle Therapy*, 1(2):357–367.

Charnes, A. and Cooper, W. W. (1959). Chance-constrained programming. *Management Science*, 6(1):73–79.

Charnes, A. and Cooper, W. W. (1962). Programming with linear fractional functionals. *Naval Research logistics quarterly*, 9(3-4):181–186.

Charnes, A. and Cooper, W. W. (1963). Deterministic equivalents for optimizing and satisficing under chance constraints. *Operations research*, 11(1):18–39.

Chen, M., Lu, W., Chen, Q., Ruchala, K., and Olivera, G. (2008). Adaptive fractionation therapy: Ii. biological effective dose. *Physics in Medicine & Biology*, 53(19):5513.

Chen, W., Sim, M., Sun, J., and Teo, C.-P. (2010). From cvar to uncertainty set: Implications in joint chance-constrained optimization. *Operations research*, 58(2):470–485.

Chen, W., Unkelbach, J., Trofimov, A., Madden, T., Kooy, H., Bortfeld, T., and Craft, D. (2012). Including robustness in multi-criteria optimization for intensity-modulated proton therapy. *Physics in Medicine & Biology*, 57(3):591.

Chetty, I. J., Rosu, M., Tyagi, N., Marsh, L. H., McShan, D. L., Balter, J. M., Fraass, B. A., and Ten Haken, R. K. (2003). A fluence convolution method to account for respiratory motion in three-dimensional dose calculations of the liver: A monte carlo study. *Medical physics*, 30(7):1776–1780.

Chu, M., Zinchenko, Y., Henderson, S. G., and Sharpe, M. B. (2005). Robust optimization for intensity modulated radiation therapy treatment planning under uncertainty. *Physics in Medicine and Biology*, 50(23):5463.

Chvetsov, A. V., Calvetti, D., Sohn, J. W., and Kinsella, T. J. (2005). Regularization of inverse planning for intensity-modulated radiotherapy. *Medical physics*, 32(2):501–514.

Cotrutz, C. and Xing, L. (2003). Method for determining a dose distribution in radiation therapy. US Patent App. 10/388,201.

de la Zerda, A., Armbruster, B., and Xing, L. (2007). Formulating adaptive radiation therapy (art) treatment planning into a closed-loop control framework. *Physics in Medicine and Biology*, 52(14):4137.

Dias, J., Rocha, H., Ventura, T., Ferreira, B., and do Carmo Lopes, M. (2016). Automated fluence map optimization based on fuzzy inference systems. *Medical physics*, 43(3):1083–1095.

Engelsman, M., Sharp, G., Bortfeld, T., Onimaru, R., and Shirato, H. (2005). How much margin reduction is possible through gating or breath hold? *Physics in Medicine and Biology*, 50(3):477.

Erridge, S. C., Seppenwoolde, Y., Muller, S. H., van Herk, M., De Jaeger, K., Belderbos, J. S., Boersma, L. J., and Lebesque, J. V. (2003). Portal imaging to assess set-up errors, tumor motion and tumor shrinkage during conformal radiotherapy of non-small cell lung cancer. *Radiotherapy and Oncology*, 66(1):75–85.

Fager, M., Toma-Dasu, I., Kirk, M., Dolney, D., Diffenderfer, E. S., Vapiwala, N., and Carabe, A. (2015). Linear energy transfer painting with proton therapy: a means of reducing radiation doses with equivalent clinical effectiveness. *International Journal of Radiation Oncology* Biology* Physics*, 91(5):1057–1064.

Ferreira, B. C., do Carmo Lopes, M., Mateus, J., Capela, M., and Mavroidis, P. (2010). Radiobiological evaluation of forward and inverse imrt using different fractionations for head and neck tumours. *Radiation Oncology*, 5(1):57.

Fowler, J. F. (2010). 21 years of biologically effective dose. *The British journal of radiology*, 83(991):554–568.

Fredriksson, A. and Bokrantz, R. (2014). A critical evaluation of worst case optimization methods for robust intensity-modulated proton therapy planning. *Medical physics*, 41(8Part1):081701.

Fredriksson, A., Forsgren, A., and Hårdemark, B. (2011). Minimax optimization for handling range and setup uncertainties in proton therapy. *Medical Physics*, 38(3):1672–1684.

Frese, M. C., Wilkens, J. J., Huber, P. E., Jensen, A. D., Oelfke, U., and Taheri-Kadkhoda, Z. (2011). Application of constant vs. variable relative biological effectiveness in treatment planning of intensity-modulated proton therapy. *International Journal of Radiation Oncology* Biology* Physics*, 79(1):80–88.

Geletu, A., Klöppel, M., Zhang, H., and Li, P. (2013). Advances and applications of chance-constrained approaches to systems optimisation under uncertainty. *International Journal of Systems Science*, 44(7):1209–1232.

Ghate, A. (2011). Dynamic optimization in radiotherapy. In *Transforming Research into Action*, pages 60–74. INFORMS.

Ghilezan, M., Yan, D., and Martinez, A. (2010). Adaptive radiation therapy for prostate cancer. In *Seminars in Radiation Oncology*, volume 20, pages 130–137. Elsevier.

Giantsoudi, D., Grassberger, C., Craft, D., Niemierko, A., Trofimov, A., and Paganetti, H. (2013). Linear energy transfer-guided optimization in intensity modulated proton therapy: feasibility study and clinical potential. *International Journal of Radiation Oncology* Biology* Physics*, 87(1):216–222.

Gillin, M. T., Sahoo, N., Bues, M., Ciangaru, G., Sawakuchi, G., Poenisch, F., Arjomandy, B., Martin, C., Titt, U., and Suzuki, K. (2010). Commissioning of the discrete spot scanning proton beam delivery system at the university of texas md anderson cancer center, proton therapy center, houston. *Medical physics*, 37(1):154–163.

Goodhead, D. T. (1994). Initial events in the cellular effects of ionizing radiations: clustered damage in dna. *International journal of radiation biology*, 65(1):7–17.

Grassberger, C. and Paganetti, H. (2011). Elevated let components in clinical proton beams. *Physics in Medicine & Biology*, 56(20):6677.

Grassberger, C., Trofimov, A., Lomax, A., and Paganetti, H. (2011). Variations in linear energy transfer within clinical proton therapy fields and the potential for biological treatment planning. *International Journal of Radiation Oncology* Biology* Physics*, 80(5):1559–1566.

Guan, F., Bronk, L., Titt, U., Lin, S. H., Mirkovic, D., Kerr, M. D., Zhu, X. R., Dinh, J., Sobieski, M., and Stephan, C. (2015a). Spatial mapping of the biologic effectiveness

of scanned particle beams: towards biologically optimized particle therapy. *Scientific reports*, 5:9850.

Guan, F., Peeler, C., Bronk, L., Geng, C., Taleei, R., Randeniya, S., Ge, S., Mirkovic, D., Grosshans, D., and Mohan, R. (2015b). Analysis of the track-and dose-averaged let and let spectra in proton therapy using the geant4 monte carlo code. *Medical physics*, 42(11):6234–6247.

Gunther, J. R., Sato, M., Chintagumpala, M., Ketonen, L., Jones, J. Y., Allen, P. K., Paulino, A. C., Okcu, M. F., Su, J. M., and Weinberg, J. (2015). Imaging changes in pediatric intracranial ependymoma patients treated with proton beam radiation therapy compared to intensity modulated radiation therapy. *International Journal of Radiation Oncology* Biology* Physics*, 93(1):54–63.

Hamacher, H. W. and Küfer, K.-H. (1999). Inverse radiation therapy planning: A multiple objective optimisation approach. In *Monitoring, Evaluating, Planning Health Services*, pages 177–189. World Scientific.

Hernández, T. G., González, A. V., Peidro, J. P., Ferrando, J. V. R., González, L. B., Cabañero, D. G., and Torrecilla, J. L. (2013). Radiobiological comparison of two radiotherapy treatment techniques for high-risk prostate cancer. *Reports of Practical Oncology & Radiotherapy*, 18(5):265–271.

Ho, K. F., Fowler, J. F., Sykes, A. J., Yap, B. K., Lee, L. W., and Slevin, N. J. (2009). Imrt dose fractionation for head and neck cancer: variation in current approaches will make standardisation difficult. *Acta Oncologica*, 48(3):431–439.

Hoeffding, W. (1963). Probability inequalities for sums of bounded random variables. *Journal of the American statistical association*, 58(301):13–30.

Hoffmann, A. L., den Hertog, D., Siem, A. Y., Kaanders, J. H., and Huizenga, H. (2008). Convex reformulation of biologically-based multi-criteria intensity-modulated radiation

therapy optimization including fractionation effects. *Physics in Medicine & Biology*, 53(22):6345.

Holder, A. (2003). Designing radiotherapy plans with elastic constraints and interior point methods. *Health care management science*, 6(1):5–16.

Huang, Z., Mayr, N. A., Yuh, W. T., Lo, S. S., Montebello, J. F., Grecula, J. C., Lu, L., Li, K., Zhang, H., and Gupta, N. (2010). Predicting outcomes in cervical cancer: a kinetic model of tumor regression during radiation therapy. *Cancer Research*, 70(2):463–470.

IBM Analytics (2019). The ilog cplex. *www.ilog.com/products/cplex/.*

ICRU (2011). Fundamental quantities and units for ionizing radiation. *(ICRU Report 85) J. ICRU 11 1-31.*

Institute, N. C. (2019). Types of treatment. *www.cancer.gov about-cancer treatment types.*

Jia, X., Men, C., Lou, Y., and Jiang, S. B. (2011). Beam orientation optimization for intensity modulated radiation therapy using adaptive l2, 1-minimization. *Physics in Medicine & Biology*, 56(19):6205.

Juloori, A., Ward, M. C., Joshi, N. P., Greskovich, J. F., Xia, P., Murray, C. E., Dorfmeyer, C. A., Potter, J., and Koyfman, S. A. (2015). Adaptive radiation therapy for head and neck cancer. *Applied Radiat Oncol*, 4(3):12–17.

Kall, P., Wallace, S. W., and Kall, P. (1994). *Stochastic programming*. Springer.

Kamjoo, A., Maheri, A., Dizqah, A. M., and Putrus, G. A. (2016). Multi-objective design under uncertainties of hybrid renewable energy system using nsga-ii and chance constrained programming. *International Journal of Electrical Power & Energy Systems*, 74:187–194.

Kardar, L. (2014). *Radiation Therapy Optimization under Uncertainty for Lung Cancer: Interplay Effects and Tumor Shrinkage*. PhD thesis.

Karlsson, K. H. and Stenerlöw, B. (2004). Focus formation of dna repair proteins in normal and repair-deficient cells irradiated with high-let ions. *Radiation research*, 161(5):517–527.

Keller, H., Ritter, M. A., and Mackie, T. R. (2003). Optimal stochastic correction strategies for rigid-body target motion. *International Journal of Radiation Oncology* Biology* Physics*, 55(1):261–270.

Key, R. (2019). Bragg peak. *www.radiologykey.comproton-beam-therapy.*

Khaled, S. and Held, K. D. (2012). Radiation biology: a handbook for teachers and students.

Kim, M., Ghate, A., and Phillips, M. H. (2009). A markov decision process approach to temporal modulation of dose fractions in radiation therapy planning. *Physics in Medicine & Biology*, 54(14):4455.

Kim, M., Ghate, A., and Phillips, M. H. (2012). A stochastic control formalism for dynamic biologically conformal radiation therapy. *European Journal of Operational Research*, 219(3):541–556.

Knap, M. M., Hoffmann, L., Nordsmark, M., and Vestergaard, A. (2010). Daily cone-beam computed tomography used to determine tumour shrinkage and localisation in lung cancer patients. *Acta Oncologica*, 49(7):1077–1084.

Koshani, R., Balter, J. M., Hayman, J. A., Henning, G. T., and van Herk, M. (2006). Short-term and long-term reproducibility of lung tumor position using active breathing control (abc). *International Journal of Radiation Oncology* Biology* Physics*, 65(5):1553–1559.

Lee, E. K., Fox, T., and Crocker, I. (2003). Integer programming applied to intensity-modulated radiation therapy treatment planning. *Annals of Operations Research*, 119(1-4):165–181.

Lee, E. K., Fox, T., and Crocker, I. (2006). Simultaneous beam geometry and intensity map optimization in intensity-modulated radiation therapy. *International Journal of Radiation Oncology* Biology* Physics*, 64(1):301–320.

Lim, G. (2008). An introduction to radiation therapy planning optimization. *Optimization in Medicine and Biology*, 16:197–221.

Lim, G. J. and Cao, W. (2012). A two-phase method for selecting imrt treatment beam angles: Branch-and-prune and local neighborhood search. *European Journal of Operational Research*, 217(3):609–618.

Lim, G. J., Choi, J., and Mohan, R. (2008). Iterative solution methods for beam angle and fluence map optimization in intensity modulated radiation therapy planning. *OR Spectrum*, 30(2):289–309.

Lim, G. J., Ferris, M. C., Shepard, D. M., Wright, S. J., and Earl, M. A. (2007). An optimization framework for conformal radiation treatment planning. *INFORMS Journal on Computing*, 19(3):366–380.

Lim, G. J., Kardar, L., and Cao, W. (2014). A hybrid framework for optimizing beam angles in radiation therapy planning. *Annals of Operations Research*, 217(1):357–383.

Liu, W., Li, Y., Li, X., Cao, W., and Zhang, X. (2012a). Influence of robust optimization in intensity-modulated proton therapy with different dose delivery techniques. *Medical physics*, 39(6Part1):3089–3101.

Liu, W., Zhang, X., Li, Y., and Mohan, R. (2012b). Robust optimization of intensity modulated proton therapy. *Medical physics*, 39(2):1079–1091.

Lof, J., Lind, B. K., and Brahme, A. (1995). Optimal radiation beam profiles considering the stochastic process of patient positioning in fractionated radiation therapy. *Inverse Problems*, 11(6):1189.

Lomax, A. (1999). Intensity modulation methods for proton radiotherapy. *Physics in Medicine & Biology*, 44(1):185.

Lomax, A. (2008). Intensity modulated proton therapy and its sensitivity to treatment

uncertainties 1: the potential effects of calculational uncertainties. *Physics in Medicine & Biology*, 53(4):1027.

Lu, W., Olivera, G. H., Chen, Q., Ruchala, K. J., Haimerl, J., Meeks, S. L., Langen, K. M., and Kupelian, P. A. (2006). Deformable registration of the planning image (kvct) and the daily images (mvct) for adaptive radiation therapy. *Physics in Medicine and Biology*, 51(17):4357.

Lujan, A. E., Ten Haken, R. K., Larsen, E. W., and Balter, J. M. (1999). Quantization of setup uncertainties in 3-d dose calculations. *Medical physics*, 26(11):2397–2402.

Manning, M. A., Wu, Q., Cardinale, R. M., Mohan, R., Lauve, A. D., Kavanagh, B. D., Morris, M. M., and Schmidt-Ullrich, R. K. (2001). The effect of setup uncertainty on normal tissue sparing with IMRT for head-and-neck cancer. *International Journal of Radiation Oncology* Biology* Physics*, 51(5):1400–1409.

Matuszak, M. M., Larsen, E. W., and Fraass, B. A. (2007). Reduction of imrt beam complexity through the use of beam modulation penalties in the objective function. *Medical physics*, 34(2):507–520.

McNamara, A. L., Schuemann, J., and Paganetti, H. (2015). A phenomenological relative biological effectiveness (rbe) model for proton therapy based on all published in vitro cell survival data. *Physics in Medicine & Biology*, 60(21):8399.

McShan, D., Kessler, M., Vineberg, K., and Fraass, B. (2006). Inverse plan optimization accounting for random geometric uncertainties with a multiple instance geometry approximation (miga). *Medical physics*, 33(5):1510–1521.

Miller, B. L. and Wagner, H. M. (1965). Chance constrained programming with joint constraints. *Operations Research*, 13(6):930–945.

Mitin, T. and Zietman, A. L. (2014). Promise and pitfalls of heavy-particle therapy. *Journal of Clinical Oncology*, 32(26):2855.

Mohan, R., Zhang, X., Wang, H., Kang, Y., Wang, X., Liu, H., Ang, K. K., Kuban, D., and Dong, L. (2005). Use of deformed intensity distributions for on-line modification of image-guided IMRT to account for interfractional anatomic changes. *International Journal of Radiation Oncology* Biology* Physics*, 61(4):1258–1266.

Nemirovski, A. and Shapiro, A. (2006). Convex approximations of chance constrained programs. *SIAM Journal on Optimization*, 17(4):969–996.

Nieves, J. F. and Ubriaco, M. R. (2015). Simple linear model of tumor growth in a changing environment. *Applied Mathematics*, 6(07):1139.

Nohadani, O. and Roy, A. (2017). Robust optimization with time-dependent uncertainty in radiation therapy. *IISE Transactions on Healthcare Systems Engineering*, 7(2):81–92.

Olafsson, A. and Wright, S. J. (2006). Efficient schemes for robust IMRT treatment planning. *Physics in Medicine and Biology*, 51(21):5621.

Paganetti, H., Niemierko, A., Ancukiewicz, M., Gerweck, L. E., Goitein, M., Loeffler, J. S., and Suit, H. D. (2002). Relative biological effectiveness (rbe) values for proton beam therapy. *International Journal of Radiation Oncology* Biology* Physics*, 53(2):407–421.

Pedicini, P., Strigari, L., and Benassi, M. (2013). Estimation of a self-consistent set of radiobiological parameters from hypofractionated versus standard radiation therapy of prostate cancer. *International Journal of Radiation Oncology* Biology* Physics*, 85(5):e231–e237.

Peeler, C. R., Mirkovic, D., Titt, U., Blanchard, P., Gunther, J. R., Mahajan, A., Mohan, R., and Grosshans, D. R. (2016). Clinical evidence of variable proton biological effectiveness in pediatric patients treated for ependymoma. *Radiotherapy and Oncology*, 121(3):395–401.

Pflugfelder, D., Wilkens, J., and Oelfke, U. (2008). Worst case optimization: a method to account for uncertainties in the optimization of intensity modulated proton therapy. *Physics in Medicine and Biology*, 53(6):1689.

Pinter, J. (1989). Deterministic approximations of probability inequalities. *Zeitschrift für Operations-Research*, 33(4):219–239.

Polster, L., Schuemann, J., Rinaldi, I., Burigo, L., McNamara, A. L., Stewart, R. D., Attili, A., Carlson, D. J., Sato, T., and Méndez, J. R. (2015). Extension of topas for the simulation of proton radiation effects considering molecular and cellular endpoints. *Physics in Medicine & Biology*, 60(13):5053.

Prékopa, A. (2013). *Stochastic programming*, volume 324. Springer Science & Business Media.

Qin, A., Sun, Y., Liang, J., and Yan, D. (2015). Evaluation of online/offline image guidance/adaptation approaches for prostate cancer radiation therapy. *International Journal of Radiation Oncology* Biology* Physics*, 91(5):1026–1033.

Ramakrishnan, J., Craft, D., Bortfeld, T., and Tsitsiklis, J. N. (2012). A dynamic programming approach to adaptive fractionation. *Physics in Medicine & Biology*, 57(5):1203.

Reemtsen, R. and Alber, M. (2009). Continuous optimization of beamlet intensities for intensity modulated photon and proton radiotherapy. In *Handbook of Optimization in Medicine*, pages 1–40. Springer.

Reilly, M., Kavanaugh, J., Green, O., and Mutic, S. (2016). Quantitative and dosimetric evaluation of offline adaptive radiation therapy toward establishing a decision support framework for evaluating the necessity for real-time adaptation. *International Journal of Radiation Oncology Biology Physics*, 96(2):S226.

Romeijn, H. E., Ahuja, R. K., Dempsey, J. F., Kumar, A., and Li, J. G. (2003). A novel linear programming approach to fluence map optimization for intensity modulated radiation therapy treatment planning. *Physics in Medicine and Biology*, 48(21):3521.

Romeijn, H. E. and Dempsey, J. F. (2008). Intensity modulated radiation therapy treatment plan optimization. *Top*, 16(2):215.

Sabin, N. D., Merchant, T. E., Harreld, J. H., Patay, Z., Klimo, P., Qaddoumi, I., Armstrong, G. T., Wright, K., Gray, J., and Indelicato, D. J. (2013). Imaging changes in very young children with brain tumors treated with proton therapy and chemotherapy. *American Journal of Neuroradiology*, 34(2):446–450.

Saka, B., Rardin, R. L., Langer, M. P., and Dink, D. (2011). Adaptive intensity modulated radiation therapy planning optimization with changing tumor geometry and fraction size limits. *IIE Transactions on Healthcare Systems Engineering*, 1(4):247–263.

Schuemann, J., Dowdell, S., Grassberger, C., Min, C., and Paganetti, H. (2014). Site-specific range uncertainties caused by dose calculation algorithms for proton therapy. *Physics in Medicine & Biology*, 59(15):4007.

Shepard, D. M., Ferris, M. C., Olivera, G. H., and Mackie, T. R. (1999). Optimizing the delivery of radiation therapy to cancer patients. *Siam Review*, 41(4):721–744.

Spirou, S. V. and Chui, C.-S. (1998). A gradient inverse planning algorithm with dose-volume constraints. *Medical physics*, 25(3):321–333.

Steel, G. G., McMillan, T. J., and Peacock, J. (1989). The 5Rs of radiobiology. *International Journal of Radiation Biology*, 56(6):1045–1048.

Stone, H. B., Coleman, C. N., Anscher, M. S., and McBride, W. H. (2003). Effects of radiation on normal tissue: consequences and mechanisms. *The lancet oncology*, 4(9):529–536.

Thames, H. D. and Hendry, J. H. (1987). *Fractionation in radiotherapy*. Taylor and Franc's London et al.

Trofimov, A., Rietzel, E., Lu, H.-M., Martin, B., Jiang, S., Chen, G. T., and Bortfeld, T. (2005). Temporo-spatial IMRT optimization: concepts, implementation and initial results. *Physics in Medicine and Biology*, 50(12):2779.

Trofimov, A., Unkelbach, J., DeLaney, T. F., and Bortfeld, T. (2012). Visualization of a variety of possible dosimetric outcomes in radiation therapy using dose-volume histogram bands. *Practical Radiation Oncology*, 2(3):164–171.

Unkelbach, J., Bortfeld, T., Martin, B. C., and Soukup, M. (2009). Reducing the sensitivity of impt treatment plans to setup errors and range uncertainties via probabilistic treatment planning. *Medical physics*, 36(1):149–163.

Unkelbach, J., Botas, P., Giantsoudi, D., Gorissen, B. L., and Paganetti, H. (2016). Reoptimization of intensity modulated proton therapy plans based on linear energy transfer. *International Journal of Radiation Oncology* Biology* Physics*, 96(5):1097–1106.

Unkelbach, J., Chan, T. C., and Bortfeld, T. (2007). Accounting for range uncertainties in the optimization of intensity modulated proton therapy. *Physics in Medicine & Biology*, 52(10):2755.

Unkelbach, J., Craft, D., Hong, T., Papp, D., Ramakrishnan, J., Salari, E., Wolfgang, J., and Bortfeld, T. (2014). Exploiting tumor shrinkage through temporal optimization of radiotherapy. *Physics in Medicine and Biology*, 59(12):3059.

Unkelbach, J. and Oelfke, U. (2004). Inclusion of organ movements in imrt treatment planning via inverse planning based on probability distributions. *Physics in Medicine & Biology*, 49(17):4005.

van Ackooij, W., Henrion, R., Möller, A., and Zorgati, R. (2014). Joint chance constrained programming for hydro reservoir management. *Optimization and Engineering*, 15(2):509–531.

van de Schoot, A. J., de Boer, P., Visser, J., Stalpers, L. J., Rasch, C. R., and Bel, A. (2017). Dosimetric advantages of a clinical daily adaptive plan selection strategy compared with a non-adaptive strategy in cervical cancer radiation therapy. *Acta Oncologica*, 56(5):667–674.

Van Herk, M. (2004). Errors and margins in radiotherapy. In *Seminars in radiation oncology*, volume 14, pages 52–64. Elsevier.

Webb, S. (2004). *Contemporary IMRT: developing physics and clinical implementation*. CRC Press.

Wilkens, J. and Oelfke, U. (2004). A phenomenological model for the relative biological effectiveness in therapeutic proton beams. *Physics in Medicine & Biology*, 49(13):2811.

Wilkens, J. J., Alaly, J. R., Zakarian, K., Thorstad, W. L., and Deasy, J. O. (2007). Imrt treatment planning based on prioritizing prescription goals. *Physics in Medicine & Biology*, 52(6):1675.

Wilkens, J. J. and Oelfke, U. (2005). Optimization of radiobiological effects in intensity modulated proton therapy. *Medical physics*, 32(2):455–465.

Withers, H. R. (1975). The four r's of radiotherapy. *Adv Radiat Biol*, 5(3):241–271.

Withers, H. R., Thames, H. D., and Peters, L. J. (1983). A new isoeffect curve for change in dose per fraction. *Radiotherapy and Oncology*, 1(2):187–191.

Wong, J. R., Grimm, L., Uematsu, M., Oren, R., Cheng, C. W., Merrick, S., and Schiff, P. (2005). Image-guided radiotherapy for prostate cancer by ct–linear accelerator combination: Prostate movements and dosimetric considerations. *International Journal of Radiation Oncology* Biology* Physics*, 61(2):561–569.

Wu, Q. and Mohan, R. (2002). Multiple local minima in imrt optimization based on dose–volume criteria. *Medical physics*, 29(7):1514–1527.

Wu, Q. J., Thongphiew, D., Wang, Z., Mathayomchan, B., Chankong, V., Yoo, S., Lee, W. R., and Yin, F.-F. (2008). On-line re-optimization of prostate IMRT plans for adaptive radiation therapy. *Physics in Medicine and Biology*, 53(3):673.

Yang, C., Liu, F., Ahunbay, E., Chang, Y.-W., Lawton, C., Schultz, C., Wang, D., Firat, S., Erickson, B., and Li, X. A. (2014). Combined online and offline adaptive radiation therapy: A dosimetric feasibility study. *Practical radiation oncology*, 4(1):e75–e83.

Yepes, P. P., Eley, J. G., Liu, A., Mirkovic, D., Randeniya, S., Titt, U., and Mohan, R. (2016). Validation of a track repeating algorithm for intensity modulated proton therapy: clinical cases study. *Physics in Medicine & Biology*, 61(7):2633.

Yoon, M., Park, S. Y., Shin, D., Lee, S. B., Pyo, H. R., Kim, D. Y., and Cho, K. H. (2007). A new homogeneity index based on statistical analysis of the dose–volume histogram. *Journal of Applied Clinical Medical Physics*, 8(2):9–17.

Zaghian, M., Cao, W., Liu, W., Kardar, L., Randeniya, S., Mohan, R., and Lim, G. (2017). Comparison of linear and nonlinear programming approaches for "worst case dose" and "minmax" robust optimization of intensity-modulated proton therapy dose distributions. *Journal of Applied Clinical Medical Physics*, 18(2):15–25.

Zaghian, M., Lim, G., Liu, W., and Mohan, R. (2014). An automatic approach for satisfying dose-volume constraints in linear fluence map optimization for impt. *Journal of Cancer Therapy*, 5(2):198.

Zaghian, M., Lim, G. J., and Khabazian, A. (2018). A chance-constrained programming framework to handle uncertainties in radiation therapy treatment planning. *European Journal of Operational Research*, 266(2):736–745.

Zymler, S., Kuhn, D., and Rustem, B. (2013). Distributionally robust joint chance constraints with second-order moment information. *Mathematical Programming*, pages 1–32.

Appendix A

Models and figures for Manuscript "A feasibility study of a risk-based stochastic optimization approach for radiation treatment planning under setup uncertainty"

A.1 CCP model under Normal distribution (CCP-N)

First, consider dose contribution vector $\tilde{\mathbf{d}}_i$ is assumed to be normally distributed with mean $E(\tilde{\mathbf{d}}_i)$ and standard deviation $\sigma(\tilde{\mathbf{d}}_i)$. So, we have

$$
\begin{aligned}
&\min \quad -\lambda_T^- \theta_L + \lambda_T^+ \theta_U + \lambda_O^+ \varphi && \text{(A.1.1)}\\
&s.t.\\
&E(\tilde{\mathbf{D}}_T(\mathbf{w})) - \Phi^{-1}(1-\alpha_T^-)\sigma(\tilde{\mathbf{D}}_T(\mathbf{w})) \geq \theta_L, \qquad \forall \mathcal{T},\\
&E(\tilde{\mathbf{D}}_T(\mathbf{w})) + \Phi^{-1}(1-\alpha_T^+)\sigma(\tilde{\mathbf{D}}_T(\mathbf{w})) \leq \theta_U, \qquad \forall \mathcal{T},\\
&E(\tilde{\mathbf{D}}_O(\mathbf{w})) + \Phi^{-1}(1-\alpha_O^+)\sigma(\tilde{\mathbf{D}}_O(\mathbf{w})) \leq \varphi, \qquad \forall \mathcal{O},\\
&\underline{\theta}_L \leq \theta_L \leq \bar{\theta}_L,\ \underline{\theta}_U \leq \theta_U \leq \bar{\theta}_U,\\
&\varphi, \mathbf{w} \geq 0,
\end{aligned}
$$

as a deterministic equivalent of CCP model (4.2.3). The cumulative distribution of a normal standard probability density is represented with $\Phi(\cdot)$.

A.2 CCP model under uniform distribution (CCP-U)

Similarly, under uniform distributional assumption, the deterministic linear equivalents of the chance constraints (4.2.3) are provided.

Assuming, vector $\tilde{\mathbf{d}}_i - E(\tilde{\mathbf{d}}_i)$ is distributed uniformly in the ellipsoid $\varepsilon = \{\xi = Qz : \|z\| \leq 1\}$, where $Q = \upsilon\Gamma_f, \Gamma = \sigma^2(\tilde{d}_i) \succ 0, \upsilon = \sqrt{n+3}, \Gamma_f \in R^n$, and υ is a full rank factor such that $\Gamma = \Gamma_f\Gamma_f^T$, the deterministic equivalence of model (4.2.3) can be formulated as follows:

$$
\begin{aligned}
&\min \quad -\lambda_T^- \theta_L + \lambda_T^+ \theta_U + \lambda_O^+ \varphi && \text{(A.2.1)}\\
&s.t.\\
&E(\tilde{\mathbf{D}}_T(\mathbf{w})) - \upsilon\sqrt{\Psi_{beta}^{-1}(1-2\alpha_T^-)}\,\sigma(\tilde{\mathbf{D}}_T(\mathbf{w})) \geq \theta_L, \qquad \forall\mathcal{T},\\
&E(\tilde{\mathbf{D}}_T(\mathbf{w})) + \upsilon\sqrt{\Psi_{beta}^{-1}(1-2\alpha_T^+)}\,\sigma(\tilde{\mathbf{D}}_T(\mathbf{w})) \leq \theta_U, \qquad \forall\mathcal{T},\\
&E(\tilde{\mathbf{D}}_O(\mathbf{w})) + \upsilon\sqrt{\Psi_{beta}^{-1}(1-2\alpha_O^+)}\,\sigma(\tilde{\mathbf{D}}_O(\mathbf{w})) \leq \varphi, \qquad \forall\mathcal{O},\\
&\underline{\theta}_L \leq \theta_L \leq \bar{\theta}_L,\ \underline{\theta}_U \leq \theta_U \leq \bar{\theta}_U,\\
&\varphi, \mathbf{w} \geq 0,
\end{aligned}
$$

where $\Psi_{beta}(\cdot)$ is the cumulative distribution of a $\beta(1/2; n/2+1)$ probability density.

Models (A.1.1) and (A.2.1) were developed to optimize the thresholds (θ_L, θ_U, and φ) of the constraints while guaranteeing the constraints hold a pre-specified probability.

A.3 Dose-volume histogram for the prostate cancer cases, the pancreatic, and pediatric cancer cases

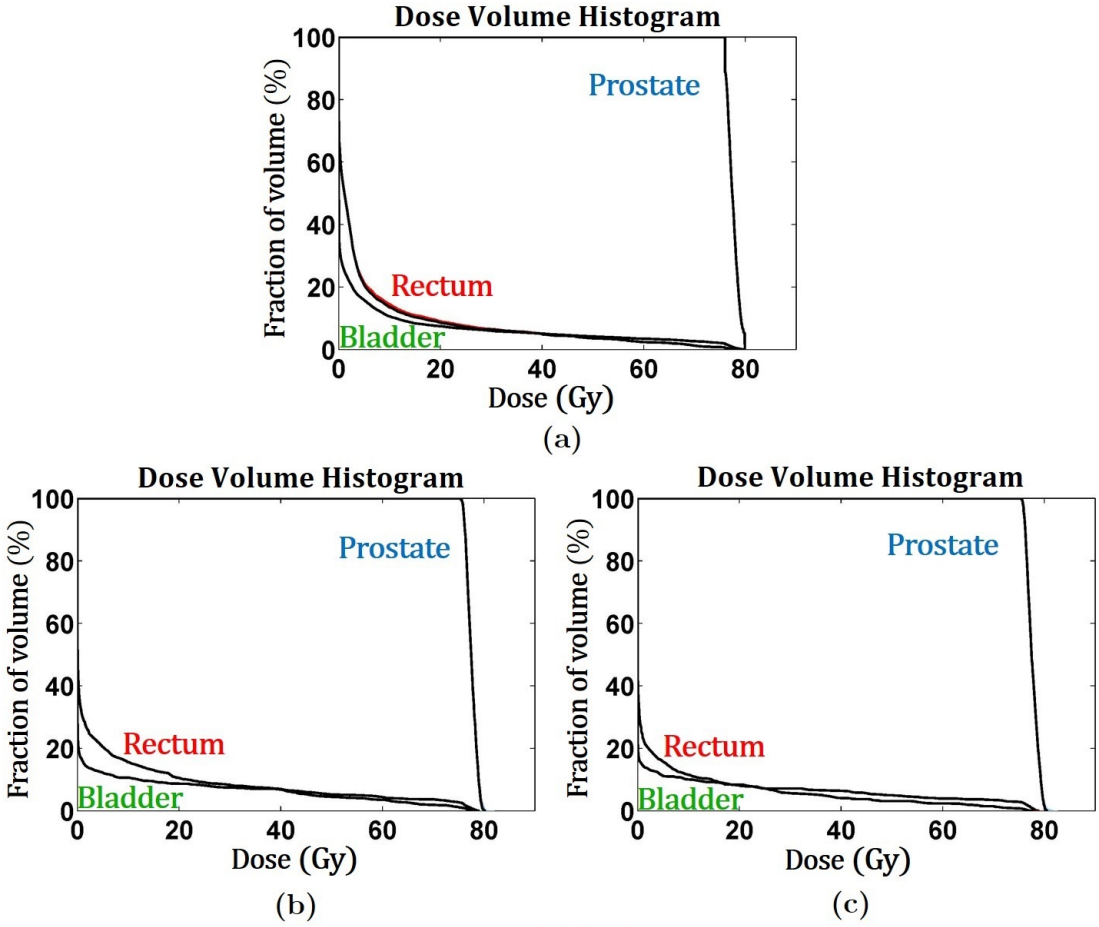

Figure A.1: Prostate cancer (case I) dose-volume histogram bands for target and organs-at-risk dose distributions covering all setup uncertainties, resulting from (a) robust optimization, (b) chance-constrained programming under the normality assumption, and (c) chance-constrained programming under the uniformity assumption.

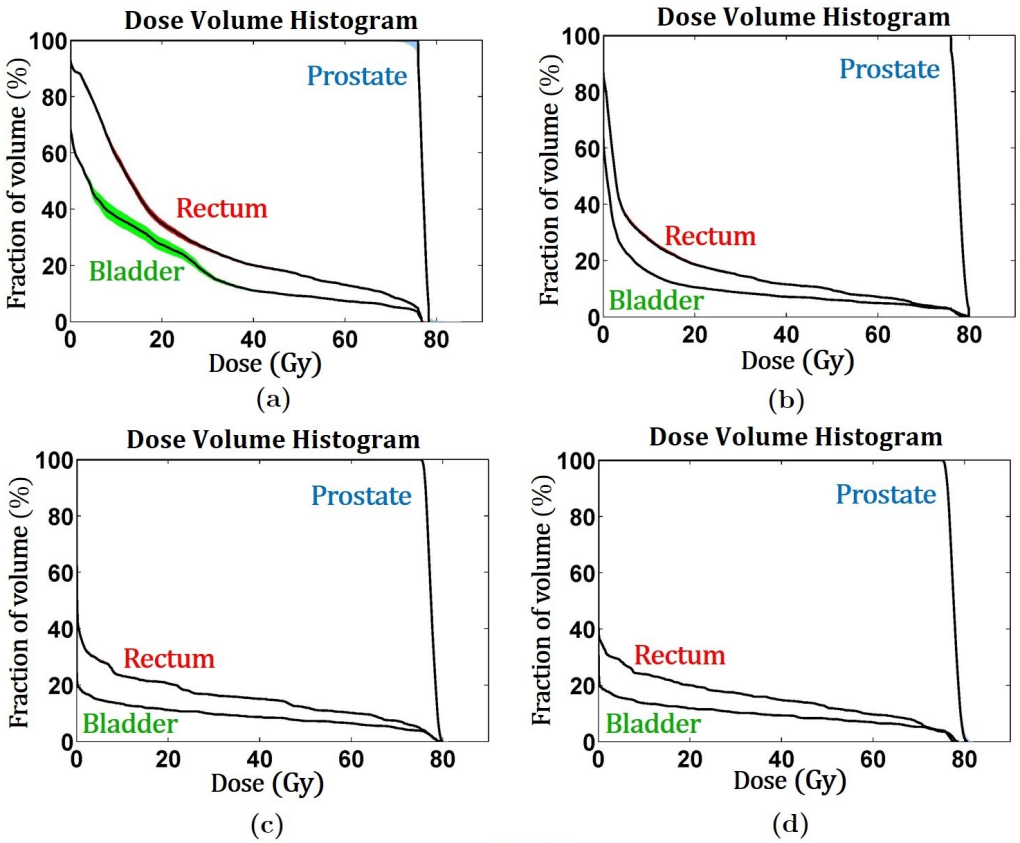

Figure A.2: Prostate cancer (case II) dose-volume histogram bands for target and organs-at-risk dose distributions covering all setup uncertainties, resulting from (a) the deterministic approach, (b) robust optimization, (c) chance-constrained programming under the normality assumption, and (d) chance-constrained programming under the uniformity assumption.

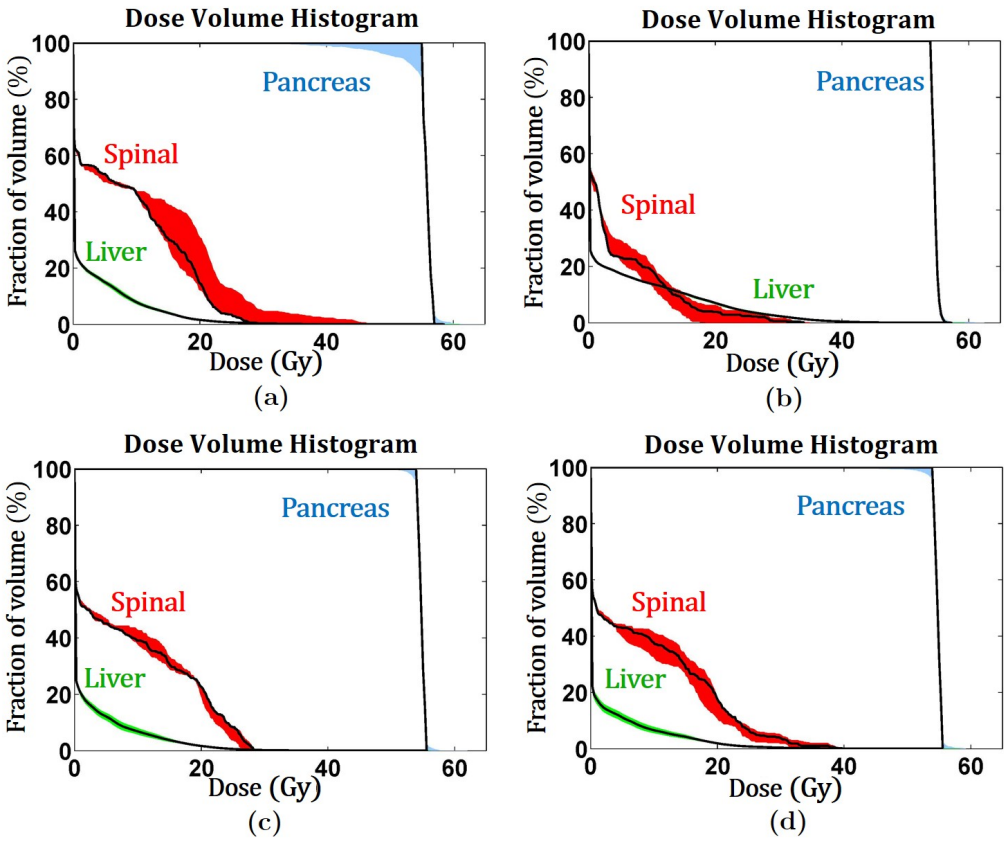

Figure A.3: Pancreatic cancer dose-volume histogram bands for target and organs-at-risk dose distributions covering all setup uncertainties, resulting from (a) the deterministic approach, (b) robust optimization, (c) chance-constrained programming under the normality assumption, and (d) chance-constrained programming under the uniformity assumption.

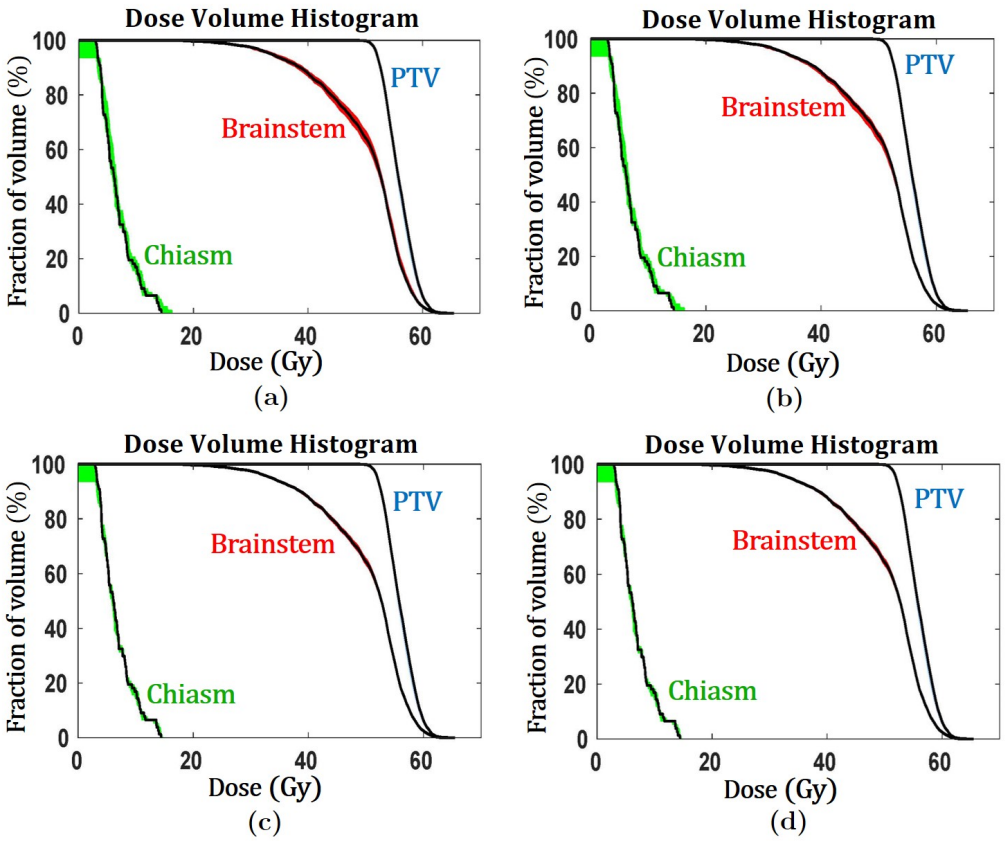

Figure A.4: Pediatric cancer dose-volume histogram bands for target and organs-at-risk dose dose distributions covering all setup uncertainties, resulting from (a) the deterministic approach, (b) robust optimization, (c) chance-constrained programming under the normality assumption, and (d) chance-constrained programming under the uniformity assumption.

Appendix B

Figures for Manuscript "Distributionally Robust Chance-Constrained Programming in Radiation Therapy Treatment Planning"

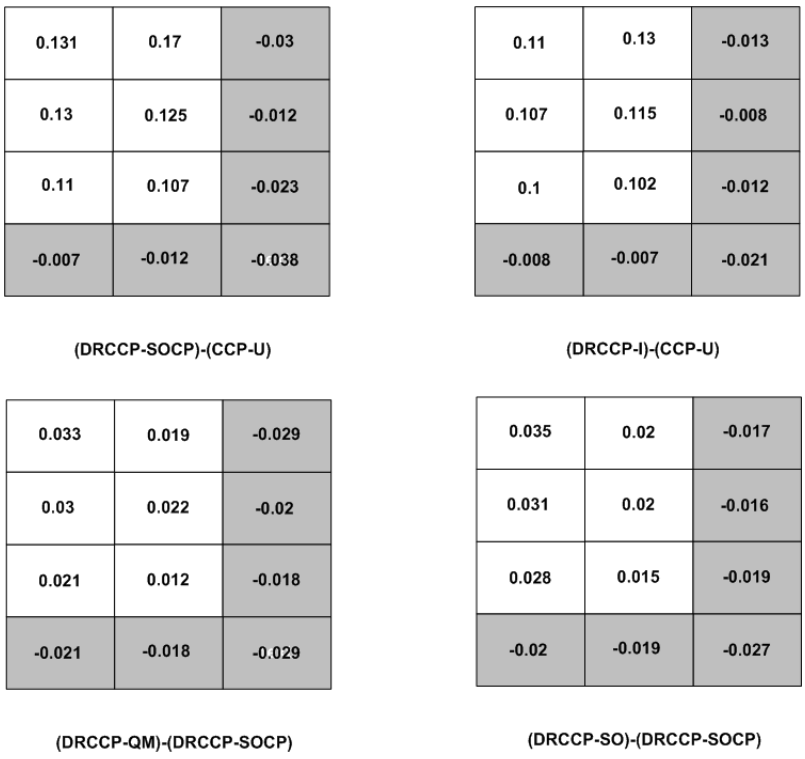

Figure B.1: Differences between the mean-dose per voxel

Appendix C

Figures for Manuscript "Linear energy transfer incorporated intensity modulated proton therapy optimization"

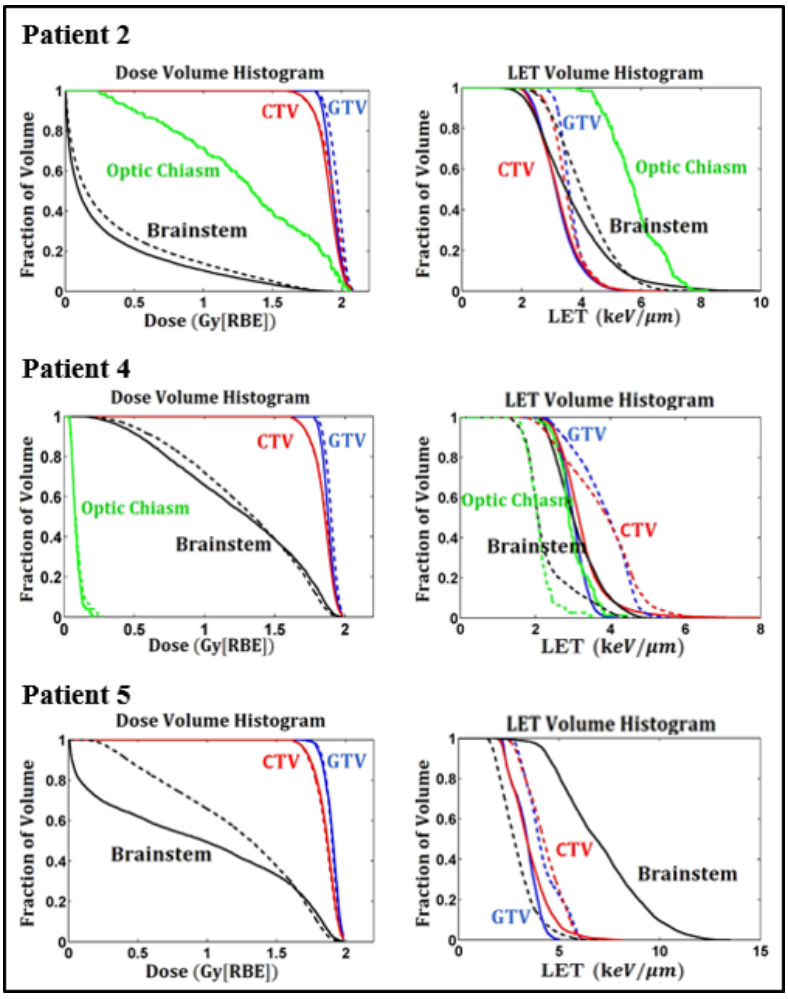

Figure C.1: Dose- and LETd-volume histograms of the IMPT plans optimized by DoseOpt (solid lines) and LETOpt (dashed lines) for Patient 2, 4 and 5.

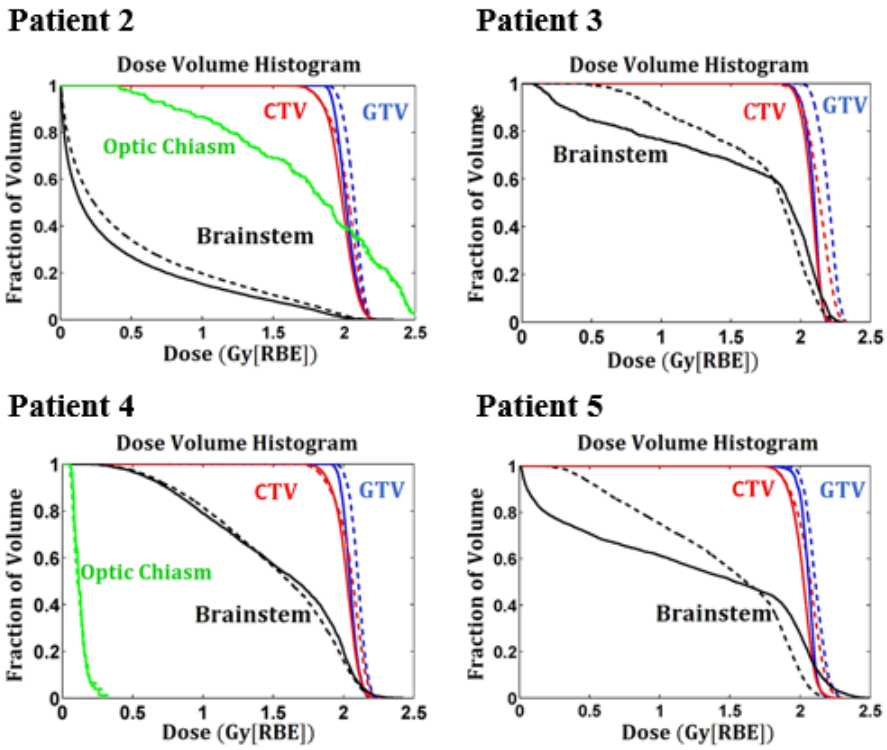

Figure C.2: Dose volume histograms of the IMPT plans optimized by DoseOpt (solid lines) and LETOpt (dashed lines) for Patient 1, 2, 4 and 5. The RBE here is variable and calculated based on a recently published RBE model (McNamara et al., 2015). The required tissue parameters are obtained from literature (Frese et al., 2011).